R. & M. No. 3653

MINISTRY OF AVIATION SUPPLY

AERONAUTICAL RESEARCH COUNCIL
REPORTS AND MEMORANDA

Low-Speed Three-Dimensional Turbulent Boundary-Layer Data
Parts 1 and 2

By L. F. EAST and R. P. HOXEY

Aerodynamics Dept., R.A.E., Bedford

LONDON: HER MAJESTY'S STATIONERY OFFICE
1971
PRICE £2 4s 0d [£2·20] NET

Low-Speed Three-Dimensional Turbulent Boundary-Layer Data
Part 1

By L. F. EAST and R. P. HOXEY

Aerodynamics Dept., R.A.E., Bedford

Reports and Memoranda No. 3653*

March, 1969

Summary.

A comprehensive low-speed experiment on a three-dimensional turbulent boundary layer is described and the results are presented in detail. The flow caused by an obstruction placed in a thick two-dimensional boundary layer is investigated at a free-stream velocity of 200 ft/s. The boundary-layer momentum-thickness Reynolds numbers are approximately 50 000.

The investigation is reported in two parts. This part is concerned with the area of the flow directly up-stream of the obstruction, which includes the axis of symmetry of the flow and extends down-stream as far as the saddle separation point and the adjacent boundary-layer separation lines. Part 2 is concerned with the flow to one side of the obstruction and the main characteristic of this region is that it contains a free-stream inflexion.

Referring to the area of the flow investigated in this part, it is shown that polar plots of the velocity vector through the boundary layer are well represented by Johnston's triangular model. The extension of the law of the wall to three dimensions is discussed. Simple extensions to three dimensions of existing methods of representing two-dimensional profiles, using Cole's wake function and Thompson's weighting function, are shown not to fit the data.

*Part 1 replaces R.A.E. Technical Report 69 041—A.R.C. 31 362.
Part 2 replaces R.A.E. Technical Report 69 137—A.R.C. 31 721.

LIST OF CONTENTS

1. *Introduction.*

The development of three-dimensional turbulent boundary layers is of considerable interest since, in practice, the majority of boundary layers are of this type. The particular aspects of the flow which are of most interest at low speeds are probably the occurrence of three-dimensional separation, which for example causes the stalling of lifting bodies; the skin friction field, from which the overall skin-friction drag can be determined, and the effective displacement thickness which will be required to predict the pressure field about three-dimensional bodies. These requirements necessitate calculating the development of a three-dimensional boundary layer in a given pressure field up to separation and ideally beyond separation to cover the complete surface. However many flow configurations which include a significant region of separated flow will be deemed unsatisfactory and an alternative configuration sought. The immediate aims of low-speed three-dimensional turbulent boundary layer research are thus taken to be the prediction of separation, skin friction and effective displacement thickness by a calculation method capable of predicting the boundary layer development up to and including separation.

The work reported here is concerned solely with a turbulent three-dimensional boundary layer and the problems of the initial laminar and subsequent transitional flows are not considered.

As with turbulent two-dimensional boundary-layers no theoretical solution to the development of turbulent three-dimensional boundary layers can be expected in the foreseeable future. Consequently a mixture of theory and empiricism will have to suffice.

The theoretical contribution is generally obtained from the time averaged forms of the continuity equation and the three-dimensional Navier-Stokes equations. After making suitable assumptions about the magnitude of the various terms in the three Navier-Stokes equations, two equations[1] are obtained which are applicable to the three-dimensional boundary layer flow over a plane surface. These are normally referred to as the boundary-layer equations though there are boundary-layer configurations to which they do not apply such as when the surface has significant curvature, when the flow is along a corner and quite possibly in the vicinity of separation from a plane surface.

The boundary layer equations cannot be solved analytically on account of the turbulent shear stress terms. The general method of obtaining a solution with the assistance of empirical results is to integrate a form of these equations over the total boundary-layer thickness and so produce equations which are less dependent upon the shear stress. The simplest forms of such equations are the momentum equations which only involve the value of the shear stress at the wall. The so called energy equations, derived in the same way, require more detailed information about the shear stress distribution across the boundary layer. A result of these integrations is to increase the number of dependent variables so that the equations can only be solved if sufficient auxiliary equations are formed. It is the choice of these auxiliary equations which characterise most of the calculation methods published[2] for two-dimensional boundary layers*. To extend these methods to three dimensions further equations have to be introduced and an improved understanding of three-dimensional flows is needed if these equations are to be reliable.

Previous low speed experimental work on three-dimensional turbulent boundary layers (reviewed in Ref. 4) has consisted of making measurements of selected profiles. Such measurements can provide useful information about the nature of three-dimensional profiles and, if accompanied by measurements of skin friction, may lead to a relationship between this important quantity and the characteristics of the profiles corresponding to the two-dimensional logarithmic-law. Such measurements cannot however give information about the development of the boundary layer. The terms of the momentum equations cannot be determined as these contain gradients of the profile integrals. If these terms could be measured, the relative importance of each term could be determined for a particular flow and the effectiveness of proposed auxiliary equations could be tested by using them in the momentum equations in place of some of the measured values and comparing the resultant computed development with the measured development. This is essentially the same procedure that is used to test two-dimensional calculation methods.

*A recent two-dimensional method[3] uses the momentum equation without integration in combination with the time averaged form of the turbulent energy equation along a mean streamline. This method solves the equations directly by the use of a computer but relies on auxiliary equations relating the time averages of various turbulent quantities.

Also it may be possible to deduce the shear-stress distribution from the momentum equations by, in effect, evaluating all the remaining terms in the equations experimentally. To obtain the required experimental data it is necessary to measure profiles and related information over an area of the surface. The selection of which profiles should be measured is somewhat arbitrary. Hall[5], working in a supersonic nozzle, followed free stream streamlines. This has the advantage that the integrated boundary-layer equations are normally written in streamline co-ordinates but requires the streamlines to be first measured and computed, and unless sufficient streamlines are followed the information obtained along the orthogonals is inadequate. An alternative is to measure the profiles on an arbitrary rectangular grid and to calculate the information along streamlines and their orthogonals subsequently by interpolation. However the equations are probably much easier to use in conjunction with experimental data if they are written in rectangular co-ordinates rather than curvilinear co-ordinates as the difficult curvature and axes-stretching quantities arising in the latter are avoided. The quantity of measurements that must be made is likely to be the same in both cases. In the work reported here a square grid of points was used.

The flow studied was formed by placing an obstruction in a thick two-dimensional boundary layer. The strong pressure gradients imposed by the obstruction, which is photographed in Fig. 1, caused the boundary layer to become three-dimensional and to separate. The flow is characterised by the rapid transformation of an essentially two-dimensional boundary layer into a three-dimensional layer by strong pressure gradients. Considerations of the magnitudes of the terms in the Navier Stokes equations, when applied to this type of flow, shows that in the outer region of the boundary layer the shear-stress terms become small compared with the inertial terms and the normal stress and normal pressure gradient terms are second order throughout the layer. Consequently the boundary-layer equations can be applied to this flow, except possibly very close to separation, although in the momentum integral equations the wall shear-stress terms will be small. Throughout the inner region of the flow the shear-stress terms are of first order showing that although this flow is dominated by the pressure gradient it does retain the essential characteristics of a viscous boundary layer. In interpreting the data presented and in using them to test calculation methods care should be exercised and account should be taken of the characteristics of the flow which are representative of three-dimensional boundary layers in strong pressure gradients.

The experiment was conducted in two parts and the regions of the flow examined in each part are shown in Fig. 2. The measurements were made in the three-dimensional boundary layer upstream of and including the three-dimensional separation at a constant freestream reference velocity of 200 ft/s throughout. As the data was primarily intended for use with integral calculation methods the time-mean velocity measurements were made using a three tube yaw probe which was chosen in preference to a hot wire arrangement because the former is more robust and easier to use and turbulence measurements were not required.

This Report is essentially a data report giving in full the data obtained and a description of the experimental details. An analysis of the profiles is also included and a comparison with existing profile representations made. The first part of the experiment, which is reported here, was made in the 13ft × 9ft low speed tunnel at R.A.E. Bedford during October to December 1966.

2. *Experimental Arrangement.*

2.1. *General Description.*

A photograph of the flow obstruction, the floor surface and those parts of the traverse gear which were exposed to the airflow is reproduced in Fig. 1. The leading part of the obstruction was semi-circular (Fig. 3). The diameter was made as large as whas thought possible without causing the resulting three-dimensional flow to be signifcantly affected by the tunnel fillets. The downstream part of the obstruction was a simple streamlined shape intended to inhibit additional flow separation and keep the flow as steady as possible. Oil flow on the surface of the obstruction showed that the flow was attached along its length.

The obstruction was mounted directly on to the tunnel floor and the bulk of the traverse gear was housed within it. The traverse gear could consequently be of massive construction, which is desirable for obtaining good positional accuracy, and only a single arm (Fig. 1) extended into the flow. A smooth false floor (Fig. 4) was laid over the tunnel floor which provided a uniform surface for the boundary layer to develop on. This arrangement also enabled the surface to be instrumented.

2.2. *Obstruction and Traverse Gear.*

The leading section of the obstruction was made of fibre-glass and the remainder of ply-wood. The dimensions are shown in Fig. 3. Part of the forward section of the obstruction was cut away to permit the traversing arm to move through an angle of approximately 105° in the horizontal plane and through a vertical displacement of about $7\frac{1}{4}$ in. A cylinder was mounted on the traverse gear which moved with the arm and sealed this opening at all times; a part of the cylinder is visible in Fig. 1. With the exception of the arm itself the shape of the flow obstruction was the same for all arm positions though the cut-out made the configuration slightly assymmetric about the centreline.

The traverse gear had four movements, each driven by a remotely controlled motor. Positions in the horizontal plane were obtained by rotating the arm (θ) and by moving the probe carriage along the arm (r). The arm could also be moved vertically to obtain the required displacement of the probe from the floor (y). Finally the probe was rotated about its tip by a mechanism mounted on the probe carriage (ϕ). The range, resolution and accuracy of these movements will be discussed in Section 3.2. The position of each movement was obtained from the output of a commutator transmitter and was displayed on a counter as well as being recorded on an electronic counter for read-out. The system used to control the traverse gear and obtain the data is shown schematically in Fig. 5. The control of the vertical and probe rotational movements were supplemented by feed-back loops. In the case of the vertical movement this was provided by an electronic relay connected between the traverse gear and the aluminium plate that formed the floor. When the probe touched the plate the relay stopped the vertical drive motor which, being fitted with a magnetic brake, stopped the probe in less than 0·010 in. This arrangement protected the probe against damage and the electronic relay could then be used to zero the vertical movement (*see* Section 3.2). A feed-back on the probe rotating mechanism was provided when the three-tube yaw-probe was fitted. The pressure difference between the two side tubes of the yaw probe was measured on a differential pressure transducer and the output fed into a potentiometric controller. If the out of balance signal exceeded a certain set value the controller operated the probe rotating motor so as to reduce the error. This constituted a simple nulling system which was useful in keeping the probe roughly aligned with the flow at all times. In this way the pressure difference applied to the transducer was kept small so the effects of hysteresis on the zero reading could be kept small. When taking measurements the probe was operated by hand and the transducer was used to determine the null position. The transducer used had a range of ± 8 in of water and was of variable inductance construction.

2.3. *False Floor.*

The obstruction was positioned on the tunnel centreline and surrounded by a smooth false floor (*see* Fig. 4). The false floor was 1·6in thick and 21ft 10in long extending 13ft 10in forward of the model. The leading and trailing edges were tapered down to the tunnel floor and oil flow showed that the flow over the leading edge ramp was attached. The false floor was made of ply-wood panels except for a 4ft × 3ft panel in the area where the measurements were made which was made of aluminium. The aluminium panel contained 220 magnets of 0·4in diameter each containing a static hole of 0·030in diameter. The static holes were arranged on a 2in × 2in grid and covered an area slightly larger than that covered by the traverse gear. The magnets and static tappings were used to measure the local skin friction stress by the Preston tube[6] and razor blade[7] techniques.

2.4. *Probes.*

Three types of interchangeable probes were used on the traverse gear. The yaw probe (Fig. 6) comprised a three tube yaw head constructed of tubes of 0·020in o/d with a static probe of 0·060in o/d positioned 5in from it. The method of using the probe is explained in Section 4.2. For the static pressure profile a probe consisting of a single 0·080in o/d static head was used. The Preston tube measurements were obtained from a probe carrying a single square-cut pitot-head of 0·080in o/d.

2.5. *Pressure Measurements.*

The pressure measurements were made with two specially constructed transducers. The transducers consisted of a single bellows which exerted an axial force proportional to the pressure difference across its surface. The force was measured by a strain-gauged arm. The advantage of these transducers was that they could be used with existing standard R.A.E. strain-gauge equipment to provide a digital read-out. The transducers had a range of about ± 40in of water and the calibrated accuracy was found to be determined entirely by the auxiliary electronic equipment. The auxiliary equipment had a full scale read-out of 1000 units and the sensitivity could be adjusted to cover any required pressure range.

2.6. *Data Recording.*

The data was recorded using the tunnel's standard read-out apparatus. The recording took the form of punched cards for subsequent analysis and a type-written copy for immediate use. Seven quantities were recorded comprising a data point number, the four positions of the probe and the two pressure transducer readings.

3. *Experimental Accuracy and Setting-up Procedures.*

3.1. *Introduction.*

As this is essentially a data report, the likely accuracy of the experimental results and possible sources of additional unmeasured errors are now considered. An overall determination of the accuracy of the results can only be obtained from an analysis of the data itself. The scatter of the individual quantities and the balance of the momentum integral equations will probably give the best indication of the extent to which the data may be trusted and the point to which refinement of analysis may reasonably be taken.

An estimate of the accuracy of the component parts of the experimental arrangement can be obtained from calibrations but aerodynamic effects such as arise from traverse gear interference or flow unsteadiness are more difficult to estimate. As the way in which the apparatus is used also effects the accuracy of the results, the setting-up procedures and checks used will be discussed in conjunction with the topic of accuracy.

3.2. *Probe Position.*

The estimated accuracy of the four movements of the traverse gear are tabulated below. The likely standard deviation (σ) of the error is listed so that 60 per cent of all measurements should be within $\pm\sigma$ and virtually all within $\pm 3\sigma$.

Quantity	Range	Resolution	Setting up σ	Measurement σ
r	14in to 30·8in	0·01in	0·005in	0·01in
θ	$-10°$ to $95°$	0·01°	0·01°	0·02°
y	0 to 7·25in	0·001in	0·001in	$y < 1$in, 0·001in $y > 1$in, 0·001 y
ϕ	$\pm 180°$	0·01°	0·02°	$q = q_0$, 0·03° $q = 0{\cdot}1 q_0$, 0·10°

The quantities r and θ were set up relative to the aluminium plate with zero tunnel flow and the figures given do not contain any estimate of the wind effect. The deflexion of the traverse gear and of the probe is small but the θ movement did have significant back-lash. This was partly overcome by a constant tension spring but in use the arm was always rotated onto a given position from the same direction so that it was driven against the back-lash spring and, in general, the wind forces. The y movement was zeroed using the electronic relay which proved very satisfactory. This was done for every profile with the wind on and a high accuracy can be expected for small values of y. The probe angle, ϕ, was set up aerodynamically. An arbitrary point in the flow was selected as having zero flow angle and was used as a datum. The point selected was $r = 30{\cdot}00$in, $\theta = 0$, $y = 7{\cdot}000$in. The calibration of ϕ showed a maximum non-linearity of 0·6° and back-lash of 0·35°. Consequently in use the probe was always aligned from the same direction and a calibration correction has been used in the computer programme which calculated the results given in this Report. With this procedure the calibrated error of the probe rotating mechanism is about 0·03°. An additional error will arise if the zero of the transducer used to balance the yaw probe is not repeatable. Frequent checks of the transducer suggest that in use its zero repeatability was equivalent to about 0·01° with the probe in a flow having the reference kinetic pressure q_0. This error is small compared with the mechanical error of 0·03°, since the combined error is equal to the square root of the sum of the squares of the individual errors, but if the probe is in a flow of 0·1 q_0 then the transducer error, equivalent to 0·1°, will predominate. Larger errors than these may occur in some areas due to flow unsteadiness.

3.3. *Probe Calibration and Pressure Measurement.*

The probes used were calibrated in the free stream of the empty tunnel. The static probe of the combined yaw and static probe was of non-standard proportions so as to minimise the effect of the thick stem downstream of it. The geometry of the probe needed to give a small correction was obtained experimentally and calibration showed that a correction of $-0{\cdot}0145\ q$ was required. The other probes required no correction.

The transducers used to measure the tunnel reference pressure and the probe pressure have been described in Section 2.5. Calibration of the transducers and their associated electronics showed that the accuracy was determined by the electronics and was equal to about 0·1 per cent of the full scale pressure which depended upon the sensitivity setting of the electronics. The sensitivity was selected so that the full scale corresponded to the local free stream kinetic pressure, q, and so the pressures recorded have an error σ of 0·001 q. A frequent check calibration procedure was used whereby the transducers were arranged to measure $P_s - P_w = 232{\cdot}0$ mm of water and $P_w - P_w = 0$ and the outputs corresponding to these two values were recorded and used in the computer programme. During the calibration readings the tunnel kinetic pressure was held accurately at 232·0 mm of water as measured by a Betz water manometer, but at other times the pressure was allowed to drift a little. The values obtained of the ratio of the local velocity to the local free stream velocity, $\mathbf{u}/U$, will have an error σ of about 0·0005. This error will be substantially increased in some areas of the flow because of unsteadiness. Also, in regions of very low velocity, particularly when accompanied by significant static pressure gradients in the y direction, the value of $\mathbf{u}/U$ will be much less accurate.

4. *Experimental Procedure.*

4.1. *Introduction.*

The main problem in an experiment of this type is in maintaining a constant standard of work throughout a long period of tunnel running. The apparatus described in Section 2 was designed with this in mind. Nevertheless, the average time taken to produce one complete traverse was about one hour and the total time taken to produce the data given in this Report was 230 hours. The main features of the experiment are now described but many preliminary and check observations that were made will not be specifically described but may be referred to in passing.

4.2. *Velocity Profiles.*

The principal part of the experiment was obtaining the velocity profiles. In the interests of establishing a routine and of easing subsequent computation all the profiles were obtained in exactly the same way. The positions of the profiles were decided in advance and were arranged on a one inch grid as shown in Fig. 7. The distances from the floor surface to the profile points (y) were also decided in advance. Over the inner part of the boundary layer the values of y were chosen to be a geometric series since, in general, the flow characteristics tend to be well conditioned functions of log y. The actual values used are given by

$$y = 0{\cdot}010(2)^{n/2} \text{ in},$$

for $0{\cdot}010 \leqq y \leqq 1{\cdot}280$ where n is an integer. This series of ordinates has the additional advantage that integrals with respect to y are easily computed since

$$\int f(y)\, dy = \int y f(y)\, d(\log y)$$

and the series gives equal steps of log y. Over the outer part of the boundary layer equal steps of half an inch were taken between 1·5in and 7·0in so as to give sufficient detail.

At the start of each profile an overall calibration of the transducers was recorded as described in Section 3.3. The yaw probe was zeroed onto the aluminium plate, using the electronic relay and the read-out was set to a value of half the probe height* (0·010in). The probe was rotated until a null on the yaw balancing transducer was obtained and a set of data recorded (*see* Section 2.6). The two pressures recorded were the probe pressure relative to P_w and the tunnel reference pressure $P_s - P_w$. Having repeated the procedure for all the values of y up to 7·000 in the potentiometer controller was switched off and the probe lowered to the $y = 3{\cdot}000$in position. This brought the separate static probe to $y = 7{\cdot}000$ in correctly aligned in yaw with the flow and enabled a measure of the static pressure to be obtained with which to calculate the velocity profiles (*see* Section 5). The pressure leads were then switched and the static pressure recorded on a card. Finally the transducers were calibrated again as at the beginning of the profile. After every second profile the probe was moved to the reference point ($r = 30$in, $\theta = 0$, $y = 7$in) and the zero of ϕ was checked and reset if necessary. If an adjustment of more than about 0·05° was required the tunnel was stopped and the zero of the balancing transducer was checked, otherwise this check was normally made every four profiles. 123 profiles were measured and these were followed by 10 repeat profiles. These repeat profiles were made when the original profile was thought to be in error and were not therefore a check on the normal repeatability of the technique. Doubt about a profile arose either as the result of the tunnel unsteadiness caused by the atmospheric wind or from irregularities in the plot of free stream angle ($y = 7{\cdot}000$in) and surface flow angle ($y = 0{\cdot}010$in) which were made during the experiment. In the data presented in the next Section seven of the repeat profiles are given in place of the originals. As an additional check the values of free stream angle ($y = 7{\cdot}000$in) were surveyed successively over the whole area.

4.3. *Extended Velocity Profiles.*

It is frequently assumed that the free stream outside a three-dimensional boundary layer on a flat plate is such that the conditions of the flow along traverses taken normal to the flat surface are constant. This is a convenient and, no doubt, reasonable assumption, but in practice it is not, and cannot be, strictly accurate. An immediate difficulty that arises from the variation of conditions in the free stream is that of defining the free stream direction and this will be discussed further in Section 5. To obtain a measure of the extent of the three-dimensionality of the free stream, profiles were extended up to 11·5in. This was done on a 2in × 2in grid using 31 profiles. Only the yaw angle and total head were measured and this was achieved by sliding the probe up about $4\frac{1}{2}$ inches in its holder so as to extend the effective range of the traverse gear.

---

*No displacement effect has been applied to the y co-ordinate. Preliminary tests with identical probes constructed of tubes of 0·028, 0·020 and 0·012in outside diameter were unable to isolate the displacement. It is expected to be of order 0·004in but may not be the same for total head as for yaw balance. This would complicate any correction considerably.

4.4. *Static Profiles.*

The normal assumptions made in deriving the boundary layer equations yield the result that the static pressure through the boundary layer is constant*. This approximation is generally valid in three-dimensional boundary layer flow but cannot be taken for granted particularly in the vicinity of separation. To obtain direct information about the validity of this approximation in the present flow static profiles were measured. This was done on the same 2in × 2in grid as was used for the extended profiles (Section 4.3). A separate 0·080in diameter static probe was traversed through the boundary layer and was positioned so that its static holes were centred on the axis of the traverse. The probe was aligned with the flow in yaw by setting it to the angle obtained from the velocity profiles corresponding to the position of its geometric centre. The probe could not be aligned with the flow in pitch but, as the maximum pitch angle of the unseparated part of the flow will be of order one degree, errors due to this misalignment should be very small.

4.5. *Preston Tube and Razor Blade Measurements.*

Various methods are available for measuring the skin friction but none has the clear advantage of definitely yielding the correct results. The direct measuring floating element method has the disadvantage of being affected by the pressure gradients by an amount that cannot be estimated accurately. It also measures the vector average over a comparatively large area which must reduce its accuracy. Even so, it would be worth using if the necessary equipment and instrumentation were available. The necessary equipment was not available and the task of surveying an area of the surface in this way was considered too formidable to attempt at present. Of the indirect methods Preston tubes, razor blades and hot films are all possibilities. As the necessary apparatus for using hot films was not available the use of both Preston tubes[6] and razor blades[7] was thought adequate. A further method of obtaining the skin friction is due to Clauser[9] and involves plotting the velocity profiles on particular log-linear axes. This method is very useful in two-dimensional flows and its extension to three-dimensional flows is discussed in Section 6.2.

Preston tube and razor blade measurements were made on the same 2in × 2in grid as used for the extended profiles (Section 4.3) with one additional row of points. At these grid points static pressure tappings and flush mounted magnets had been set in the aluminium ground plate. A 0·080in diameter Preston tube was attached to the traverse gear and set on the surface at the angle previously obtained from the velocity profiles at $y = 0{\cdot}010$in. The same pressure transducer and read-out was used as for the velocity profiles. The razor blades, which were only 0·0050in high were set to the same surface flow angle by hand. Because the boundary layer was so thick the skin friction was low and the pressure differences recorded by the razor blades were very small (typically $0{\cdot}02\,q_0$). As this small pressure difference was obtained from two measurements of pressure, made at different times, one with the blade in position and other with it removed, a single Betz manometer was used to improve accuracy. Even so this method makes extreme demands on the repeatability of tunnel conditions and so the results from the razor blades may be significantly less repeatable than those from the Preston tube.

5. *Experimental Results.*

The experimental data are given in Tables 1 to 5 and are deduced directly from the measurements with no smoothing applied. In Table 1 the displacement and momentum integrals are given together with the free stream direction and static pressure. The two measured values of skin friction are listed in Table 2 and the detailed velocity profiles are given in Table 3. Throughout this Report the individual profiles are

---

*According to Rotta[8]

$$C_p + 2\left(\frac{\bar{v}^2}{U^2}\right) = \text{constant}.$$

On the surface $\bar{v}^2/U^2$ is zero and is negligible in the free stream. A typical maximum value of $\sqrt{\bar{v}^2}/U$ is 0·05 so that C_p may be expected to be reduced by about 0·005 within the boundary layer.

referred to by a number obtained by combining the Z and X co-ordinates. Thus the profile at $Z = 6$in, $X = 24$in is number 624, that at $Z = -2$in, $X = 30$in is -230 and at $Z = 0$, $X = 22$in is 22. For clarity the profile co-ordinates are listed in Table 3 together with the profile numbers. In Table 3 the velocity is the apparent velocity obtained by assuming that the static pressure through the boundary layer is constant and equal to the values measured at $y = 7{\cdot}000$in which is given in Table 1. For a few profiles, close to the saddle separation point, the measured total head was less than the free stream static pressure and in these cases the velocity has been printed as zero. This results from static gradients normal to the surface and very low velocities, and, in the case of profile 21, from reversed flow. As the integrals in Table 1 were obtained using the values given in Table 3, the data for these few profiles may be in significant error. The data obtained from the measurements of static pressure across the boundary layer are listed in Table 4 and in general the static gradients are small. The values of pressure coefficient given for $y = 0$ were obtained from the surface static tapping and are in quite close agreement with the probe data. The difference increases to about 0·01 near separation and is probably due to differing effects of turbulence on the static tapping and static probe and to the gradient in the y direction of flow direction which will cause the static probe to register a low pressure. There is a fairly constant difference of about 0·005 between the values obtained at $y = 7{\cdot}000$in from the separate static probe and from combined yaw and static probe. This is probably due to traverse gear interference though differing characteristics of the static probes in curved flows may also contribute. The effect of this possible error on the velocity profiles will be small and should not exceed 0·015 for the lowest values of $\mathbf{u}/U$ and will be negligible over most of the boundary layer. The cross flow angles measured on the extended profiles are given in Table 5 and in all cases the total pressure was constant and equal to the tunnel total pressure.

In two-dimensional boundary layers the edge of the boundary layer is normally defined experimentally by

$$y = \delta \quad \text{at} \quad u/U = 0{\cdot}995\,.$$

The same definition has been used in presenting the data and the free stream flow direction (α) has been taken as the flow direction at $y = \delta$, though the three-dimensionality of the free stream makes this definition rather arbitrary. In addition α was measured relative to the flow direction at $X = 30{\cdot}00$in, $y = 7{\cdot}000$in and $Z = 0$ which is also arbitrary. A set of values of α which have been smoothed and corrected are given in Table 6. The values of α given in Table 1 were first smoothed by an iterative two-dimensional process. The true undisturbed flow direction was then estimated by assuming that it occurs at the upstream end of the data where the transverse velocity integral (δ_2) is zero. This is shown in Fig. 8 to occur at $Z = 0{\cdot}4$in. A plot of this corrected value of α, (α^*), against Z is shown in Fig. 9. It is suggested that the point $X = 30{\cdot}00$, $Z = 0{\cdot}40$in would be a suitable origin for a free stream streamline co-ordinate system.

Also shown in Fig. 9 are curves obtained from the two-dimensional potential flow around a cylinder with the same section as the obstruction. The flow field was obtained by representing the body by a distribution of source elements and the strength of these elements was determined by satisfying the solid boundary condition[10]. The tunnel walls were represented by computing the flow through an infinite cascade of bodies. The computation was made both for an infinite flow and for tunnel walls at 13ft spacing. The latter case is shown in Fig. 9 though the difference between the two calculated results is much less than between the calculated results and the experimental results shown in Fig. 9. These differences are attributed to the three-dimensionality of the free stream arising from the tunnel fillets, which at floor level are only 9ft 9in apart, the limited height of the obstruction, which did not span the tunnel, and the variations of the floor displacement thickness. The points obtained at $y = 11{\cdot}5$in (Fig. 9) are seen to be slightly closer to the potential solution near the axes of symmetry ($|Z| \simeq 2$in). Further information on the comparison between the computed and measured free stream will be given in Part 2.

The region of the flow investigated in this Report is illustrated in Fig. 7 together with the positions of each profile. Using the measured flow directions free-hand streamlines have been drawn which give approximately the surface flow and free-stream streamline patterns. The surface flow pattern is in close visual agreement with the oil flow pattern in Fig. 10. The area of the test will be seen to include the axis of symmetry of the flow and also the three-dimensional separation line.

6. *Profile Analysis.*

6.1. *Polar Plot.*

The polar plot of the velocity vector is a useful representation of the three-dimensional profile. The importance of this plot is that on it many profiles have been found to take the form of a triangle[11] (Fig. 11). The cross flow can then be represented by the equations

$$\frac{w}{U} = \frac{u}{U} \tan \beta_0 \tag{1}$$

in Region I and,

$$\frac{w}{U} = A\left(1 - \frac{u}{U}\right) \tag{2}$$

in Region II. In relation to the y co-ordinate this plot entails a large distortion since about 99 per cent of the boundary layer thickness can be in Region II. For the purposes of relating the momentum integrals it may be sufficient to assume that Region II extends over the whole boundary layer, then

$$\left.\begin{aligned} &\theta_{12} = A\,(H-1)\,\theta_{11}\,, \quad \theta_{21} = -A\,\theta_{11}\,, \quad \theta_{22} = -A^2\,(H-1)\,\theta_{11} \\ &\text{and} \\ &\delta_2 = -A\,H\,\theta_{11} \\ &\text{where} \quad H = \delta_1/\theta_{11}\,. \end{aligned}\right\} \tag{3}$$

Agreement with this simple model has been found in several flows[11,12] in which the lateral pressure gradient is monotonic. The present pressure field is of the type and the data fit this representation well. A selection of profiles is shown in Fig. 12.

It has been shown[11] by inviscid theory that if the free stream is two-dimensional

$$\underset{u \to U}{Lt}\ (A) = 2U^2 \int_0^{\alpha} U^{-2}\, d\alpha \tag{4}$$

and if the streamwise pressure gradient is zero

$$\underset{u \to U}{Lt}\ (A) = 2\alpha\,. \tag{5}$$

A minus sign has been omitted from both equations (4) and (5) because the sign of α given in this Report has been defined so as to be positive when Z is positive. This is opposite to the sign convention used in the theory of Ref. 11.

These relationships only apply in the limit and the polar plot in Region II should in general be curved. The empirical observation that in many cases the whole Region II approximates to a straight line on the polar plot suggests that equations (4) and (5) may be used in equation (2). Lines corresponding to $A = 2\alpha^*$ are shown in Fig. 12 and are in good agreement with the data particularly as u/U approaches unity.

If the relationships in (3) are accepted then a variety of additional methods of determining A from the data is available. The simplest form appears to be $A = -\delta_2/\delta_1$ and in Fig. 13 this function is plotted against α^* for all the data except the profiles on $Z = 0$. There is clearly a strong correlation between the functions though, as expected from the polar plots, in general $-\delta_2/\delta_1 > 2\alpha^*$. Using equation (4) in place of equation (5) would make the correlation worse. The three-dimensionality of the free stream could contribute to this discrepancy particularly near the axis of symmetry.

Johnston used the triangular model to relate the surface flow direction (β_0) to A and the component of skin friction in the local free stream direction (C_{fx}). To do this he assumed that Region I corresponded to the laminar sub-layer so that $\mathbf{u}/U = y\,u_\tau/\nu$. By assuming in addition that the apex of the triangle corresponds to a particular value of $y\,u_\tau/\nu$ he obtained the relationship

$$\frac{\tan\beta_0}{A} = 0{\cdot}1\left[\frac{(1+\tan^2\beta_0)^{\frac{1}{4}}}{\sqrt{C_{fx}}}\right]-1\,. \tag{6}$$

The assumption that the apex of the triangle corresponds to a constant value of $y\,u_\tau/\nu$ has been disputed[12]. In practice it is difficult to measure the correct value of $y\,u_\tau/\nu$ since it is first necessary to determine the position of the apex of the polar plot and then to infer by some criterion the corresponding value of $y\,u_\tau/\nu$. Considering that successive points of Fig. 12 represent 41 per cent increases of $y\,u_\tau/\nu$ this is a very inaccurate process. If however the triangular form of the polar plot is accepted it is sufficient to postulate that the apex is given by

$$(\mathbf{u}/U)_{\text{apex}} = K\,u_\tau/U \tag{7}$$

where K is the same constant as Johnston[11] used. By applying the sine rule to the triangular model in Fig. 11,

$$\sin(\beta_0+\gamma) = (K\,u_\tau/U)^{-1}\sin\gamma$$

hence

$$\beta_0 = \sin^{-1}\{(K\,u_\tau/U)^{-1}\sin\gamma\}-\gamma\,. \tag{8}$$

Equations (6) and (8) are congruent. The experimental data are compared with equation (8) in Fig. 14 using $\gamma = \tan^{-1}2\alpha^*$ and u_τ/U given by the Preston tube. Putting $\gamma = \tan^{-1}2\alpha^*$ will in general imply a different fit of the triangular model to the data from that obtained graphically, as shown in Fig. 12. Promising agreement is obtained with a value of K of 14 but the scatter includes a definite trend. This is particularly so when additional data to be given in Part 2 are added. However this trend can be reduced by non-dimensionalising u_τ with regard to U_0 rather than U. Equation (8) then becomes

$$\beta_0 = \sin^{-1}\{(K\,u_\tau/U_0)^{-1}\sin\gamma\}-\gamma\,, \tag{9}$$

which is no longer related to the triangular model on the polar plot. The data are compared with equation (9) in Fig. 15. A value of K of 17·5 is used and the experimental values of β_0 are linear extrapolations through $y = 0{\cdot}014$in and $y = 0{\cdot}028$in. The agreement is considered satisfactory for all the data and the systematic trend is reduced. Two profiles (620 and 820) do not yield real solutions to equation (9), which implies that the measured values of α^* and u_τ/U_0 are such that the polar triangle does not meet up. The limiting form, when $\gamma+\beta_0 = 90°$, gives values of β_0 for these profiles of 70° and 67° which compare reasonably with the measured values of 74° and 62°.

U_0 is a constant for all the data so that the correct method of non-dimensionalising u_τ in equation (9) is now in doubt. Many alternative forms could be written down but further data will be required before the optimum non-dimensional form can be decided. However the agreement obtained in Figs. 14 and 15 suggest that equations (8) and (9) may be useful, particularly in monotonic flows.

6.2. *Logarithmic Plot.*

The plot of u/u_τ against $\log (y\, u_\tau/\nu)$ has proved very useful in the analysis of two-dimensional boundary layers in moderate pressure gradients. In the inner 10 per cent or so of the boundary layer this representation of the profile gives a unique curve. For values of $(y\, u_\tau/\nu) \geqq 30$ the curve is straight and is given by the equation of the 'logarithmic law', which is

$$u/u_\tau = A \log (y\, u_\tau/\nu) + B\,. \tag{10}$$

Clauser[9] wrote this equation as,

$$u/U = (u_\tau/U)\,\{A \log (y\, U/\nu) + A \log (u_\tau/U) + B\}$$

which enables straight lines of constant u_τ/U to be drawn on a plot of u/U against $\log (y\, U/\nu)$. This plot provides a quick way of deducing the value of u_τ/U from a given velocity profile.

Some examples of the present data are shown in Fig. 16 plotted as $\mathbf{u}/U$ against $\log_{10} (y\, U/\nu)$. Lines are also shown corresponding to the values of u_τ/U obtained from the Preston tube and razor blades. In Fig. 16 a displacement correction of +0·004in has been applied to y. Profiles 30 and 26 are almost collateral though the adverse pressure gradients are severe. The curves agree at their lower ends with the razor blade lines and a limited logarithmic region is present in Profile 30. The remaining profiles in Fig. 16 are three-dimensional to varying extents. In addition to $\mathbf{u}/U$, w/U is plotted and also u/U, where it differs significantly from $\mathbf{u}/U$. As might be expected there is general agreement between the $\mathbf{u}/U$ profiles and the positions of the straight lines corresponding to the values of u_τ/U obtained from the Preston tube and razor blades. There is, however, a tendency for the profiles to be curved such that in the region of $\log_{10} (y\, U/\nu)$ equals 4·0 to 4·5 they drop below the Clauser line which fits the points at $\log_{10} (y\, U/\nu)$ equals 3·0 to 3·5. This is particularly clear in Fig. 16 Profile 820. Joubert and Perry[13] found the same curved form and proposed an alternative plot. They observed that s/U given by

$$s/U = U^{-1} \int_0^u \left(1 + \left(\frac{dw}{du} \right)^2 \right)^{\frac{1}{2}} du\,,$$

produced a more nearly linear region and by extending mixing-length theory to three dimensions deduced the general form that s/U should take. The function s/U, which is the length of the curve on the polar plot, is plotted on Fig. 16 and will be seen to be a little closer to the logarithmic law though in Profiles 824 and 820, in particular, it is continuously curved. Joubert and Perry did not obtain very satisfactory agreement between the experimental form of s/U and the form deduced by mixing-length theory, and a few exploratory calculations on the present data were also unsatisfactory.

Another method that is sometimes adopted is to deduce the skin friction from the u/U profile as if it is two-dimensional and to call the value of the skin-friction velocity obtained $u_{\tau x}$. This method is used because the u/U profile generally exhibits a linear region, as shown in Fig. 16 (e.g. Profile 820 is linear from $\log_{10} (y\, U/\nu)$ equals 3·0 to 4·0), but it does not follow that the correct value of skin friction is deduced. Johnston[14] has proposed an improved method of deducing the skin-friction velocity from the observed linear region and this method is now considered in detail.

The law of the wall in two dimensions states that u/u_τ is a unique function of $(y\, u_\tau/\nu)$. Thus,

$$u/u_\tau = f\,(y\, u_\tau/\nu)\,. \tag{11}$$

In three dimensions equation (11) may be expected to be true in the limit as y tends to zero. In this limit equation (11) becomes,

$$\mathbf{u}/u_\tau = f\,(y\, u_\tau/\nu)\,, \tag{12}$$

and also

$$\mathbf{u} = u \sec \beta_0 .$$

Hence,

$$u \sec \beta_0 / u_\tau = f\,(y\, u_\tau / \nu) \qquad \text{as} \qquad y \to 0 . \tag{13}$$

For any particular profile ($\sec \beta_0 / u_\tau$) is a constant. The left hand side of equation (13), $u \sec \beta_0/u_\tau$, is therefore proportional to u/U which, as mentioned above, has been found experimentally to exhibit a logarithmic region. It is proposed, therefore, that equation (13) be applied throughout the normal law of the wall region. In the logarithmic region equation (13) then becomes

$$u \sec \beta_0 / u_\tau = A \log (y\, u_\tau / \nu) + B \tag{14}$$

where A and B are the log-law constants for two-dimensional boundary layers. To obtain the Clauser plot, equation (14) is written as

$$u \sec \beta_0 / U = (u_\tau / U) \{A \log (y\, U/\nu) + A \log (u_\tau / U) + B\} . \tag{15}$$

Thus a plot of ($u \sec \beta_0/U$) against $\log (y\, U/\nu)$ should enable the skin-friction velocity (u_τ/U) to be deduced. This plot is also shown in Fig. 16 wherever ($u \sec \beta_0/U$) differs significantly from $\mathbf{u}/U$. Linear regions are produced which generally follow log-law lines and the form of the ($u \sec \beta_0/U$) profiles are similar to the $\mathbf{u}/U$ profiles on the centreline (e.g. Profile 424 is in a strong adverse pressure gradient and the ($u \sec \beta_0/U$) profile is similar to the centreline Profile 26 which is also in a strong adverse pressure gradient). This similarity suggests that the effects of pressure gradients are significant and that in a more moderate pressure field the ($u \sec \beta_0/U$) profiles will have longer log-law regions.

On the present evidence the above method of plotting ($u \sec \beta_0/U$) on a conventional two-dimensional Clauser plot appears to give the correct value of u_τ/U providing the pressure gradients are not too severe. This conclusion implies that a direct plot of u/U will give neither u_τ/U nor $u_{\tau x}/U$. However, for small cross flows, when $\sqrt{\sec \beta_0} \simeq 1$, a plot of u/U will be sufficiently accurate to give the value of $u_{\tau x}/U$.

It is tempting at this stage to regard the whole of the ($u \sec \beta_0/U$) profile as a two-dimensional equivalent of the real three-dimensional profile. If this is done, existing skin-friction laws can be applied to the equivalent profile and the skin-friction obtained. Any skin-friction law can be used providing the actual pressure gradient comes within its range of application. A simple table of equivalent quantities can be drawn up as follows

Two-dimensional quantity	Equivalent three-dimensional quantity
θ	θ_{11}
H	H
R_θ	$R_{\theta_{11}} \sec \beta_0$
C_f	$C_f \cos^2 \beta_0$

The present data do not provide a good test of this concept because the pressure gradients are such that no known skin-friction law would be applicable even if the flow were two-dimensional. A tentative comparison is shown in Fig. 17. A skin-friction relationship due to Green[15] has been modified to take account of the severe adverse pressure gradients by making it give approximate agreement with the data along the centreline. This modified relationship has then been applied in the manner suggested above to the three-dimensional data and the results are shown in Fig. 17. The comparison is inevitably inconclusive but it is suggested that this method of extending two-dimensional skin-friction laws to three-dimensional flows may be effective in more moderate flows.

6.3. *Mager's cross-flow profile.*

Mager[16] proposed that the cross flow could be related to the streamwise profile by the equation

$$w/u = (1-y/\delta)^2 \tan \beta_0 . \tag{16}$$

This equation is a particular form of Prandtl's[17] more general suggestion that

$$w/u = g\,(y/\delta) \tan \beta_0 \tag{17}$$

and was obtained from the data of Gruschwitz[18]. Mager demonstrated that equation (16) does not represent the data of Burgess[19] well and Fig. 18 shows that it does not represent the present data. If the bottom 10 per cent of the boundary layer is ignored then equation (16) becomes a tolerable representation and part of the inadequacies of equation (16) can probably be attributed to a lack of reliable data in the inner region in old data. It is possible that another polynomial form of $g(y/\delta)$ in equation (17) may give better overall results but it seems likely that the form of equation (17) is too simple and restrictive to represent quickly changing flows of this type.

6.4. *Coles's and Thompson's profiles.*

The two most successful profile representations in two-dimensional flows are due to Coles[20] and Sarnecki[21]. Sarnecki's method has been developed further by Thompson[22]. The methods are similar in that they use as a basis the well established logarithmic law and extrapolate it to the edge of the boundary layer. Coles then adds a function of y/δ of fixed shape and correct magnitude to satisfy the end condition $u = U$ at $y = \delta$: this function is generally called the wake function. Coles's representation does not satisfy the condition $du/dy = 0$ at $y = \delta$. Sarnecki and Thompson overcame this limitation by compounding the velocity from a proportion of the velocity given by the logarithmic law and the remainder of free stream velocity. The proportions vary through the boundary layer according to a weighting function. This representation satisfies both the end conditions $u = U$ and $du/dy = 0$ at $y = \delta$.

Coles suggested that his representation could be extended to three dimensions by treating the two component parts as vectors and taking the logarithmic-law vector in the direction of the surface shear stress. The magnitude and direction of the wake function is then given by the free stream condition. It follows that the profile of the velocity component normal to the surface shear stress should have the form of the wake function. Hornung and Joubert[12] have shown that this is not true for their data and Fig. 19 shows that it is also not true for the present data. A similar procedure might be followed for extending Thompson's profiles to three dimensions. The three-dimensional profile could be constructed by taking the vector sum of the logarithmic-law vector and the free stream vector in the proportions given by the weighting function. If this is done the profile of the velocity component normal to the surface shear stress vector will have the form of the weighting function. As the wake function and one minus the weighting function are closely similar both are shown in Fig. 19 by the same curve and so this extension of Thompson's profiles is not confirmed experimentally.

Both Coles's and Thompson's profiles are based upon data obtained in slowly changing two-dimensional boundary layers and it is probable therefore that the proposed extensions to three dimensions would be more successful if they were applied to slowly changing three-dimensional flows than they are shown to be for the present rapidly changing flow.

7. *Conclusions.*

Extensive information is given of a turbulent three-dimensional boundary layer produced by an obstruction placed in a two-dimensional boundary layer flow. The area of the flow studied is directly upstream of the obstruction and extends downstream as far as the boundary layer separation line. The flow is dominated by the large pressure gradients produced by the obstruction and the influence of the shear stress is mainly restricted to the region of the flow close to the surface. Also, in the region of the separation line, the normal boundary layer approximations are invalidated by significant pressure gradients through the layer.

The analysis presented in this Report suggests that the experimental data have been obtained with an acceptable accuracy and the data, which were obtained primarily for improving integral calculation methods, have been compared with several existing theories of two- and three-dimensional boundary layers.

The velocity profiles are shown to be in good agreement with Johnston's triangular model. A relationship between the magnitude and direction of the skin-friction vector and the local free stream conditions is proposed and verified experimentally. This relationship, like the triangular model, is probably valid in flows with monotonic transverse pressure gradients. The use of the logarithmic plot in three dimensions is discussed and methods of deducing the magnitude of the skin-friction vector considered. The effects of pressure gradients on the log-law are shown to be significant both on the axis of symmetry of the flow and elsewhere.

Mager's cross-flow profile is shown not to fit the present data and simple extensions to three dimensions of existing methods of representing two-dimensional profiles, using Coles's wake function and Thompson's weighting function, are also shown not to fit the data. The failure of these methods is attributed, at least in part, to the severity of the pressure gradients present in the flow studied.

LIST OF SYMBOLS

A	Defined by equation (2). Also used as a constant in equation (10)
B	Constant in equation (10)
C_f	Skin-friction coefficient based on local free stream kinetic pressure
C_{fx}	Component of C_f in $\mathbf{U}$ direction
C_p	Static-pressure coefficient
H	$H = \delta_1/\theta_{11}$
K	Constant (*see* equation (7))
P_s	Settling chamber reference pressure
P_w	Working section reference pressure
q	Kinetic pressure
q_0	Working section reference kinetic pressure
R_θ	Momentum thickness Reynolds number
r	Radial position of probe
s	Arc length measured along polar plot of profile $s = \int_0^u \left(1+\left(\frac{dw}{du}\right)^2\right)^{\frac{1}{2}} du$ (*see* Section 6.2)
U	Free stream velocity
U_0	Working section reference velocity
$\mathbf{u}$	Local velocity vector within boundary layer
u	Component of $\mathbf{u}$ parallel to $\mathbf{U}$
u_τ	Skin friction velocity defined by $u_\tau = \sqrt{\tau/\rho}$
$u_{\tau x}$	Component of u_τ parallel to $\mathbf{U}$, equal to $u_\tau \cos^{\frac{1}{2}} \beta_0$
w	Component of $\mathbf{u}$ normal to $\mathbf{U}$
X	Cartesian co-ordinate (*see* Fig. 3)
y	Displacement of probe centre from surface
Z	Cartesian co-ordinate (*see* Fig. 3)
α	Angular displacement of free stream
β	Boundary layer cross flow angle. The angle between $\mathbf{u}$ and $\mathbf{U}$
β_0	Value of β in the limit as y tends to zero
γ	$\gamma = \tan^{-1} A$ (*see* Fig. 11)
δ	Boundary layer thickness $y = \delta$ at $\mathbf{u}/U = 0{\cdot}995$

δ_1	$\int_0^\delta \left(1-\frac{u}{U}\right) dy$
δ_2	$-\int_0^\delta \frac{w}{U} dy$
θ	Traverse gear arm angular position
θ_{11}	$\int_0^\delta \left(1-\frac{u}{U}\right)\frac{u}{U} dy$
θ_{12}	$\int_0^\delta \left(1-\frac{u}{U}\right)\frac{w}{U} dy$
θ_{21}	$-\int_0^\delta \frac{uw}{U^2} dy$
θ_{22}	$-\int_0^\delta \frac{w^2}{U^2} dy$
ν	Kinematic viscosity of fluid
ρ	Density of fluid
τ	Skin friction
ϕ	Angular position of probe measured relative to traverse gear arm

REFERENCES

No.	Author(s)	Title, etc.
1	J. C. Cooke and M. G. Hall ..	Boundary layers in three dimensions. *Progress in Aeronautical Sciences*, Vol. 2 (1962).
2	B. G. J. Thompson	A critical review of existing methods of calculating the turbulent boundary layer. A.R.C. R. & M. 3447 (1964).
3	P. Bradshaw, D. H. Ferriss and W. P. Atwell	Calculation of boundary layer development using the turbulent energy equation. *J. Fluid Mech.* 28 (1967).
4	G. P. Francis and N. A. Cumpsty	Three-dimensional turbulent boundary layers in incompressible flow. Lockheed-Georgia Research ER-8144 (1965).
5	M. G. Hall and H. B. Dickens	Measurements in a three-dimensional turbulent boundary layer in supersonic flow. A.R.C. R. & M. 3537 (1966).
6	V. C. Patel	Calibration of the Preston tube and limitations on its use in pressure gradients. *J. Fluid Mech.* 23 (1965).
7	L. F. East	Measurement of skin friction at low subsonic speeds by the razor-blade technique. A.R.C. R. & M. 3525 (1966).
8	J. C. Rotta	Turbulent boundary layers in incompressible flow. *Progress in Aeronautical Sciences*, Vol. 2 (1962).
9	F. H. Clauser	Turbulent boundary layers in adverse pressure gradients. *J. Aeronaut. Sci.*, 21, No. 2 (1954).
10	A. M. O. Smith and J. L. Hess	Calculations of potential flow about arbitrary bodies. *Progress in Aeronautical Sciences*, Vol. 8 (1966).
11	J. P. Johnston	On the three-dimensional turbulent boundary layer generated by secondary flow. *Journal of Basic Engineering*, Trans. ASME Series D, 82 (1960).
12	H. G. Hornung and P. N. Joubert	The mean velocity profile in three-dimensional turbulent layers. *J. Fluid Mech.* 15 (1963).
13	N. E. Perry and P. N. Joubert	A three-dimensional turbulent boundary layer. *J. Fluid Mech.* 22 (1965).
14	J. P. Johnston	Three-dimensional turbulent boundary layer. M.I.T. Gas Turbine Lab. Rep. 39 (1957).

No.	*Author(s)*	*Title, etc.*
15	J. F. Green	R.A.E. (unpublished).
16	A. Mager	Generalization of boundary layer momentum-integral equations to three-dimensional flow, including those of rotating systems. NACA Report 1067 (1952).
17	L. Prandtl	On boundary layers in three-dimensional flow. Reps. and Trans. 64, British NAP (1946).
18	E. Gruschwitz	Turbulent reibunsschichten mit Seckundasstromung. *Ingenierer-Archin*, Vol. 4 (1935).
19	S. M. Burgess	Some considerations on the development of boundary layers in the case of flows having a rotational component. *Nederl, Akad van Wetenschappen*, 44, Nos. 1–5 (1941).
20	D. Coles	The law of the wake in the turbulent boundary layer. *J. Fluid Mech.* 1 (1956).
21	A. J. Sarnecki	Ph.D. Dissertation. Cambridge University (1959).
22	B. G. J. Thompson	A new two-parameter family of mean velocity profiles for incompressible turbulent boundary layers on smooth walls. A.R.C. R. & M. 3463 (1967).

TABLE 1

Boundary Layer Displacement and Momentum Thicknesses.

Profile No.	Z	X	α	Cp	δ	δ_1	δ_2	θ_{11}	θ_{12}	θ_{22}	H
	inches	inches	degrees		inches	inches	inches	inches	inches	inches	
-230	-2	30	-1.06	0.294	5.22	0.8670	0.0404	0.6158	-0.0112	-0.0005	1.4080
-229	-2	29	-1.21	0.310	5.32	0.9167	0.0441	0.6414	-0.0131	-0.0006	1.4291
-228	-2	28	-1.32	0.328	5.34	0.9420	0.0533	0.6509	-0.0161	-0.0009	1.4473
-227	-2	27	-1.52	0.348	5.41	0.9828	0.0639	0.6692	-0.0201	-0.0013	1.4686
-226	-2	26	-1.70	0.366	5.43	1.0340	0.0730	0.6887	-0.0246	-0.0018	1.5014
-225	-2	25	-2.08	0.388	5.49	1.1006	0.0941	0.7140	-0.0335	-0.0029	1.5416
-224	-2	24	-2.37	0.411	5.54	1.1823	0.1154	0.7389	-0.0443	-0.0045	1.6000
-223	-2	23	-2.78	0.435	5.60	1.2923	0.1362	0.7624	-0.0580	-0.0064	1.6951
-222	-2	22	-3.21	0.469	5.65	1.5095	0.1504	0.7756	-0.0732	-0.0075	1.9463
-221	-2	21	-3.81	0.492	5.72	1.7959	0.1356	0.7199	-0.0636	-0.0063	2.4945
-220	-2	20	-4.40	0.528	5.72	2.1908	0.0781	0.5936	-0.0349	-0.0027	3.6906
-130	-1	30	-0.52	0.296	5.12	0.8403	0.0292	0.5996	-0.0074	-0.0002	1.4013
-129	-1	29	-0.57	0.315	5.11	0.8687	0.0326	0.6130	-0.0087	-0.0003	1.4171
-128	-1	28	-0.64	0.334	5.22	0.9103	0.0380	0.6317	-0.0108	-0.0004	1.4410
-127	-1	27	-0.70	0.351	5.28	0.9433	0.0455	0.6456	-0.0132	-0.0006	1.4612
-126	-1	26	-0.79	0.371	5.30	0.9912	0.0525	0.6672	-0.0162	-0.0008	1.4855
-125	-1	25	-0.95	0.394	5.25	1.0388	0.0612	0.6797	-0.0198	-0.0011	1.5283
-124	-1	24	-1.09	0.416	5.46	1.1389	0.0751	0.7143	-0.0265	-0.0017	1.5943
-123	-1	23	-1.24	0.444	5.57	1.2741	0.0883	0.7452	-0.0356	-0.0024	1.7096
-122	-1	22	-1.48	0.469	5.62	1.4521	0.1011	0.7604	-0.0466	-0.0032	1.9096
-121	-1	21	-1.73	0.506	5.78	1.7875	0.0840	0.7016	-0.0348	-0.0022	2.5478
30	0	30	-0.01	0.298	4.90	0.7933	0.0078	0.5674	-0.0017	-0.0000	1.3980
29	0	29	0.01	0.314	5.03	0.8114	0.0115	0.5760	-0.0023	-0.0000	1.4087
28	0	28	-0.04	0.333	5.15	0.8694	0.0142	0.6057	-0.0029	-0.0000	1.4355
27	0	27	-0.02	0.354	5.19	0.9048	0.0163	0.6205	-0.0034	-0.0001	1.4581
26	0	26	0.06	0.375	5.38	0.9536	0.0205	0.6402	-0.0045	-0.0001	1.4895
25	0	25	-0.01	0.397	5.28	1.0085	0.0150	0.6624	-0.0034	-0.0001	1.5225
24	0	24	0.04	0.423	5.28	1.0756	0.0197	0.6781	-0.0049	-0.0001	1.5862
23	0	23	0.03	0.449	5.58	1.1775	0.0185	0.7017	-0.0047	-0.0001	1.6779
22	0	22	-0.02	0.483	5.36	1.3519	0.0171	0.7175	-0.0051	-0.0001	1.8841
21	0	21	-0.08	0.524	5.44	1.5896	0.0159	0.6692	-0.0050	-0.0001	2.3752
130	1	30	0.26	0.296	4.95	0.7843	-0.0152	0.5624	0.0041	-0.0001	1.3946
129	1	29	0.37	0.314	4.78	0.8036	-0.0145	0.5675	0.0044	-0.0001	1.4161
128	1	28	0.43	0.331	4.91	0.8390	-0.0205	0.5859	0.0060	-0.0001	1.4318
127	1	27	0.48	0.351	4.84	0.8645	-0.0216	0.5933	0.0071	-0.0002	1.4570
126	1	26	0.55	0.373	4.91	0.9161	-0.0260	0.6158	0.0090	-0.0003	1.4877
125	1	25	0.77	0.395	5.20	0.9865	-0.0369	0.6458	0.0127	-0.0005	1.5276
124	1	24	1.03	0.418	5.15	1.0013	-0.0469	0.6400	0.0171	-0.0008	1.5645
123	1	23	1.26	0.446	5.15	1.1159	-0.0564	0.6752	0.0234	-0.0013	1.6528
122	1	22	1.41	0.475	5.33	1.3160	-0.0701	0.6959	0.0328	-0.0018	1.8911
121	1	21	1.64	0.517	5.16	1.6324	-0.0515	0.6304	0.0216	-0.0010	2.5895

TABLE 1—*continued*

Boundary Layer Displacement and Momentum Thicknesses.

Profile No.	Z	X	α	C_p	δ	δ_1	δ_2	θ_{11}	θ_{12}	θ_{22}	H
	inches	inches	degrees		inches	inches	inches	inches	inches	inches	
230	2	30	0.89	0.293	4.94	0.8044	-0.0307	0.5743	0.0086	-0.0003	1.4005
229	2	29	0.92	0.309	4.93	0.8133	-0.0360	0.5777	0.0100	-0.0004	1.4080
228	2	28	1.09	0.327	5.06	0.8460	-0.0417	0.5918	0.0122	-0.0006	1.4294
227	2	27	1.31	0.348	4.90	0.8755	-0.0489	0.6023	0.0154	-0.0009	1.4536
226	2	26	1.52	0.368	4.89	0.9370	-0.0613	0.6283	0.0202	-0.0013	1.4913
225	2	25	1.83	0.389	5.10	0.9586	-0.0816	0.6309	0.0272	-0.0023	1.5195
224	2	24	2.30	0.412	5.19	1.0594	-0.0919	0.6707	0.0352	-0.0032	1.5794
223	2	23	2.49	0.438	5.09	1.1320	-0.1255	0.6768	0.0495	-0.0054	1.6725
222	2	22	3.16	0.467	5.22	1.2895	-0.1379	0.6975	0.0642	-0.0070	1.8489
221	2	21	3.63	0.495	5.13	1.5365	-0.1316	0.6593	0.0586	-0.0061	2.3306
330	3	30	1.22	0.292	5.36	0.8277	-0.0577	0.5923	0.0152	-0.0010	1.3974
329	3	29	1.53	0.305	5.21	0.8453	-0.0675	0.6000	0.0181	-0.0014	1.4088
328	3	28	1.92	0.325	5.17	0.8729	-0.0716	0.6127	0.0208	-0.0017	1.4246
327	3	27	2.14	0.341	5.09	0.9066	-0.0878	0.6264	0.0263	-0.0025	1.4474
326	3	26	2.55	0.362	5.16	0.9413	-0.1027	0.6357	0.0324	-0.0035	1.4807
325	3	25	3.02	0.383	5.14	1.0114	-0.1195	0.6646	0.0405	-0.0048	1.5218
324	3	24	3.48	0.404	5.24	1.0822	-0.1487	0.6871	0.0534	-0.0073	1.5751
323	3	23	4.10	0.429	5.43	1.2016	-0.1727	0.7163	0.0714	-0.0106	1.6776
322	3	22	4.69	0.454	5.29	1.3757	-0.2007	0.7281	0.0951	-0.0140	1.8895
321	3	21	5.27	0.480	5.29	1.5355	-0.2267	0.7051	0.1168	-0.0173	2.1777
430	4	30	2.01	0.287	4.97	0.8314	-0.0757	0.5950	0.0209	-0.0019	1.3973
429	4	29	2.29	0.302	5.13	0.8626	-0.0865	0.6108	0.0243	-0.0024	1.4123
428	4	28	2.63	0.319	5.17	0.8953	-0.0954	0.6275	0.0279	-0.0030	1.4268
427	4	27	2.99	0.336	5.22	0.9386	-0.1103	0.6472	0.0340	-0.0040	1.4503
426	4	26	3.43	0.353	5.24	0.9812	-0.1296	0.6648	0.0421	-0.0057	1.4760
425	4	25	3.89	0.374	5.41	1.0393	-0.1595	0.6854	0.0547	-0.0086	1.5162
424	4	24	4.41	0.392	5.39	1.1046	-0.1958	0.7050	0.0714	-0.0129	1.5667
423	4	23	5.16	0.414	5.47	1.2023	-0.2296	0.7298	0.0931	-0.0185	1.6476
422	4	22	5.86	0.438	5.47	1.3357	-0.2791	0.7456	0.1274	-0.0277	1.7914
421	4	21	6.78	0.461	5.43	1.5165	-0.3206	0.7319	0.1671	-0.0359	2.0722
530	5	30	2.68	0.279	5.26	0.8747	-0.0853	0.6235	0.0247	-0.0025	1.4027
529	5	29	2.97	0.294	5.28	0.8988	-0.0974	0.6350	0.0289	-0.0032	1.4154
528	5	28	3.35	0.311	5.14	0.9243	-0.1132	0.6461	0.0346	-0.0044	1.4307
527	5	27	3.73	0.324	5.36	0.9619	-0.1389	0.6651	0.0429	-0.0063	1.4462
526	5	26	4.31	0.345	5.34	1.0135	-0.1576	0.6876	0.0522	-0.0085	1.4740
525	5	25	4.84	0.362	5.51	1.0700	-0.1867	0.7088	0.0661	-0.0123	1.5096
524	5	24	5.43	0.379	5.43	1.1196	-0.2351	0.7209	0.0867	-0.0191	1.5529
523	5	23	6.02	0.396	5.44	1.1756	-0.2850	0.7306	0.1113	-0.0281	1.6091
522	5	22	6.99	0.419	5.42	1.2781	-0.3376	0.7423	0.1464	-0.0404	1.7219
521	5	21	8.08	0.437	5.54	1.4333	-0.3933	0.7495	0.1945	-0.0557	1.9124

TABLE 1—*continued*

Boundary Layer Displacement and Momentum Thicknesses.

Profile No	Z	X	α	C_p	δ	δ_1	δ_2	θ_{11}	θ_{12}	θ_{22}	H
	inches	inches	degrees		inches	inches	inches	inches	inches	inches	
630	6	30	3.10	0.272	5.16	0.8864	-0.0976	0.6301	0.0284	-0.0032	1.4068
629	6	29	3.51	0.286	5.30	0.9162	-0.1074	0.6461	0.0328	-0.0041	1.4181
628	6	28	3.97	0.302	5.32	0.9384	-0.1243	0.6534	0.0394	-0.0055	1.4362
627	6	27	4.39	0.315	5.22	0.9637	-0.1534	0.6652	0.0486	-0.0081	1.4488
626	6	26	4.94	0.330	5.32	0.9956	-0.1830	0.6802	0.0603	-0.0017	1.4639
625	6	25	5.60	0.347	5.51	1.0513	-0.2198	0.7041	0.0748	-0.0164	1.4932
624	6	24	6.24	0.363	5.41	1.0964	-0.2687	0.7166	0.0958	-0.0245	1.5300
623	6	23	7.07	0.380	5.48	1.1619	-0.3167	0.7380	0.1205	-0.0347	1.5743
622	6	22	8.28	0.395	5.50	1.2317	-0.3655	0.7471	0.1524	-0.0486	1.6486
621	6	21	9.29	0.410	5.54	1.3489	-0.4435	0.7577	0.2049	-0.0717	1.7804
620	6	20	10.42	0.428	5.60	1.5343	-0.5037	0.7600	0.2678	-0.0935	2.0187
730	7	30	3.40	0.264	5.20	0.8737	-0.1096	0.6226	0.0320	-0.0042	1.4034
729	7	29	4.16	0.277	5.18	0.8882	-0.1184	0.6267	0.0363	-0.0051	1.4174
728	7	28	4.55	0.289	5.18	0.9124	-0.1444	0.6378	0.0444	-0.0073	1.4307
727	7	27	4.99	0.305	5.26	0.9561	-0.1673	0.6592	0.0530	-0.0096	1.4506
726	7	26	5.59	0.319	5.28	0.9912	-0.1967	0.6744	0.0640	-0.0131	1.4697
725	7	25	6.47	0.332	5.38	1.0455	-0.2287	0.6990	0.0783	-0.0180	1.4958
724	7	24	7.26	0.346	5.49	1.0945	-0.2690	0.7156	0.0978	-0.0257	1.5295
723	7	23	8.02	0.359	5.45	1.1411	-0.3280	0.7343	0.1231	-0.0378	1.5541
722	7	22	9.08	0.372	5.67	1.2256	-0.3958	0.7625	0.1601	-0.0564	1.6074
721	7	21	10.14	0.382	5.65	1.3104	-0.4736	0.7674	0.2098	-0.0823	1.7075
720	7	20	11.45	0.393	5.59	1.4397	-0.5540	0.7773	0.2737	-0.1146	1.8522
829	8	29	4.50	0.266	4.92	0.8366	-0.1340	0.5962	0.0388	-0.0064	1.4032
828	8	28	5.05	0.278	5.12	0.8685	-0.1566	0.6132	0.0459	-0.0084	1.4162
827	8	27	5.73	0.290	5.15	0.8964	-0.1767	0.6270	0.0537	-0.0109	1.4297
826	8	26	6.38	0.304	5.26	0.9414	-0.2029	0.6500	0.0648	-0.0146	1.4484
825	8	25	7.12	0.314	5.37	0.9781	-0.2393	0.6642	0.0790	-0.0202	1.4726
824	8	24	7.92	0.326	5.34	1.0352	-0.2804	0.6901	0.0974	-0.0279	1.4999
823	8	23	8.77	0.335	5.38	1.0934	-0.3437	0.7134	0.1246	-0.0415	1.5327
822	8	22	9.69	0.345	5.45	1.1635	-0.4022	0.7341	0.1570	-0.0583	1.5851
821	8	21	10.90	0.354	5.58	1.2526	-0.4848	0.7562	0.2043	-0.0854	1.6564
820	8	20	12.36	0.360	5.58	1.3556	-0.5585	0.7736	0.2602	-0.1186	1.7524
929	9	29	5.19	0.255	4.94	0.7645	-0.1388	0.5523	0.0380	-0.0070	1.3842
928	9	28	5.74	0.266	4.94	0.7855	-0.1581	0.5632	0.0444	-0.0091	1.3947
927	9	27	6.18	0.277	4.93	0.8326	-0.1816	0.5890	0.0532	-0.0118	1.4136
926	9	26	6.91	0.286	5.14	0.8634	-0.2065	0.6047	0.0629	-0.0156	1.4278
925	9	25	7.72	0.297	5.00	0.9013	-0.2430	0.6219	0.0769	-0.0216	1.4492
924	9	24	8.49	0.304	5.08	0.9398	-0.2898	0.6396	0.0946	-0.0303	1.4693
923	9	23	9.29	0.312	5.26	0.9934	-0.3480	0.6606	0.1186	-0.0428	1.5039
922	9	22	10.38	0.320	5.20	1.0648	-0.4062	0.6890	0.1480	-0.0591	1.5455
921	9	21	11.57	0.325	5.31	1.1518	-0.4719	0.7207	0.1868	-0.0823	1.5983
920	9	20	12.65	0.325	5.49	1.2437	-0.5586	0.7506	0.2388	-0.1180	1.6570

TABLE 2

Skin Friction.

Profile Number	Preston Tube		Razor Blade	
	U/u_τ	$C_f \times 10^3$	U/u_τ	$C_f \times 10^3$
−230	37·63	1·413	38·73	1·334
−228	40·78	1·203	41·84	1·143
−226	45·54	0·964	47·37	0·891
−224	56·83	0·619	61·55	0·528
−222	90·68	0·243	68·84	0·422
030	37·20	1·445	38·62	1·341
028	40·37	1·227	41·25	1·176
026	44·79	0·997	46·12	0·940
024	58·18	0·591	63·28	0·499
022	93·87	0·227	—	0
230	36·70	1·485	39·00	1·315
228	39·34	1·292	40·67	1·210
226	43·85	1·040	45·09	0·984
224	54·70	0·668	54·75	0·667
222	90·12	0·246	98·06	0·208
430	37·40	1·430	38·45	1·353
428	39·32	1·294	39·85	1·259
426	42·86	1·089	42·54	1·105
424	50·83	0·774	47·62	0·882
422	60·21	0·552	53·48	0·699
630	37·51	1·422	36·93	1·467
628	39·01	1·314	38·17	1·373
626	41·28	1·174	39·50	1·282
624	44·65	1·003	42·60	1·102
622	45·59	0·962	45·72	0·957
620	40·37	1·227	37·43	1·427
828	37·86	1·395	37·09	1·453
826	39·47	1·284	38·01	1·385
824	40·36	1·228	38·68	1·336
822	40·62	1·212	39·19	1·302
820	36·19	1·527	34·99	1·633
1028	35·61	1·577	35·88	1·554
1026	36·31	1·517	36·57	1·496
1024	37·08	1·455	36·12	1·533
1022	37·10	1·453	35·52	1·586
1020	34·51	1·679	33·81	1·750

TABLE 3

Velocity Profiles.

Profile No	-230		-229		-228		-227		-226		-225	
y	u/U	beta	u/U	beta	u/U	beta	u/U	beta	u/U	beta	u/U	beta
0.010	0.346	-3.33	0.333	-3.69	0.311	-4.92	0.304	-6.26	0.310	-10.01	0.264	-11.55
0.014	0.374	-3.33	0.348	-3.86	0.335	-4.92	0.325	-6.36	0.321	-8.51	0.277	-11.73
0.020	0.389	-3.21	0.361	-3.92	0.357	-4.80	0.338	-6.12	0.334	-7.90	0.294	-11.60
0.028	0.408	-3.21	0.383	-3.95	0.374	-4.57	0.354	-5.87	0.342	-7.46	0.304	-11.28
0.040	0.422	-3.15	0.410	-3.62	0.392	-4.44	0.374	-5.61	0.354	-7.21	0.329	-10.67
0.057	0.448	-2.90	0.428	-3.54	0.410	-4.33	0.399	-5.21	0.375	-6.70	0.348	-10.08
0.080	0.467	-2.80	0.452	-3.40	0.435	-4.13	0.420	-5.03	0.393	-6.30	0.358	-9.18
0.113	0.493	-2.57	0.472	-3.08	0.458	-3.84	0.443	-4.65	0.414	-5.79	0.382	-8.63
0.160	0.523	-2.39	0.502	-2.86	0.481	-3.37	0.466	-4.26	0.443	-5.18	0.423	-7.33
0.226	0.545	-2.14	0.529	-2.66	0.517	-3.15	0.497	-3.83	0.470	-4.71	0.448	-6.47
0.320	0.574	-1.92	0.561	-2.27	0.550	-2.84	0.533	-3.46	0.511	-4.17	0.470	-5.72
0.453	0.613	-1.69	0.592	-1.93	0.581	-2.43	0.562	-2.89	0.539	-3.59	0.518	-4.82
0.640	0.651	-1.42	0.632	-1.64	0.624	-2.01	0.597	-2.51	0.581	-3.00	0.557	-3.94
0.905	0.689	-1.15	0.676	-1.38	0.663	-1.59	0.659	-2.04	0.630	-2.50	0.615	-3.20
1.280	0.737	-0.92	0.728	-1.04	0.719	-1.26	0.709	-1.62	0.691	-1.92	0.679	-2.40
1.500	0.768	-0.81	0.750	-0.91	0.745	-1.12	0.733	-1.33	0.718	-1.64	0.707	-2.10
2.000	0.814	-0.63	0.805	-0.68	0.801	-0.81	0.788	-0.97	0.788	-1.12	0.762	-1.55
2.500	0.863	-0.45	0.851	-0.51	0.848	-0.57	0.845	-0.76	0.833	-0.76	0.822	-1.06
3.000	0.903	-0.31	0.894	-0.34	0.889	-0.44	0.885	-0.51	0.877	-0.55	0.871	-0.68
3.500	0.936	-0.25	0.930	-0.25	0.929	-0.31	0.922	-0.33	0.916	-0.40	0.912	-0.43
4.000	0.960	-0.13	0.955	-0.11	0.954	-0.17	0.950	-0.17	0.948	-0.18	0.941	-0.25
4.500	0.979	-0.07	0.976	-0.05	0.977	-0.06	0.973	-0.11	0.973	-0.07	0.972	-0.19
5.000	0.992	-0.01	0.990	0.01	0.990	-0.00	0.991	-0.03	0.986	0.01	0.984	-0.01
5.500	0.998	0.01	0.997	-0.01	0.997	-0.00	0.996	0.00	0.996	-0.00	0.995	-0.00
6.000	0.999	0.01	0.999	-0.01	0.999	-0.00	0.999	-0.01	1.000	-0.00	0.998	-0.02
6.500	1.000	0.01	1.000	0.01	1.000	-0.00	1.000	-0.05	1.000	0.03	1.000	-0.00
7.000	1.000	0.01	1.000	0.04	1.000	-0.00	1.000	-0.01	1.000	0.03	1.001	-0.00

Profile No	-224		-223		-222		-221		-220		-130	
y	u/U	beta	u/U	beta	u/U	beta	u/U	beta	u/U	beta	u/U	beta
0.010	0.249	-17.08	0.193	-26.36	0.045	-50.73	0.000	-94.33	0.000	-109.24	0.350	-1.97
0.014	0.255	-16.98	0.195	-26.54	0.067	-50.23	0.000	-96.51	0.000	-107.47	0.368	-1.97
0.020	0.269	-16.50	0.220	-26.12	0.050	-49.56	0.000	-96.51	0.000	-106.79	0.388	-1.97
0.028	0.276	-15.68	0.223	-25.80	0.079	-48.76	0.000	-96.51	0.000	-108.71	0.408	-1.97
0.040	0.298	-14.78	0.232	-23.84	0.087	-45.47	0.000	-93.65	0.000	-114.46	0.428	-1.97
0.057	0.310	-14.01	0.237	-21.77	0.082	-41.16	0.000	-91.76	0.000	-112.98	0.446	-1.85
0.080	0.324	-12.99	0.267	-19.74	0.131	-37.52	0.000	-85.77	0.000	-111.26	0.474	-1.80
0.113	0.345	-11.80	0.288	-17.42	0.132	-32.48	0.000	-74.02	0.000	-112.87	0.492	-1.62
0.160	0.373	-10.66	0.296	-15.28	0.190	-26.43	0.000	-59.64	0.000	-114.54	0.526	-1.52
0.226	0.403	-9.21	0.354	-13.00	0.194	-22.61	0.000	-45.44	0.000	-113.28	0.548	-1.43
0.320	0.440	-7.94	0.387	-10.91	0.255	-16.88	0.000	-34.97	0.000	-109.20	0.589	-1.21
0.453	0.479	-6.46	0.425	-9.06	0.319	-13.49	0.101	-24.08	0.000	-105.62	0.620	-1.11
0.640	0.526	-5.27	0.486	-6.97	0.403	-9.98	0.256	-16.10	0.000	-47.18	0.655	-0.91
0.905	0.586	-4.08	0.547	-5.26	0.468	-7.26	0.335	-11.24	0.000	-22.85	0.699	-0.75
1.280	0.651	-2.93	0.621	-3.72	0.555	-5.02	0.486	-7.43	0.262	-10.81	0.743	-0.66
1.500	0.686	-2.53	0.657	-3.13	0.606	-4.11	0.537	-5.79	0.343	-7.89	0.772	-0.57
2.000	0.748	-1.84	0.732	-2.11	0.697	-2.65	0.646	-3.45	0.581	-3.80	0.821	-0.46
2.500	0.809	-1.26	0.796	-1.51	0.761	-1.74	0.738	-2.06	0.682	-2.23	0.871	-0.32
3.000	0.859	-0.92	0.845	-0.97	0.824	-1.17	0.808	-1.35	0.781	-1.16	0.904	-0.26
3.500	0.904	-0.59	0.892	-0.62	0.877	-0.72	0.863	-0.77	0.851	-0.60	0.940	-0.23
4.000	0.937	-0.35	0.933	-0.39	0.920	-0.34	0.910	-0.44	0.911	-0.36	0.965	-0.16
4.500	0.965	-0.12	0.960	-0.17	0.955	-0.18	0.951	-0.25	0.950	-0.11	0.983	-0.07
5.000	0.984	-0.03	0.980	-0.07	0.978	-0.05	0.975	-0.13	0.975	0.02	0.994	-0.01
5.500	0.995	-0.00	0.994	-0.00	0.992	0.00	0.991	-0.01	0.991	-0.01	0.997	0.03
6.000	0.998	0.04	0.998	-0.02	1.000	-0.02	0.998	-0.01	0.998	0.03	0.999	0.03
6.500	1.001	0.03	1.000	-0.00	1.000	-0.02	1.000	-0.03	1.000	-0.08	0.999	0.03
7.000	1.001	0.03	1.001	-0.02	1.000	-0.02	1.001	-0.07	1.001	-0.09	1.001	0.03

Profile No	-129		-128		-127		-126		-125		-124	
y	u/U	beta	u/U	beta	u/U	beta	u/U	beta	u/U	beta	u/U	beta
0.010	0.337	-2.37	0.320	-2.95	0.310	-3.60	0.289	-4.63	0.266	-6.71	0.227	-10.15
0.014	0.363	-2.37	0.335	-3.03	0.329	-3.60	0.307	-5.05	0.298	-6.58	0.244	-9.96
0.020	0.377	-2.37	0.360	-2.95	0.350	-3.70	0.336	-4.96	0.298	-6.48	0.255	-9.83
0.028	0.396	-2.37	0.372	-2.76	0.366	-3.61	0.348	-4.84	0.312	-6.30	0.269	-9.57
0.040	0.413	-2.27	0.396	-2.80	0.382	-3.41	0.361	-4.51	0.337	-5.88	0.286	-9.00
0.057	0.436	-2.18	0.419	-2.66	0.401	-3.21	0.380	-4.23	0.354	-5.60	0.290	-8.38
0.080	0.454	-2.13	0.438	-2.55	0.420	-2.98	0.401	-3.97	0.361	-5.18	0.311	-7.73
0.113	0.475	-2.00	0.464	-2.39	0.443	-2.79	0.417	-3.59	0.387	-4.74	0.343	-7.01
0.160	0.510	-1.76	0.488	-2.12	0.471	-2.55	0.446	-3.23	0.417	-4.20	0.364	-6.14
0.226	0.538	-1.60	0.520	-1.96	0.498	-2.40	0.478	-3.02	0.443	-3.71	0.386	-5.37
0.320	0.579	-1.41	0.550	-1.78	0.538	-2.17	0.521	-2.60	0.490	-3.23	0.436	-4.56
0.453	0.605	-1.25	0.585	-1.49	0.574	-1.88	0.556	-2.25	0.527	-2.80	0.496	-3.71
0.640	0.643	-1.06	0.621	-1.36	0.613	-1.61	0.594	-1.94	0.573	-2.36	0.536	-2.97
0.905	0.688	-0.94	0.676	-1.17	0.661	-1.38	0.647	-1.61	0.628	-1.92	0.595	-2.41
1.280	0.738	-0.76	0.725	-0.90	0.716	-1.09	0.712	-1.30	0.686	-1.53	0.665	-1.88
1.500	0.762	-0.65	0.761	-0.82	0.744	-0.92	0.735	-1.14	0.721	-1.30	0.699	-1.66
2.000	0.816	-0.52	0.808	-0.63	0.801	-0.78	0.788	-0.88	0.785	-1.00	0.763	-1.23
2.500	0.862	-0.35	0.855	-0.42	0.850	-0.57	0.838	-0.69	0.836	-0.72	0.822	-0.87
3.000	0.904	-0.30	0.899	-0.33	0.896	-0.37	0.891	-0.43	0.881	-0.48	0.867	-0.67
3.500	0.935	-0.20	0.938	-0.23	0.932	-0.29	0.925	-0.32	0.923	-0.40	0.910	-0.46
4.000	0.963	-0.13	0.954	-0.11	0.956	-0.16	0.949	-0.18	0.950	-0.27	0.943	-0.26
4.500	0.980	-0.10	0.980	-0.08	0.978	-0.09	0.976	-0.09	0.975	-0.03	0.970	-0.18
5.000	0.993	-0.02	0.992	-0.02	0.989	-0.03	0.990	-0.01	0.991	-0.05	0.987	-0.08
5.500	0.999	0.03	0.997	0.01	0.998	0.02	0.997	0.00	0.997	0.04	0.995	0.01
6.000	1.001	0.03	0.999	0.01	1.000	0.02	1.000	0.02	0.999	0.04	0.997	0.04
6.500	0.999	0.02	1.000	0.05	1.001	0.02	1.000	0.04	1.000	0.04	1.000	0.02
7.000	1.000	0.04	1.000	0.07	0.999	0.02	1.000	0.03	1.000	0.04	1.002	0.04

TABLE 3—*continued*
Velocity Profiles.

Profile No	-123		-122		-121		30		29		28	
y	u/U	beta	u/U	beta	u/U	beta	u/U	beta	u/U	beta	u/U	beta
0.010	0.169	-18.48	0.074	-42.77	0.000	-128.47	0.354	0.40	0.351	0.07	0.326	0.07
0.014	0.187	-17.60	0.094	-40.17	0.000	-125.42	0.374	-0.07	0.373	-0.24	0.350	-0.33
0.020	0.194	-17.36	0.099	-38.58	0.000	-124.75	0.393	-0.20	0.384	-0.35	0.358	-0.35
0.028	0.198	-16.56	0.093	-37.00	0.000	-124.75	0.416	-0.28	0.405	-0.34	0.379	-0.38
0.040	0.216	-15.14	0.115	-33.82	0.000	-124.35	0.434	-0.24	0.422	-0.29	0.406	-0.40
0.057	0.225	-14.58	0.114	-30.48	0.000	-123.45	0.459	-0.32	0.446	-0.29	0.419	-0.44
0.080	0.243	-12.56	0.109	-26.88	0.000	-105.90	0.475	-0.31	0.465	-0.25	0.441	-0.38
0.113	0.263	-10.93	0.141	-21.27	0.000	-74.16	0.503	-0.20	0.491	-0.25	0.467	-0.40
0.160	0.289	-9.65	0.174	-17.45	0.000	-43.58	0.531	-0.20	0.519	-0.29	0.495	-0.39
0.226	0.330	-8.32	0.210	-14.59	0.000	-36.18	0.559	-0.19	0.544	-0.29	0.530	-0.39
0.320	0.363	-6.60	0.263	-10.80	0.000	-23.00	0.595	-0.20	0.582	-0.29	0.560	-0.36
0.453	0.418	-5.24	0.322	-7.93	0.000	-14.18	0.625	-0.20	0.618	-0.29	0.594	-0.34
0.640	0.471	-4.28	0.416	-5.77	0.224	-9.56	0.659	-0.21	0.654	-0.29	0.632	-0.34
0.905	0.559	-3.12	0.482	-4.27	0.356	-6.13	0.709	-0.24	0.703	-0.29	0.683	-0.29
1.280	0.629	-2.33	0.578	-2.95	0.473	-4.32	0.757	-0.22	0.753	-0.23	0.730	-0.24
1.500	0.666	-2.04	0.630	-2.44	0.545	-3.48	0.779	-0.18	0.775	-0.21	0.765	-0.25
2.000	0.733	-1.41	0.708	-1.76	0.658	-2.19	0.835	-0.14	0.830	-0.21	0.820	-0.27
2.500	0.793	-0.98	0.775	-1.25	0.740	-1.49	0.878	-0.09	0.877	-0.18	0.862	-0.25
3.000	0.852	-0.78	0.838	-0.85	0.807	-0.98	0.921	-0.08	0.918	-0.11	0.912	-0.17
3.500	0.901	-0.50	0.884	-0.54	0.871	-0.70	0.949	-0.08	0.947	-0.11	0.939	-0.17
4.000	0.938	-0.33	0.928	-0.38	0.922	-0.40	0.972	0.02	0.972	-0.11	0.966	-0.14
4.500	0.965	-0.20	0.956	-0.18	0.946	-0.21	0.987	-0.04	0.986	-0.06	0.984	-0.06
5.000	0.987	-0.09	0.979	-0.08	0.977	-0.11	0.996	0.02	0.995	0.00	0.993	-0.02
5.500	0.994	-0.01	0.993	-0.01	0.990	-0.01	0.997	0.11	0.999	0.00	0.998	0.02
6.000	0.999	0.00	0.998	0.01	0.999	-0.02	0.999	0.09	1.000	0.12	0.999	0.02
6.500	1.000	0.00	1.000	-0.02	1.000	-0.02	1.000	0.09	1.000	0.12	1.000	0.03
7.000	1.001	0.01	1.001	-0.00	1.001	-0.03	1.000	0.12	1.000	0.12	1.000	0.01

Profile No	27		26		25		24		23		22	
y	u/U	beta	u/U	beta	u/U	beta	u/U	beta	u/U	beta	u/U	beta
0.010	0.316	-0.29	0.282	-0.94	0.256	0.19	0.212	-0.58	0.172	-0.74	0.000	-2.66
0.014	0.331	-0.54	0.296	-1.09	0.281	0.19	0.235	-0.53	0.187	-0.74	0.000	-2.05
0.020	0.355	-0.60	0.317	-0.95	0.291	-0.25	0.251	-0.54	0.193	-0.74	0.000	-1.93
0.028	0.364	-0.60	0.342	-0.82	0.307	-0.31	0.269	-0.59	0.215	-0.74	0.000	-1.68
0.040	0.386	-0.60	0.354	-0.71	0.321	-0.29	0.283	-0.55	0.222	-0.74	0.060	-1.55
0.057	0.403	-0.50	0.374	-0.69	0.348	-0.29	0.304	-0.55	0.244	-0.60	0.103	-1.49
0.080	0.424	-0.50	0.401	-0.73	0.367	-0.29	0.326	-0.65	0.261	-0.60	0.124	-1.46
0.113	0.457	-0.46	0.420	-0.66	0.395	-0.25	0.348	-0.65	0.279	-0.60	0.142	-1.37
0.160	0.476	-0.46	0.444	-0.62	0.420	-0.25	0.373	-0.62	0.311	-0.60	0.191	-1.22
0.226	0.510	-0.44	0.483	-0.55	0.460	-0.40	0.404	-0.59	0.342	-0.60	0.240	-0.93
0.320	0.546	-0.44	0.520	-0.55	0.490	-0.41	0.451	-0.56	0.406	-0.55	0.289	-0.75
0.453	0.573	-0.44	0.557	-0.52	0.532	-0.37	0.500	-0.53	0.435	-0.55	0.355	-0.70
0.640	0.622	-0.35	0.599	-0.49	0.580	-0.37	0.546	-0.53	0.499	-0.55	0.430	-0.54
0.905	0.669	-0.31	0.654	-0.48	0.636	-0.34	0.610	-0.45	0.564	-0.48	0.503	-0.49
1.280	0.722	-0.31	0.714	-0.41	0.696	-0.34	0.666	-0.45	0.643	-0.37	0.605	-0.41
1.500	0.747	-0.33	0.734	-0.37	0.723	-0.34	0.705	-0.45	0.686	-0.37	0.648	-0.38
2.000	0.809	-0.25	0.801	-0.33	0.797	-0.27	0.780	-0.37	0.762	-0.32	0.733	-0.32
2.500	0.865	-0.25	0.848	-0.29	0.839	-0.25	0.837	-0.31	0.824	-0.26	0.790	-0.27
3.000	0.904	-0.21	0.900	-0.22	0.886	-0.21	0.883	-0.27	0.872	-0.26	0.851	-0.24
3.500	0.943	-0.21	0.932	-0.20	0.926	-0.21	0.927	-0.27	0.920	-0.24	0.905	-0.21
4.000	0.966	-0.17	0.963	-0.22	0.956	-0.13	0.955	-0.15	0.950	-0.18	0.945	-0.16
4.500	0.980	-0.10	0.981	-0.15	0.980	-0.07	0.977	-0.11	0.975	-0.14	0.969	-0.10
5.000	0.993	-0.03	0.991	-0.08	0.992	-0.02	0.991	-0.03	0.987	-0.06	0.987	-0.06
5.500	0.997	0.03	0.996	0.02	0.997	0.02	0.997	0.01	0.994	-0.00	0.997	0.03
6.000	0.999	0.03	1.000	0.03	0.999	0.08	1.000	0.03	0.999	-0.00	0.999	0.11
6.500	1.000	0.03	1.000	0.04	1.000	0.08	1.000	0.05	1.001	-0.00	1.000	0.13
7.000	1.001	0.03	1.000	0.01	1.001	0.04	1.000	0.05	1.000	0.04	1.000	0.13

Profile No	21		130		129		128		127		126	
y	u/U	beta	u/U	beta	u/U	beta	u/U	beta	u/U	beta	u/U	beta
0.010	0.000	-6.87	0.351	2.01	0.336	2.26	0.327	2.65	0.316	3.17	0.293	3.84
0.014	0.000	-10.31	0.380	1.49	0.363	2.03	0.354	2.37	0.333	2.92	0.310	3.67
0.020	0.000	-8.57	0.400	1.40	0.384	1.89	0.376	2.33	0.356	2.61	0.331	3.35
0.028	0.000	-4.99	0.413	1.34	0.404	1.75	0.388	2.12	0.369	2.47	0.349	3.20
0.040	0.000	-3.97	0.429	1.24	0.422	1.65	0.411	2.07	0.391	2.47	0.364	2.97
0.057	0.000	-3.69	0.460	1.24	0.445	1.46	0.428	1.89	0.410	2.19	0.384	2.74
0.080	0.000	-2.98	0.479	1.15	0.467	1.26	0.450	1.84	0.429	2.12	0.406	2.68
0.113	0.000	-2.46	0.504	1.05	0.492	1.12	0.476	1.68	0.457	1.95	0.429	2.46
0.160	0.000	-2.01	0.532	0.91	0.522	1.05	0.506	1.53	0.484	1.76	0.463	2.13
0.226	0.000	-1.66	0.563	0.83	0.546	0.95	0.533	1.20	0.510	1.53	0.491	1.95
0.320	0.000	-1.37	0.595	0.72	0.579	0.78	0.569	0.99	0.546	1.36	0.524	1.64
0.453	0.170	-1.07	0.630	0.65	0.612	0.68	0.599	0.91	0.586	1.14	0.563	1.41
0.640	0.307	-0.90	0.665	0.53	0.654	0.61	0.642	0.77	0.624	0.91	0.607	1.22
0.905	0.429	-0.60	0.710	0.42	0.703	0.49	0.685	0.62	0.677	0.73	0.661	0.90
1.280	0.531	-0.52	0.763	0.35	0.751	0.37	0.743	0.46	0.734	0.54	0.713	0.61
1.500	0.586	-0.47	0.781	0.30	0.776	0.27	0.768	0.42	0.759	0.49	0.746	0.63
2.000	0.698	-0.39	0.839	0.26	0.829	0.22	0.825	0.30	0.821	0.36	0.808	0.41
2.500	0.779	-0.30	0.881	0.17	0.877	0.13	0.872	0.24	0.871	0.18	0.862	0.23
3.000	0.846	-0.21	0.918	0.13	0.918	0.04	0.915	0.16	0.912	0.11	0.900	0.10
3.500	0.896	-0.16	0.949	0.06	0.955	0.04	0.947	0.09	0.945	0.04	0.944	0.05
4.000	0.932	-0.15	0.974	0.04	0.977	0.00	0.973	0.04	0.974	-0.01	0.969	0.05
4.500	0.967	-0.09	0.988	0.01	0.990	0.02	0.988	-0.01	0.989	-0.01	0.988	-0.01
5.000	0.987	-0.06	0.996	-0.00	0.997	-0.01	0.996	-0.01	0.997	-0.01	0.996	-0.01
5.500	0.996	0.01	0.999	-0.03	0.998	-0.01	0.999	-0.05	0.999	-0.05	0.999	-0.08
6.000	1.000	0.07	0.999	-0.03	0.999	-0.01	1.000	-0.05	1.000	-0.05	1.001	-0.08
6.500	1.001	0.08	1.000	-0.03	1.000	-0.01	1.000	-0.07	1.000	-0.05	1.000	-0.08
7.000	0.999	0.08	1.000	-0.03	1.000	-0.01	0.999	-0.07	1.001	-0.05	1.000	-0.05

TABLE 3—*continued*
Velocity Profiles.

Profile No	125		124		123		122		121		230	
y	u/U	beta	u/U	beta	u/U	beta	u/U	beta	u/U	beta	u/U	beta
0.010	0.264	5.63	0.239	8.74	0.209	14.00	0.090	33.01	0.000	141.79	0.357	3.80
0.014	0.289	5.19	0.267	7.72	0.204	13.26	0.070	30.08	0.000	140.61	0.379	3.31
0.020	0.301	4.94	0.275	7.13	0.222	12.25	0.092	28.49	0.000	139.51	0.386	3.07
0.028	0.316	4.82	0.290	6.66	0.231	11.67	0.097	24.28	0.000	133.85	0.418	2.89
0.040	0.333	4.41	0.316	6.24	0.247	10.54	0.113	22.31	0.000	134.09	0.439	2.75
0.057	0.354	3.96	0.322	5.93	0.260	9.87	0.123	19.21	0.000	131.77	0.456	2.63
0.080	0.370	3.56	0.352	5.14	0.278	9.08	0.145	16.91	0.000	130.33	0.488	2.44
0.113	0.391	3.26	0.366	4.67	0.294	7.77	0.173	14.64	0.000	47.28	0.503	2.23
0.160	0.423	2.97	0.392	4.16	0.342	6.55	0.201	12.35	0.000	34.09	0.526	2.01
0.226	0.457	2.59	0.433	3.70	0.368	5.62	0.233	10.16	0.000	23.46	0.558	1.82
0.320	0.488	2.19	0.475	2.92	0.419	4.55	0.284	7.96	0.000	15.94	0.589	1.54
0.453	0.536	1.84	0.514	2.58	0.466	3.40	0.358	5.92	0.000	9.53	0.631	1.36
0.640	0.584	1.55	0.562	2.13	0.521	2.73	0.424	4.25	0.263	6.30	0.659	1.13
0.905	0.636	1.29	0.620	1.71	0.581	2.08	0.512	2.88	0.392	4.11	0.702	0.92
1.280	0.700	0.94	0.693	1.30	0.652	1.60	0.609	2.12	0.510	2.52	0.751	0.72
1.500	0.731	0.83	0.729	1.08	0.703	1.29	0.640	1.68	0.580	2.10	0.781	0.61
2.000	0.793	0.59	0.797	0.76	0.777	0.97	0.735	1.13	0.687	1.29	0.830	0.43
2.500	0.848	0.37	0.853	0.49	0.827	0.54	0.806	0.74	0.779	0.85	0.874	0.30
3.000	0.894	0.26	0.896	0.27	0.877	0.26	0.868	0.53	0.846	0.58	0.917	0.21
3.500	0.933	0.12	0.944	0.10	0.936	0.14	0.917	0.29	0.903	0.29	0.947	0.16
4.000	0.967	0.05	0.967	0.07	0.961	0.06	0.954	0.14	0.946	0.11	0.973	0.07
4.500	0.984	0.05	0.985	-0.00	0.981	0.04	0.977	0.03	0.974	0.03	0.988	0.02
5.000	0.993	0.01	0.993	-0.00	0.993	-0.04	0.991	-0.02	0.993	-0.00	0.996	-0.01
5.500	0.997	-0.02	0.998	-0.00	0.998	0.09	0.997	0.01	0.997	0.02	0.999	-0.09
6.000	0.999	-0.05	1.000	-0.00	0.999	0.01	1.000	-0.03	0.999	0.06	1.000	-0.10
6.500	1.000	-0.04	0.999	0.07	1.000	-0.05	1.000	-0.01	1.002	0.08	1.000	-0.08
7.000	1.000	0.01	1.000	-0.01	1.000	0.01	1.000	0.05	0.999	0.16	1.000	-0.03

Profile No	229		228		227		226		225		224	
y	u/U	beta	u/U	beta	u/U	beta	u/U	beta	u/U	beta	u/U	beta
0.010	0.348	4.16	0.331	4.44	0.319	5.99	0.295	7.49	0.285	10.97	0.256	15.43
0.014	0.368	3.66	0.358	4.38	0.332	5.69	0.318	7.12	0.297	10.26	0.269	14.53
0.020	0.375	3.53	0.379	4.29	0.357	5.44	0.330	7.01	0.310	9.73	0.285	14.17
0.028	0.416	3.44	0.389	4.20	0.379	5.10	0.350	6.72	0.334	9.36	0.296	13.23
0.040	0.429	3.30	0.404	3.88	0.404	4.95	0.366	6.47	0.346	8.94	0.304	12.47
0.057	0.441	3.08	0.434	3.84	0.407	4.69	0.383	6.06	0.370	8.49	0.317	11.72
0.080	0.470	2.91	0.450	3.49	0.440	4.37	0.416	5.57	0.392	7.83	0.353	10.56
0.113	0.492	2.57	0.479	3.19	0.453	3.99	0.431	5.28	0.412	6.99	0.365	9.95
0.160	0.520	2.39	0.509	2.95	0.490	3.55	0.460	4.65	0.432	6.40	0.391	8.83
0.226	0.550	2.11	0.523	2.69	0.514	3.06	0.489	4.24	0.462	5.73	0.422	7.63
0.320	0.588	1.77	0.571	2.27	0.549	2.81	0.518	3.61	0.499	4.88	0.454	6.59
0.453	0.620	1.53	0.599	1.88	0.583	2.42	0.558	3.07	0.546	4.14	0.504	5.55
0.640	0.662	1.32	0.642	1.57	0.630	1.91	0.610	2.57	0.591	3.38	0.549	4.49
0.905	0.699	1.02	0.686	1.24	0.674	1.66	0.643	2.04	0.637	2.70	0.608	3.38
1.280	0.754	0.80	0.741	0.93	0.728	1.22	0.715	1.57	0.703	2.06	0.680	2.58
1.500	0.769	0.70	0.768	0.83	0.756	1.11	0.748	1.34	0.743	1.88	0.712	2.04
2.000	0.831	0.54	0.824	0.61	0.819	0.66	0.804	0.91	0.802	1.20	0.781	1.30
2.500	0.873	0.36	0.872	0.40	0.867	0.45	0.857	0.64	0.854	0.75	0.840	0.78
3.000	0.916	0.26	0.908	0.29	0.910	0.40	0.900	0.40	0.904	0.50	0.886	0.56
3.500	0.946	0.20	0.949	0.18	0.943	0.16	0.935	0.23	0.938	0.34	0.926	0.21
4.000	0.974	0.08	0.971	0.13	0.968	0.19	0.962	0.14	0.967	0.22	0.960	0.17
4.500	0.987	0.05	0.990	0.06	0.987	-0.04	0.988	0.02	0.986	0.17	0.981	0.07
5.000	0.996	-0.01	0.995	-0.00	0.997	-0.02	0.996	-0.02	0.994	0.04	0.992	0.01
5.500	1.001	-0.09	0.998	-0.02	1.002	-0.10	1.000	-0.07	0.999	-0.08	0.999	-0.03
6.000	1.001	-0.12	1.000	-0.11	1.002	-0.02	1.002	0.00	1.000	0.01	1.000	-0.11
6.500	0.999	-0.09	1.002	-0.08	1.002	-0.16	1.001	-0.06	1.000	0.01	1.000	-0.12
7.000	1.001	-0.06	0.998	-0.08	0.998	-0.08	0.998	-0.06	1.001	0.01	1.000	-0.13

Profile No	223		222		221		330		329		328	
y	u/U	beta	u/U	beta	u/U	beta	u/U	beta	u/U	beta	u/U	beta
0.010	0.215	23.02	0.136	42.46	0.000	94.50	0.351	5.22	0.356	6.13	0.340	7.37
0.014	0.220	21.56	0.136	41.29	0.000	91.95	0.369	4.93	0.366	5.81	0.355	7.11
0.020	0.244	21.37	0.166	40.28	0.000	91.22	0.395	4.68	0.385	5.64	0.373	6.87
0.028	0.250	20.07	0.159	37.93	0.000	92.17	0.416	4.43	0.403	5.49	0.391	6.60
0.040	0.253	19.29	0.156	33.45	0.000	90.24	0.436	4.27	0.435	5.23	0.415	6.22
0.057	0.273	18.00	0.220	32.00	0.000	83.[illegible]	0.456	4.15	0.446	5.01	0.432	5.87
0.080	0.292	16.18	0.192	28.00	0.000	73.24	0.475	3.92	0.465	4.63	0.456	5.46
0.113	0.315	14.34	0.223	25.04	0.000	63.76	0.497	3.61	0.493	4.36	0.477	5.13
0.160	0.326	12.86	0.245	20.55	0.000	46.30	0.528	3.24	0.520	4.00	0.503	4.73
0.226	0.354	10.97	0.269	16.56	0.000	36.73	0.559	2.94	0.547	3.72	0.533	4.28
0.320	0.413	9.28	0.322	13.64	0.081	25.47	0.589	2.55	0.578	3.19	0.566	3.77
0.453	0.448	7.68	0.369	10.42	0.200	18.31	0.620	2.27	0.612	2.73	0.600	3.28
0.640	0.513	6.08	0.444	8.26	0.338	12.54	0.659	1.95	0.647	2.26	0.642	2.67
0.905	0.580	4.61	0.513	6.09	0.436	8.48	0.701	1.61	0.696	1.88	0.682	2.16
1.280	0.651	3.31	0.610	4.20	0.540	5.69	0.753	1.32	0.744	1.44	0.734	1.66
1.500	0.686	2.78	0.664	3.24	0.590	4.52	0.778	1.12	0.771	1.31	0.766	1.42
2.000	0.772	1.96	0.734	2.18	0.713	2.96	0.824	0.90	0.823	1.00	0.821	1.03
2.500	0.822	1.35	0.811	1.41	0.785	1.77	0.871	0.64	0.869	0.72	0.862	0.80
3.000	0.886	0.94	0.864	0.95	0.850	1.07	0.908	0.46	0.910	0.55	0.903	0.49
3.500	0.926	0.59	0.917	0.49	0.903	0.59	0.941	0.35	0.938	0.37	0.937	0.37
4.000	0.961	0.30	0.958	0.22	0.946	0.34	0.966	0.21	0.964	0.33	0.960	0.21
4.500	0.983	0.08	0.982	0.06	0.976	0.16	0.985	0.09	0.982	0.11	0.984	0.08
5.000	0.994	-0.00	0.993	-0.00	0.993	0.02	0.994	0.05	0.992	0.06	0.993	0.04
5.500	0.999	-0.01	0.997	-0.00	0.999	-0.02	0.996	-0.00	0.998	-0.06	0.998	-0.06
6.000	1.001	-0.06	0.999	-0.04	1.000	0.05	1.000	0.06	0.999	-0.05	1.000	-0.03
6.500	1.000	0.02	1.000	-0.04	1.001	0.14	0.999	0.01	1.000	-0.10	1.001	-0.03
7.000	0.999	0.02	1.001	-0.04	0.999	0.14	1.001	0.01	1.000	-0.04	0.999	-0.06

TABLE 3—*continued*
Velocity Profiles.

Profile No	327		326		325		324		323		322	
y	u/U	beta	u/U	beta	u/U	beta	u/U	beta	u/U	beta	u/U	beta
0.010	0.323	9.37	0.305	11.86	0.287	15.69	0.260	21.60	0.204	32.74	0.154	52.96
0.014	0.342	8.86	0.321	11.44	0.304	14.93	0.279	20.36	0.209	32.74	0.175	52.44
0.020	0.370	8.33	0.341	11.04	0.319	14.30	0.292	19.86	0.242	31.05	0.183	50.68
0.028	0.380	8.15	0.358	10.27	0.334	13.71	0.302	18.92	0.247	30.50	0.183	49.72
0.040	0.401	7.88	0.374	9.73	0.349	12.61	0.312	18.14	0.261	28.81	0.175	48.08
0.057	0.419	7.42	0.394	9.28	0.368	12.26	0.334	17.18	0.283	25.33	0.191	43.73
0.080	0.439	6.95	0.413	8.86	0.388	11.21	0.355	15.54	0.297	23.38	0.200	40.28
0.113	0.462	6.43	0.438	7.86	0.408	10.32	0.372	14.43	0.312	21.77	0.198	36.49
0.160	0.484	5.87	0.458	7.29	0.433	9.23	0.400	12.90	0.338	18.89	0.228	30.66
0.226	0.512	5.11	0.494	6.49	0.459	8.09	0.421	11.24	0.363	16.37	0.254	25.15
0.320	0.549	4.55	0.533	5.68	0.500	6.99	0.460	9.41	0.405	13.63	0.302	20.86
0.453	0.589	3.91	0.563	4.79	0.533	5.90	0.504	7.85	0.444	10.95	0.368	15.45
0.640	0.627	3.35	0.608	3.92	0.586	4.92	0.554	6.38	0.507	8.37	0.423	11.84
0.905	0.670	2.72	0.651	3.23	0.630	3.92	0.610	4.99	0.566	6.21	0.500	8.84
1.280	0.724	2.06	0.716	2.53	0.691	2.94	0.674	3.61	0.644	4.72	0.593	5.94
1.500	0.751	1.86	0.746	2.24	0.724	2.58	0.708	3.20	0.678	4.02	0.630	4.93
2.000	0.814	1.29	0.803	1.63	0.790	1.85	0.771	2.23	0.747	2.67	0.713	3.35
2.500	0.857	0.88	0.857	1.04	0.842	1.43	0.830	1.61	0.816	1.86	0.780	2.21
3.000	0.900	0.73	0.896	0.70	0.891	0.93	0.881	1.12	0.865	1.21	0.857	1.45
3.500	0.931	0.40	0.933	0.48	0.924	0.54	0.920	0.74	0.913	0.70	0.907	0.82
4.000	0.963	0.26	0.964	0.32	0.957	0.26	0.956	0.51	0.948	0.41	0.945	0.50
4.500	0.980	0.14	0.984	0.13	0.978	0.13	0.976	0.24	0.974	0.26	0.968	0.14
5.000	0.994	-0.00	0.992	0.02	0.993	0.04	0.991	0.06	0.989	0.00	0.989	0.06
5.500	0.997	0.04	0.999	-0.03	0.998	-0.08	0.998	-0.05	0.996	0.00	0.997	-0.04
6.000	0.999	0.04	0.999	-0.07	0.999	-0.14	0.999	-0.10	1.000	-0.06	0.999	-0.08
6.500	1.000	-0.00	1.000	-0.07	1.000	-0.14	1.000	-0.07	0.999	-0.06	1.000	-0.08
7.000	1.000	-0.00	1.001	-0.07	1.000	-0.14	1.001	-0.04	1.001	-0.06	1.001	-0.04

Profile No	321		430		429		428		427		426	
y	u/U	beta	u/U	beta	u/U	beta	u/U	beta	u/U	beta	u/U	beta
0.010	0.090	85.91	0.360	6.91	0.355	8.06	0.345	9.62	0.328	12.21	0.314	15.36
0.014	0.083	85.33	0.379	6.54	0.372	7.73	0.359	9.26	0.343	11.64	0.337	14.47
0.020	0.090	84.93	0.401	6.41	0.389	7.43	0.379	9.01	0.357	11.27	0.348	14.08
0.028	0.107	84.51	0.413	6.14	0.412	7.20	0.396	8.77	0.382	10.62	0.364	13.61
0.040	0.122	83.18	0.436	6.02	0.425	6.89	0.417	8.25	0.401	10.16	0.384	12.91
0.057	0.117	77.72	0.452	5.61	0.447	6.54	0.439	7.89	0.412	9.52	0.400	12.12
0.080	0.107	74.36	0.478	5.36	0.464	6.14	0.458	7.41	0.433	8.99	0.420	11.47
0.113	0.094	68.09	0.502	5.01	0.495	5.78	0.481	6.75	0.465	8.23	0.439	10.53
0.160	0.112	58.07	0.531	4.50	0.520	5.35	0.509	6.14	0.486	7.45	0.468	9.49
0.226	0.121	47.53	0.556	4.15	0.545	4.74	0.524	5.62	0.518	6.69	0.491	8.35
0.320	0.173	35.75	0.594	3.64	0.575	4.19	0.567	4.96	0.548	5.97	0.530	7.27
0.453	0.264	25.87	0.622	3.15	0.614	3.66	0.602	4.29	0.584	5.05	0.558	6.18
0.640	0.347	17.85	0.659	2.72	0.649	3.05	0.635	3.48	0.622	4.26	0.608	5.15
0.905	0.452	12.53	0.698	2.22	0.689	2.57	0.679	2.88	0.666	3.46	0.653	4.15
1.280	0.558	8.19	0.754	1.83	0.742	2.01	0.729	2.15	0.720	2.58	0.716	3.26
1.500	0.596	6.69	0.778	1.67	0.765	1.76	0.758	1.88	0.749	2.27	0.735	2.80
2.000	0.694	4.19	0.824	1.17	0.818	1.36	0.809	1.38	0.798	1.62	0.786	1.89
2.500	0.777	2.65	0.866	0.81	0.860	0.96	0.859	1.02	0.847	1.17	0.845	1.43
3.000	0.842	1.65	0.904	0.48	0.902	0.62	0.898	0.74	0.891	0.83	0.886	0.92
3.500	0.894	0.91	0.939	0.36	0.938	0.47	0.932	0.51	0.925	0.56	0.921	0.59
4.000	0.937	0.41	0.968	0.22	0.965	0.28	0.959	0.31	0.960	0.34	0.953	0.34
4.500	0.966	0.19	0.982	0.08	0.981	0.11	0.981	0.15	0.978	0.13	0.980	0.18
5.000	0.989	0.02	0.995	-0.00	0.993	0.03	0.993	0.04	0.991	0.04	0.991	0.05
5.500	0.997	-0.01	0.998	-0.02	0.998	-0.07	0.998	-0.05	0.998	-0.03	0.998	-0.04
6.000	0.998	-0.04	0.999	-0.05	1.000	-0.09	1.000	-0.05	1.000	-0.06	1.000	-0.08
6.500	1.000	0.04	1.000	-0.05	1.001	-0.09	1.001	-0.08	1.000	-0.10	1.000	-0.08
7.000	1.000	0.11	1.000	-0.05	0.999	-0.09	1.000	-0.08	1.001	-0.06	1.001	-0.08

Profile No	425		424		423		422		421		530	
y	u/U	beta	u/U	beta	u/U	beta	u/U	beta	u/U	beta	u/U	beta
0.010	0.299	20.01	0.275	27.10	0.244	38.84	0.201	56.75	0.166	78.55	0.362	8.33
0.014	0.308	19.63	0.300	26.48	0.259	37.31	0.214	55.56	0.177	78.10	0.376	8.13
0.020	0.325	18.71	0.303	25.79	0.267	36.60	0.227	54.89	0.189	77.38	0.395	7.66
0.028	0.336	18.15	0.322	24.83	0.282	35.55	0.225	53.99	0.203	76.09	0.411	7.34
0.040	0.359	16.86	0.339	23.17	0.297	33.61	0.239	52.01	0.206	73.90	0.433	7.10
0.057	0.372	16.20	0.353	21.95	0.312	30.68	0.254	48.93	0.215	73.13	0.451	6.77
0.080	0.390	15.27	0.372	20.21	0.319	28.51	0.260	45.15	0.207	71.17	0.476	6.39
0.113	0.407	13.83	0.386	18.31	0.341	26.30	0.273	41.94	0.210	65.80	0.499	5.97
0.160	0.439	12.37	0.400	16.61	0.355	23.36	0.290	36.60	0.213	59.86	0.528	5.40
0.226	0.468	10.86	0.440	14.59	0.387	20.37	0.324	30.58	0.223	50.64	0.552	4.94
0.320	0.502	9.59	0.466	12.65	0.423	17.02	0.354	25.41	0.252	41.53	0.586	4.38
0.453	0.537	8.03	0.509	10.43	0.468	13.82	0.402	20.32	0.309	30.68	0.618	3.85
0.640	0.586	6.54	0.558	8.44	0.519	11.10	0.466	15.35	0.378	22.47	0.647	3.25
0.905	0.631	5.15	0.610	6.59	0.572	8.42	0.534	11.19	0.467	15.51	0.689	2.62
1.280	0.692	3.99	0.678	5.00	0.649	6.18	0.619	7.99	0.564	10.55	0.739	2.00
1.500	0.718	3.46	0.703	4.17	0.690	5.03	0.649	6.74	0.607	8.70	0.764	1.71
2.000	0.780	2.43	0.768	2.90	0.752	3.55	0.730	4.46	0.695	5.53	0.816	1.24
2.500	0.837	1.73	0.820	2.11	0.810	2.37	0.796	2.92	0.774	3.55	0.856	0.90
3.000	0.880	1.20	0.871	1.49	0.861	1.60	0.845	1.91	0.833	2.18	0.897	0.61
3.500	0.918	0.74	0.907	0.98	0.908	1.06	0.903	1.15	0.889	1.28	0.933	0.43
4.000	0.951	0.42	0.950	0.60	0.942	0.60	0.933	0.60	0.936	0.67	0.957	0.20
4.500	0.972	0.23	0.974	0.26	0.965	0.24	0.965	0.28	0.962	0.31	0.978	0.09
5.000	0.989	0.05	0.990	0.10	0.985	0.06	0.983	0.12	0.987	0.12	0.991	0.03
5.500	0.996	-0.01	0.996	-0.02	0.995	-0.00	0.996	-0.01	0.996	-0.01	0.997	-0.00
6.000	1.001	-0.12	0.999	-0.05	1.000	-0.04	1.000	-0.05	1.000	-0.01	1.000	0.05
6.500	1.001	-0.16	1.001	-0.05	1.000	-0.04	1.000	-0.05	0.999	0.05	1.001	0.05
7.000	0.999	-0.09	1.000	-0.02	1.001	-0.04	1.000	0.03	1.000	0.20	1.000	0.02

TABLE 3—*continued*
Velocity Profiles.

Profile No	529		528		527		526		525		524	
y	u/U	beta	u/U	beta	u/U	beta	u/U	beta	u/U	beta	u/U	beta
0.010	0.355	9.91	0.344	11.75	0.329	14.60	0.332	18.31	0.309	23.23	0.298	31.10
0.014	0.367	9.51	0.364	11.37	0.357	13.94	0.335	17.44	0.329	22.23	0.311	29.51
0.020	0.389	9.31	0.388	11.03	0.372	13.41	0.356	16.96	0.343	21.84	0.323	29.08
0.028	0.409	8.98	0.397	10.57	0.383	13.12	0.369	16.35	0.354	21.25	0.332	27.98
0.040	0.424	8.47	0.419	10.14	0.405	12.54	0.391	15.45	0.371	20.27	0.347	27.19
0.057	0.453	7.93	0.440	9.66	0.420	11.97	0.410	14.77	0.386	19.20	0.366	25.56
0.080	0.471	7.52	0.461	9.09	0.440	11.17	0.425	13.79	0.408	17.89	0.382	23.72
0.113	0.493	6.92	0.480	8.49	0.463	10.44	0.450	12.76	0.428	16.15	0.407	21.62
0.160	0.520	6.32	0.500	7.58	0.490	9.30	0.468	11.56	0.448	14.84	0.417	19.65
0.226	0.541	5.66	0.532	6.91	0.515	8.46	0.495	10.42	0.476	13.01	0.451	17.45
0.320	0.572	5.05	0.557	5.96	0.551	7.43	0.530	9.20	0.505	11.42	0.481	14.89
0.453	0.608	4.33	0.597	5.08	0.584	6.39	0.562	7.77	0.546	9.79	0.526	12.38
0.640	0.639	3.69	0.635	4.35	0.621	5.29	0.604	6.48	0.583	8.12	0.565	10.31
0.905	0.682	2.99	0.675	3.55	0.663	4.27	0.651	5.09	0.629	6.40	0.614	8.10
1.280	0.735	2.43	0.727	2.76	0.721	3.31	0.702	3.88	0.687	4.76	0.671	6.21
1.500	0.756	2.04	0.751	2.42	0.741	2.83	0.730	3.26	0.713	4.01	0.703	5.22
2.000	0.807	1.42	0.801	1.76	0.796	2.03	0.783	2.33	0.772	2.73	0.763	3.64
2.500	0.857	1.04	0.847	1.20	0.842	1.50	0.833	1.60	0.826	1.92	0.819	2.46
3.000	0.891	0.73	0.891	0.76	0.883	1.04	0.876	1.12	0.867	1.34	0.865	1.63
3.500	0.926	0.38	0.925	0.43	0.921	0.75	0.914	0.73	0.909	0.80	0.910	1.06
4.000	0.959	0.26	0.956	0.31	0.952	0.43	0.946	0.42	0.944	0.42	0.940	0.60
4.500	0.978	0.07	0.975	0.10	0.974	0.21	0.971	0.25	0.971	0.19	0.966	0.28
5.000	0.991	0.03	0.992	0.00	0.988	0.09	0.988	0.05	0.987	0.07	0.987	0.08
5.500	0.997	-0.01	0.998	0.00	0.997	-0.02	0.997	-0.01	0.995	0.00	0.996	-0.01
6.000	0.999	0.01	0.999	0.00	0.999	-0.02	0.999	-0.01	0.998	0.00	0.999	-0.04
6.500	0.999	0.03	1.000	0.00	1.000	-0.02	1.000	0.01	1.002	0.00	1.000	-0.06
7.000	1.001	0.03	1.000	0.00	1.000	-0.01	1.000	0.01	1.000	0.00	1.001	-0.04

Profile No	523		522		521		630		629		628	
y	u/U	beta	u/U	beta	u/U	beta	u/U	beta	u/U	beta	u/U	beta
0.010	0.275	40.55	0.254	55.25	0.223	71.90	0.365	9.52	0.353	11.51	0.346	13.57
0.014	0.300	39.47	0.257	54.35	0.248	70.54	0.390	9.07	0.369	10.89	0.369	12.94
0.020	0.309	38.46	0.278	53.53	0.267	70.41	0.402	8.82	0.392	10.53	0.386	12.28
0.028	0.317	37.22	0.282	52.14	0.274	69.98	0.417	8.55	0.405	10.26	0.401	12.12
0.040	0.334	35.99	0.293	50.37	0.288	68.84	0.432	8.36	0.425	9.78	0.421	11.50
0.057	0.343	34.21	0.302	47.97	0.293	66.50	0.456	7.95	0.445	9.31	0.437	11.02
0.080	0.362	31.15	0.320	45.84	0.293	65.04	0.481	7.53	0.463	8.73	0.457	10.42
0.113	0.369	29.43	0.331	42.01	0.295	60.62	0.503	6.84	0.487	8.18	0.481	9.73
0.160	0.398	25.98	0.350	37.75	0.295	55.80	0.527	6.43	0.514	7.48	0.504	8.84
0.226	0.420	22.88	0.369	32.82	0.309	48.61	0.549	5.61	0.544	6.73	0.529	7.93
0.320	0.449	19.47	0.397	27.64	0.331	40.48	0.582	5.04	0.569	5.82	0.560	7.04
0.453	0.489	16.35	0.447	21.95	0.380	31.67	0.614	4.25	0.604	4.98	0.593	6.04
0.640	0.547	13.13	0.504	17.05	0.438	23.70	0.649	3.62	0.639	4.14	0.626	4.99
0.905	0.595	10.01	0.562	12.80	0.512	17.12	0.685	2.92	0.682	3.39	0.670	4.00
1.280	0.664	7.45	0.637	9.15	0.597	11.64	0.736	2.26	0.729	2.61	0.718	3.06
1.500	0.696	6.24	0.672	7.77	0.640	9.65	0.758	1.96	0.752	2.21	0.747	2.60
2.000	0.751	4.49	0.738	5.23	0.706	6.29	0.810	1.41	0.803	1.56	0.796	1.82
2.500	0.810	3.00	0.803	3.58	0.790	4.22	0.853	1.07	0.853	1.09	0.846	1.27
3.000	0.862	2.09	0.850	2.37	0.839	2.59	0.895	0.73	0.888	0.75	0.891	0.83
3.500	0.905	1.25	0.899	1.50	0.888	1.61	0.929	0.48	0.924	0.41	0.925	0.53
4.000	0.939	0.69	0.935	0.85	0.928	0.86	0.958	0.29	0.953	0.26	0.953	0.25
4.500	0.966	0.37	0.966	0.35	0.963	0.34	0.978	0.13	0.977	0.06	0.976	0.09
5.000	0.987	0.10	0.986	0.07	0.984	0.18	0.993	-0.01	0.990	0.01	0.991	-0.01
5.500	0.996	-0.00	0.996	-0.01	0.994	0.01	0.997	0.04	0.997	0.00	0.996	0.01
6.000	1.000	0.01	1.000	-0.06	0.999	-0.02	1.000	0.06	1.000	0.04	1.000	0.03
6.500	1.001	0.01	1.000	-0.02	1.001	0.10	1.001	0.10	1.000	0.05	1.001	0.03
7.000	1.000	0.06	1.000	-0.01	1.000	0.24	1.000	0.10	1.000	0.04	0.999	0.03

Profile No	627		626		625		624		623		622	
y	u/U	beta	u/U	beta	u/U	beta	u/U	beta	u/U	beta	u/U	beta
0.010	0.343	16.07	0.345	20.80	0.332	24.30	0.305	32.02	0.305	39.72	0.297	51.47
0.014	0.365	15.19	0.355	19.67	0.340	23.67	0.336	30.73	0.322	38.81	0.313	50.53
0.020	0.372	14.87	0.376	18.73	0.358	22.97	0.346	30.24	0.336	38.25	0.329	49.37
0.028	0.391	14.42	0.386	17.87	0.372	22.21	0.364	28.97	0.346	37.12	0.333	48.78
0.040	0.413	13.71	0.404	17.36	0.392	21.36	0.380	28.10	0.357	36.53	0.346	47.72
0.057	0.427	13.11	0.422	16.64	0.406	20.58	0.396	26.29	0.371	34.42	0.359	45.65
0.080	0.447	12.39	0.434	15.63	0.427	19.39	0.405	25.04	0.388	32.19	0.368	43.09
0.113	0.473	11.51	0.461	14.22	0.442	17.79	0.423	22.95	0.402	29.76	0.377	40.58
0.160	0.497	10.63	0.482	13.17	0.468	16.29	0.450	20.65	0.423	26.87	0.395	36.24
0.226	0.517	9.44	0.506	11.88	0.490	14.58	0.470	18.45	0.445	24.13	0.418	32.37
0.320	0.545	8.45	0.541	10.34	0.518	12.63	0.501	16.39	0.474	20.97	0.440	27.26
0.453	0.588	7.30	0.576	8.82	0.556	10.91	0.538	13.74	0.519	17.42	0.486	22.47
0.640	0.620	6.25	0.611	7.39	0.598	8.93	0.577	11.38	0.559	14.26	0.526	17.71
0.905	0.663	4.96	0.658	6.05	0.635	7.24	0.624	8.95	0.614	10.92	0.594	13.50
1.280	0.713	3.75	0.707	4.62	0.692	5.58	0.679	6.87	0.667	8.12	0.647	9.87
1.500	0.739	3.22	0.735	4.04	0.723	4.75	0.713	5.83	0.695	6.95	0.690	8.18
2.000	0.795	2.26	0.783	2.77	0.777	3.37	0.766	4.16	0.758	4.90	0.751	5.53
2.500	0.842	1.59	0.837	1.94	0.826	2.28	0.822	2.96	0.809	3.34	0.802	3.77
3.000	0.882	1.04	0.880	1.28	0.873	1.61	0.870	1.98	0.858	2.23	0.854	2.52
3.500	0.923	0.71	0.914	0.76	0.909	1.03	0.902	1.30	0.902	1.49	0.895	1.54
4.000	0.952	0.36	0.948	0.38	0.944	0.58	0.943	0.68	0.932	0.81	0.932	0.82
4.500	0.973	0.24	0.974	0.13	0.970	0.27	0.967	0.30	0.964	0.42	0.961	0.28
5.000	0.990	0.06	0.989	0.02	0.988	0.11	0.986	0.11	0.984	0.13	0.982	0.01
5.500	0.998	-0.04	0.997	-0.00	0.995	0.00	0.996	-0.01	0.995	-0.00	0.995	0.00
6.000	0.999	0.00	0.999	-0.02	1.000	0.00	0.999	-0.01	0.999	0.06	0.999	-0.02
6.500	1.000	-0.01	1.001	-0.02	1.001	0.00	1.000	0.01	1.000	0.11	1.001	0.03
7.000	1.000	0.00	0.999	-0.00	1.000	0.00	1.000	0.07	1.000	0.21	0.999	0.13

TABLE 3—*continued*
Velocity Profiles.

Profile No	521		620		730		729		728		727	
y	u/U	beta	u/U	beta	u/U	beta	u/U	beta	u/U	beta	u/U	beta
0.010	0.288	64.18	0.286	73.65	0.363	10.64	0.353	12.39	0.354	14.60	0.341	17.52
0.014	0.310	63.23	0.302	72.79	0.380	10.34	0.380	11.75	0.368	14.14	0.358	16.66
0.020	0.323	62.98	0.319	72.18	0.403	9.96	0.397	11.45	0.388	13.55	0.382	16.29
0.028	0.331	62.58	0.340	71.82	0.419	9.63	0.412	11.10	0.409	13.02	0.399	15.48
0.040	0.343	61.89	0.352	71.44	0.448	9.17	0.433	10.65	0.427	12.58	0.416	14.99
0.057	0.348	60.21	0.349	70.95	0.462	8.88	0.449	10.17	0.446	12.11	0.432	14.47
0.080	0.352	58.94	0.359	69.45	0.480	8.47	0.471	9.57	0.466	11.42	0.451	13.54
0.113	0.361	55.94	0.355	66.57	0.509	7.77	0.494	8.86	0.491	10.53	0.475	12.35
0.160	0.373	49.97	0.349	63.05	0.530	7.23	0.520	8.13	0.509	9.54	0.500	11.33
0.226	0.389	44.96	0.341	59.59	0.556	6.52	0.547	7.32	0.535	8.75	0.520	10.37
0.320	0.397	38.86	0.348	51.02	0.584	5.74	0.576	6.41	0.567	7.70	0.554	9.03
0.453	0.438	30.77	0.357	44.64	0.616	5.00	0.608	5.64	0.599	6.71	0.584	7.78
0.640	0.489	23.76	0.409	34.45	0.653	4.09	0.645	4.80	0.640	5.62	0.624	6.57
0.905	0.552	17.58	0.481	25.19	0.691	3.33	0.686	3.79	0.675	4.71	0.659	5.36
1.280	0.620	12.63	0.565	17.07	0.738	2.59	0.732	2.98	0.724	3.60	0.713	4.23
1.500	0.663	10.55	0.612	13.52	0.763	2.27	0.756	2.49	0.750	3.10	0.744	3.59
2.000	0.736	6.88	0.700	8.54	0.812	1.61	0.804	1.79	0.803	2.13	0.794	2.59
2.500	0.797	4.58	0.777	5.08	0.857	1.16	0.857	1.20	0.855	1.59	0.843	1.82
3.000	0.845	2.93	0.830	3.11	0.898	0.77	0.901	0.79	0.892	0.97	0.887	1.26
3.500	0.887	1.74	0.882	1.72	0.931	0.44	0.936	0.43	0.928	0.57	0.928	0.72
4.000	0.927	0.99	0.923	0.88	0.960	0.25	0.960	0.13	0.961	0.30	0.953	0.35
4.500	0.960	0.44	0.955	0.33	0.981	0.09	0.979	0.02	0.980	0.09	0.977	0.14
5.000	0.980	0.04	0.980	0.13	0.992	0.03	0.992	-0.01	0.992	0.01	0.991	-0.03
5.500	0.994	-0.00	0.993	-0.01	0.997	-0.01	0.998	0.02	0.998	0.01	0.997	0.04
6.000	0.998	0.08	1.001	0.14	0.999	0.07	1.000	0.06	1.000	0.07	0.998	0.07
6.500	1.001	0.21	1.000	0.29	1.001	0.05	1.000	0.10	1.001	0.13	1.000	0.10
7.000	1.001	0.35	0.999	0.46	1.000	0.11	1.000	0.05	0.999	0.13	1.001	0.10

Profile No	726		725		724		723		722		721	
y	u/U	beta	u/U	beta	u/U	beta	u/U	beta	u/U	beta	u/U	beta
0.010	0.335	20.34	0.328	25.53	0.314	31.49	0.323	38.39	0.317	48.70	0.327	59.69
0.014	0.358	19.84	0.346	24.95	0.339	30.65	0.340	38.06	0.342	47.90	0.348	58.87
0.020	0.368	19.34	0.364	24.23	0.354	30.03	0.355	37.20	0.360	46.89	0.362	58.17
0.028	0.383	18.95	0.380	23.58	0.370	29.14	0.378	36.05	0.367	46.50	0.374	57.43
0.040	0.402	18.29	0.395	22.25	0.383	28.40	0.390	35.09	0.377	45.19	0.381	56.79
0.057	0.421	17.42	0.415	21.23	0.400	27.20	0.395	33.16	0.393	43.69	0.392	56.01
0.080	0.440	16.35	0.427	20.20	0.416	25.56	0.407	31.38	0.403	41.54	0.402	53.69
0.113	0.460	15.22	0.449	18.69	0.431	23.74	0.430	29.10	0.415	39.33	0.403	51.72
0.160	0.484	13.85	0.472	16.92	0.453	21.29	0.453	26.74	0.434	35.48	0.415	47.69
0.226	0.504	12.47	0.491	15.32	0.481	19.25	0.466	24.16	0.448	32.12	0.431	42.85
0.320	0.536	10.93	0.521	13.41	0.508	16.54	0.494	20.85	0.475	27.44	0.454	36.72
0.453	0.567	9.37	0.557	11.36	0.544	14.24	0.529	17.66	0.510	22.92	0.482	30.57
0.640	0.616	7.81	0.596	9.38	0.580	11.75	0.572	14.39	0.551	18.56	0.521	23.83
0.905	0.655	6.34	0.640	7.51	0.619	9.27	0.617	11.62	0.602	14.23	0.571	18.10
1.280	0.706	4.83	0.691	5.76	0.678	6.96	0.668	8.54	0.650	10.66	0.634	13.02
1.500	0.729	4.25	0.717	4.92	0.707	5.86	0.704	7.19	0.693	8.90	0.674	10.85
2.000	0.787	3.00	0.774	3.52	0.769	4.15	0.759	5.02	0.745	6.11	0.734	7.40
2.500	0.842	2.22	0.825	2.45	0.816	2.91	0.811	3.48	0.800	4.12	0.791	5.00
3.000	0.882	1.47	0.876	1.69	0.869	1.90	0.860	2.30	0.852	2.66	0.842	3.12
3.500	0.920	0.96	0.914	1.06	0.908	1.17	0.900	1.35	0.887	1.61	0.889	1.85
4.000	0.951	0.43	0.946	0.58	0.942	0.55	0.937	0.83	0.926	0.91	0.927	0.99
4.500	0.975	0.17	0.971	0.22	0.969	0.25	0.966	0.27	0.960	0.38	0.960	0.40
5.000	0.989	0.03	0.987	0.03	0.988	0.00	0.985	0.09	0.983	0.13	0.982	0.11
5.500	0.998	0.01	0.997	0.01	0.995	0.00	0.996	-0.00	0.993	0.01	0.993	-0.00
6.000	0.999	0.09	0.999	0.05	1.000	0.04	1.000	0.03	0.998	0.01	0.998	0.05
6.500	0.999	0.15	1.000	0.06	1.001	0.04	1.001	0.09	1.001	0.11	1.000	0.17
7.000	1.001	0.13	1.000	0.07	1.000	0.08	1.000	0.13	1.000	0.22	1.001	0.31

Profile No	720		829		828		827		826		825	
y	u/U	beta	u/U	beta	u/U	beta	u/U	beta	u/U	beta	u/U	beta
0.010	0.323	67.89	0.368	13.06	0.367	14.82	0.354	17.70	0.350	22.71	0.350	25.32
0.014	0.347	67.38	0.395	12.40	0.387	14.55	0.379	17.20	0.369	20.96	0.367	24.67
0.020	0.371	67.14	0.411	12.15	0.402	14.32	0.401	16.60	0.386	20.26	0.382	24.27
0.028	0.382	66.60	0.426	11.89	0.422	13.88	0.414	16.39	0.403	19.39	0.395	23.65
0.040	0.398	66.26	0.447	11.28	0.442	13.17	0.429	15.76	0.418	18.61	0.414	22.62
0.057	0.408	65.85	0.467	10.70	0.456	12.62	0.452	14.91	0.439	17.80	0.431	21.63
0.080	0.411	64.14	0.483	10.17	0.477	11.95	0.469	13.98	0.458	16.74	0.453	20.25
0.113	0.415	62.21	0.509	9.43	0.497	11.06	0.492	13.32	0.478	15.71	0.470	18.69
0.160	0.416	58.79	0.536	8.76	0.522	10.17	0.512	12.12	0.500	14.48	0.490	17.31
0.226	0.417	54.21	0.558	7.81	0.549	9.13	0.542	10.81	0.527	12.80	0.514	15.62
0.320	0.417	48.24	0.594	6.90	0.578	8.04	0.570	9.39	0.553	11.47	0.539	13.79
0.453	0.437	40.84	0.621	6.00	0.616	6.95	0.600	8.20	0.585	9.83	0.573	11.75
0.640	0.475	32.43	0.653	5.03	0.651	5.83	0.639	6.81	0.623	8.12	0.613	9.83
0.905	0.538	24.17	0.701	4.17	0.686	4.80	0.680	5.52	0.671	6.52	0.654	7.84
1.280	0.599	17.21	0.746	3.30	0.735	3.79	0.734	4.19	0.722	5.05	0.711	5.91
1.500	0.647	13.78	0.768	2.85	0.758	3.28	0.753	3.67	0.751	4.21	0.735	5.06
2.000	0.720	8.79	0.821	2.07	0.819	2.39	0.810	2.69	0.803	3.03	0.799	3.60
2.500	0.778	5.65	0.867	1.38	0.860	1.69	0.857	1.87	0.850	2.18	0.841	2.53
3.000	0.834	3.58	0.906	0.91	0.902	1.18	0.898	1.27	0.881	1.43	0.882	1.70
3.500	0.880	2.02	0.939	0.54	0.937	0.67	0.934	0.76	0.927	0.83	0.924	1.00
4.000	0.921	0.94	0.967	0.16	0.964	0.26	0.962	0.31	0.959	0.35	0.956	0.50
4.500	0.955	0.34	0.986	0.01	0.984	0.14	0.981	0.11	0.979	0.10	0.978	0.17
5.000	0.978	-0.00	0.996	-0.01	0.993	0.01	0.992	0.00	0.992	0.00	0.990	-0.01
5.500	0.994	-0.00	0.997	0.00	0.998	0.02	0.999	0.02	0.997	0.02	0.996	0.01
6.000	0.998	0.03	1.000	0.09	0.999	0.07	1.000	0.08	1.000	0.10	1.000	0.03
6.500	1.000	0.29	1.000	0.05	1.000	0.06	1.000	0.08	1.001	0.08	1.000	0.03
7.000	1.000	0.42	1.000	0.03	1.000	0.04	1.000	0.04	1.000	0.05	1.000	0.03

TABLE 3—*concluded*

Velocity Profiles.

Profile No	824		823		822		821		820	
y	u/U	beta	u/U	beta	u/U	beta	u/U	beta	u/U	beta
0.010	0.358	29.96	0.346	37.45	0.348	45.43	0.356	54.32	0.368	61.66
0.014	0.354	29.51	0.367	36.75	0.367	44.84	0.370	53.90	0.387	61.35
0.020	0.377	29.10	0.383	35.88	0.386	43.99	0.390	53.37	0.410	61.16
0.028	0.391	28.17	0.396	35.32	0.396	43.26	0.398	52.90	0.417	60.96
0.040	0.411	27.30	0.410	34.00	0.408	42.21	0.411	51.98	0.430	60.69
0.057	0.420	26.23	0.419	33.15	0.418	41.18	0.421	51.37	0.437	59.82
0.080	0.440	24.90	0.439	30.99	0.431	38.90	0.431	49.85	0.450	58.71
0.113	0.457	22.91	0.454	28.74	0.445	36.28	0.439	47.50	0.454	56.56
0.160	0.479	21.40	0.470	26.68	0.458	33.86	0.446	44.15	0.458	54.29
0.226	0.502	19.12	0.489	23.89	0.473	30.54	0.457	40.47	0.462	49.84
0.320	0.525	16.72	0.519	20.82	0.497	26.98	0.481	35.28	0.467	44.39
0.453	0.561	14.16	0.550	17.88	0.526	22.39	0.507	29.34	0.486	37.55
0.640	0.598	11.87	0.584	14.67	0.566	18.33	0.541	23.27	0.513	30.12
0.905	0.642	9.51	0.627	11.73	0.613	14.25	0.592	17.89	0.567	22.64
1.280	0.698	7.16	0.683	8.91	0.663	10.45	0.650	12.79	0.627	16.16
1.500	0.725	6.07	0.708	7.56	0.697	8.98	0.680	10.77	0.664	13.39
2.000	0.779	4.19	0.766	5.35	0.753	6.19	0.746	7.49	0.730	8.50
2.500	0.833	2.93	0.819	3.64	0.809	4.33	0.799	5.08	0.783	5.49
3.000	0.875	1.96	0.871	2.43	0.862	2.74	0.849	3.30	0.839	3.59
3.500	0.915	1.15	0.911	1.42	0.905	1.62	0.893	2.11	0.886	2.02
4.000	0.951	0.57	0.945	0.75	0.938	0.82	0.936	1.05	0.925	0.94
4.500	0.974	0.19	0.970	0.28	0.969	0.33	0.961	0.35	0.960	0.34
5.000	0.989	0.05	0.987	0.08	0.986	0.08	0.986	0.05	0.982	0.03
5.500	0.997	-0.00	0.997	-0.01	0.996	0.00	0.994	-0.01	0.994	-0.01
6.000	1.001	0.04	0.999	0.05	1.000	0.12	0.999	0.07	1.000	0.12
6.500	0.999	0.06	1.000	0.07	1.000	0.19	1.001	0.20	0.999	0.32
7.000	1.001	0.06	1.000	0.09	0.999	0.24	1.000	0.25	1.000	0.46

Profile No	929		928		927		926		925	
y	u/U	beta	u/U	beta	u/U	beta	u/U	beta	u/U	beta
0.010	0.384	13.30	0.389	15.15	0.376	17.50	0.366	20.95	0.367	24.87
0.014	0.408	12.77	0.409	14.78	0.394	17.31	0.388	20.41	0.386	24.29
0.020	0.427	12.49	0.420	14.56	0.418	16.81	0.409	19.70	0.402	23.88
0.028	0.443	12.13	0.440	14.03	0.426	16.30	0.427	19.29	0.418	22.89
0.040	0.465	11.66	0.458	13.55	0.441	15.83	0.446	18.42	0.435	22.43
0.057	0.489	11.08	0.481	12.89	0.465	15.08	0.463	17.60	0.455	21.24
0.080	0.509	10.56	0.500	12.38	0.492	14.20	0.478	16.61	0.473	20.32
0.113	0.531	9.71	0.520	11.46	0.509	13.30	0.506	15.42	0.489	19.20
0.160	0.559	8.92	0.544	10.63	0.536	12.22	0.523	14.25	0.511	17.30
0.226	0.576	8.05	0.565	9.41	0.552	11.04	0.550	12.91	0.536	15.53
0.320	0.613	7.07	0.596	8.22	0.586	9.74	0.572	11.43	0.560	13.69
0.453	0.639	6.10	0.637	6.95	0.620	8.38	0.604	9.88	0.597	11.80
0.640	0.674	5.15	0.670	5.86	0.654	6.93	0.647	8.35	0.632	9.78
0.905	0.714	4.23	0.711	4.85	0.693	5.58	0.686	6.58	0.677	7.92
1.280	0.766	3.27	0.762	3.76	0.744	4.31	0.738	4.97	0.732	6.00
1.500	0.790	2.81	0.783	3.22	0.775	3.72	0.768	4.27	0.752	5.14
2.000	0.841	2.05	0.835	2.38	0.826	2.69	0.820	3.01	0.813	3.54
2.500	0.880	1.40	0.882	1.57	0.870	1.88	0.862	2.06	0.856	2.47
3.000	0.922	0.92	0.915	1.00	0.914	1.22	0.908	1.34	0.903	1.60
3.500	0.953	0.47	0.952	0.55	0.943	0.68	0.944	0.78	0.936	0.90
4.000	0.978	0.22	0.978	0.25	0.969	0.25	0.967	0.27	0.965	0.36
4.500	0.991	0.04	0.987	0.06	0.987	0.11	0.986	0.12	0.983	0.09
5.000	0.996	0.00	0.996	-0.00	0.996	0.00	0.994	0.01	0.995	-0.00
5.500	1.000	0.05	1.001	0.01	0.999	0.06	0.998	0.01	0.999	-0.05
6.000	1.000	0.05	1.000	0.01	1.000	0.04	1.000	0.01	0.999	-0.05
6.500	0.999	-0.03	1.001	-0.03	1.000	0.01	1.000	-0.02	0.999	-0.10
7.000	1.001	-0.11	0.999	-0.08	1.000	-0.04	0.999	-0.04	1.001	-0.07

Profile No	924		923		922		921		920	
y	u/U	beta	u/U	beta	u/U	beta	u/U	beta	u/U	beta
0.010	0.370	29.87	0.369	35.26	0.364	42.32	0.371	49.35	0.405	55.48
0.014	0.389	29.05	0.383	34.67	0.394	41.25	0.398	48.60	0.423	55.32
0.020	0.409	28.31	0.401	34.27	0.405	40.86	0.414	48.26	0.443	54.91
0.028	0.419	27.65	0.419	33.39	0.416	39.99	0.424	47.78	0.456	54.72
0.040	0.436	26.76	0.431	32.59	0.429	39.47	0.440	47.19	0.468	54.44
0.057	0.451	25.59	0.444	31.46	0.445	37.82	0.448	46.80	0.475	54.30
0.080	0.465	24.33	0.462	29.84	0.457	36.47	0.459	44.62	0.483	53.02
0.113	0.482	22.77	0.476	27.98	0.468	34.65	0.471	42.63	0.488	51.55
0.160	0.503	20.87	0.492	25.50	0.484	31.82	0.478	40.04	0.497	48.94
0.226	0.527	18.86	0.512	22.89	0.504	29.17	0.495	36.48	0.499	45.20
0.320	0.551	16.65	0.537	20.30	0.525	25.65	0.509	32.23	0.511	40.28
0.453	0.587	14.08	0.572	17.56	0.555	21.31	0.540	27.16	0.529	34.06
0.640	0.624	11.64	0.610	14.44	0.588	17.59	0.570	21.67	0.563	27.31
0.905	0.667	9.50	0.650	11.46	0.634	13.90	0.617	16.82	0.600	20.73
1.280	0.720	7.24	0.706	8.69	0.687	10.17	0.675	12.19	0.656	15.05
1.500	0.744	6.25	0.732	7.44	0.717	8.63	0.703	10.31	0.686	12.52
2.000	0.806	4.41	0.791	5.34	0.778	6.08	0.763	7.04	0.745	8.46
2.500	0.846	2.94	0.846	3.71	0.838	4.23	0.817	4.66	0.803	5.42
3.000	0.896	1.87	0.892	2.40	0.878	2.79	0.865	3.12	0.852	3.38
3.500	0.931	1.14	0.929	1.34	0.916	1.77	0.906	1.88	0.899	2.10
4.000	0.962	0.49	0.959	0.71	0.954	0.80	0.944	0.93	0.934	1.11
4.500	0.983	0.14	0.981	0.24	0.975	0.37	0.972	0.34	0.964	0.36
5.000	0.994	0.01	0.990	0.01	0.991	0.04	0.988	0.05	0.985	0.09
5.500	1.000	-0.00	0.998	0.01	0.999	-0.01	0.997	0.01	0.995	0.00
6.000	1.000	-0.00	0.999	0.01	1.001	0.04	0.999	0.10	0.999	0.18
6.500	1.000	-0.06	1.001	0.01	1.001	0.10	1.000	0.18	1.000	0.30
7.000	1.001	-0.06	1.000	0.01	0.999	0.10	1.000	0.25	1.000	0.45

TABLE 4

Static-Pressure Distributions through the Boundary Layer.

Profile	-230	-228	-226	-224	-222	30	28	26	24	22
y	c_p	c_p	c_p	c_p	c_p	c_p	c_p	c_p	c_p	c_p
0	0.304	0.343	0.387	0.435	0.473	0.307	0.348	0.393	0.445	0.486
0.08	0.304	0.339	0.381	0.428	0.466	0.303	0.338	0.382	0.429	0.476
0.16	0.300	0.339	0.382	0.428	0.465	0.303	0.339	0.380	0.428	0.474
0.32	0.300	0.337	0.381	0.425	0.465	0.302	0.338	0.380	0.427	0.472
0.61	0.298	0.338	0.381	0.426	0.462	0.300	0.337	0.379	0.427	0.471
1.28	0.300	0.338	0.378	0.422	0.461	0.301	0.338	0.380	0.426	0.470
2.00	0.302	0.337	0.378	0.420	0.456	0.302	0.338	0.381	0.426	0.469
3.00	0.301	0.337	-	0.416	0.452	0.304	0.338	0.380	0.424	0.466
4.00	0.301	0.337	0.375	0.413	0.449	0.304	0.340	0.380	0.424	0.466
5.00	0.302	0.336	0.372	0.412	0.452	0.305	0.340	0.380	0.424	0.470
6.00	0.300	0.335	0.372	0.414	0.458	0.305	0.339	0.380	0.423	0.472
7.00	0.299	0.334	0.372	0.415	0.467	0.304	0.339	0.380	0.426	0.479

Profile	230	228	226	224	222	430	428	426	424	422
y	c_p	c_p	c_p	c_p	c_p	c_p	c_p	c_p	c_p	c_p
0	0.304	0.345	0.390	0.437	0.479	0.299	0.334	0.376	0.420	0.454
0.08	0.302	0.340	0.383	0.430	0.471	0.295	0.330	0.369	0.410	0.445
0.16	0.301	0.338	0.383	0.430	0.470	0.293	0.330	0.367	0.409	0.445
0.32	0.301	0.338	0.382	0.428	0.469	0.291	0.328	0.366	0.408	0.443
0.64	0.299	0.338	0.380	0.426	0.467	0.292	0.328	0.365	0.408	0.441
1.28	0.300	0.338	0.381	0.423	0.467	0.292	0.328	0.366	0.406	0.441
2.00	0.301	0.338	0.380	0.422	0.461	0.294	0.328	0.365	0.404	0.435
3.00	0.302	0.338	0.378	0.418	0.456	0.295	0.329	0.363	0.399	0.433
4.00	0.302	0.338	0.377	0.416	0.455	0.294	0.327	0.362	0.398	0.430
5.00	0.301	0.336	0.375	0.415	0.459	0.294	0.328	0.361	0.397	0.433
6.00	0.301	0.336	0.375	0.416	0.463	0.294	0.326	0.360	0.398	0.438
7.00	0.300	0.335	0.375	0.417	0.470	0.292	0.325	0.360	0.400	0.445

Profile	630	628	626	624	622	620	828	826	824	822	820
y	c_p	c_p	c_p	c_p	c_p	c_p	c_p	c_p	c_p	c_p	c_p
0	0.285	0.316	0.351	0.387	0.413	0.420	0.293	0.323	0.350	0.369	0.364
0.08	0.282	0.312	0.346	0.380	0.406	0.407	0.289	0.318	0.343	0.360	0.353
0.16	0.281	0.311	0.346	0.378	0.404	0.403	0.288	0.317	0.343	0.360	0.348
0.32	0.280	0.310	0.345	0.379	0.403	0.394	0.289	0.316	0.342	0.358	0.344
0.64	0.279	0.309	0.343	0.377	0.402	0.398	0.288	0.315	0.340	0.357	0.346
1.28	0.280	0.310	0.343	0.375	0.399	0.401	0.288	0.315	0.337	0.354	0.350
2.00	0.280	0.309	0.343	0.373	0.396	0.397	0.288	0.315	0.337	0.350	0.345
3.00	0.282	0.309	0.341	0.368	0.391	0.393	0.289	0.314	0.334	0.348	0.340
4.00	0.282	0.310	0.340	0.368	0.390	0.398	0.288	0.313	0.333	0.346	0.343
5.00	0.282	0.308	0.339	0.368	0.392	0.405	0.286	0.312	0.332	0.346	0.347
6.00	0.280	0.308	0.339	0.368	0.395	0.422	0.286	0.310	0.332	0.348	0.356
7.00	0.279	0.307	0.339	0.369	0.400	0.433	0.285	0.310	0.332	0.352	0.366

TABLE 5

Cross-Flow Angles in the Free Stream (degrees)

Profile	-230	-228	-226	-224	-222	30	28	26	24	22
y	β	β	β	β	β	β	β	β	β	β
7.0	0.02	0.00	-.02	0.02	0.00	0.05	0.02	-.03	0.01	0.12
7.5	-.02	-.01	-.02	0.04	-.07	0.11	0.04	0.02	0.04	0.12
8.0	0.00	-.01	0.04	0.04	-.12	0.13	0.05	0.00	0.06	0.10
8.5	0.04	0.01	0.03	0.08	-.12	0.11	0.04	-.02	0.04	0.10
9.0	0.04	-.01	0.03	0.04	-.14	0.09	0.02	-.05	0.01	0.10
9.5	-.01	-.07	-.04	-.04	-.20	0.08	-.03	-.07	0.01	0.09
10.0	-.04	-.13	-.11	-.04	-.28	0.00	-.07	-.09	-.02	0.07
10.5	-.14	-.20	-.13	-.15	-.40	-.02	-.09	-.11	-.07	0.02
11.0	-.15	-.21	-.15	-.24	-.40	-.02	-.14	-.15	-.09	-.03
11.5	-.19	-.23	-.21	-.26	-.50	-.05	-.15	-.15	-.08	-.06

Profile	230	228	226	224	222	430	428	426	424	422
y	β	β	β	β	β	β	β	β	β	β
7.0	-.08	-.09	-.08	-.12	-.04	-.01	-.07	-.08	0.04	0.17
7.5	-.08	-.06	-.02	-.06	-.02	-.06	-.11	-.08	0.04	0.14
8.0	-.08	-.04	0.00	-.03	0.03	-.06	-.11	-.08	0.00	0.19
8.5	0.00	-.03	0.03	0.03	0.14	-.01	-.07	-.07	0.08	0.32
9.0	0.04	0.05	0.09	0.10	0.18	-.01	0.00	0.02	0.14	0.40
9.5	0.06	0.14	0.11	0.12	0.26	0.01	0.05	0.05	0.20	0.43
10.0	0.10	0.16	0.16	0.19	0.34	0.04	0.03	0.05	0.23	0.48
10.5	0.08	0.14	0.20	0.23	0.42	0.02	0.01	0.08	0.23	0.54
11.0	0.07	0.14	0.24	0.25	0.45	0.02	0.00	0.08	0.26	0.61
11.5	0.07	0.14	0.20	0.25	0.50	0.02	0.00	0.08	0.30	0.64

Profile	630	628	626	624	622	620	828	826	824	822	820
y	β	β	β	β	β	β	β	β	β	β	β
7.0	0.14	0.05	-.01	0.09	0.17	0.45	0.02	0.05	0.06	0.24	0.45
7.5	0.10	0.02	0.02	0.14	0.20	0.62	-.03	-.01	0.06	0.28	0.59
8.0	0.09	-.02	-.02	0.16	0.26	0.75	-.05	-.03	0.05	0.32	0.73
8.5	0.09	-.01	0.01	0.15	0.35	0.89	-.05	-.04	0.05	0.41	0.89
9.0	0.11	-.01	0.01	0.22	0.45	1.03	-.05	-.04	0.07	0.47	1.00
9.5	0.10	0.02	0.01	0.22	0.55	1.16	-.07	-.06	0.09	0.50	1.17
10.0	0.07	0.03	0.01	0.24	0.59	1.30	-.10	-.06	0.09	0.51	1.25
10.5	0.07	-.01	0.02	0.26	0.59	1.38	-.13	-.12	0.07	0.55	1.30
11.0	0.05	0.00	0.02	0.29	0.64	1.41	-.17	-.13	0.08	0.56	1.39
11.5	0.07	0.00	0.02	0.30	0.71	1.52	-.16	-.13	0.09	0.60	1.48

TABLE 6

Smoothed Values of Free Stream Angle (degrees).

X	Z					
	−2	−1	0	1	2	3
30	−1·19	−0·68	−0·16	0·26	0·73	1·30
29	−1·32	−0·74	−0·18	0·34	0·90	1·53
28	−1·47	−0·82	−0·20	0·41	1·05	1·77
27	−1·65	−0·91	−0·20	0·50	1·25	2·06
26	−1·89	−1·02	−0·19	0·64	1·51	2·41
25	−2·18	−1·16	−0·17	0·81	1·82	2·83
24	−2·51	−1·31	−0·14	1·01	2·17	3·31
23	−2·90	−1·50	−0·13	1·22	2·55	3·82
22	−3·33	−1·72	−0·12	1·44	2·97	4·43
21	−3·85	−1·96	−0·10	1·68	3·41	5·14
20	−4·50					

X	Z					
	4	5	6	7	8	9
30	1·90	2·45	2·96	3·34		
29	2·19	2·83	3·39	3·90	4·45	5·05
28	2·51	3·22	3·86	4·45	5·04	5·68
27	2·88	3·65	4·35	4·99	5·60	6·17
26	3·31	4·13	4·89	5·59	6·23	6·75
25	3·80	4·69	5·52	6·27	6·94	7·51
24	4·37	5·35	6·24	7·04	7·75	8·34
23	5·03	6·11	7·07	7·92	8·64	9·21
22	5·78	6·97	8·02	8·94	9·66	10·28
21	6·67	7·98	9·11	10·08	10·87	11·50
20			10·30	11·37	12·24	12·89

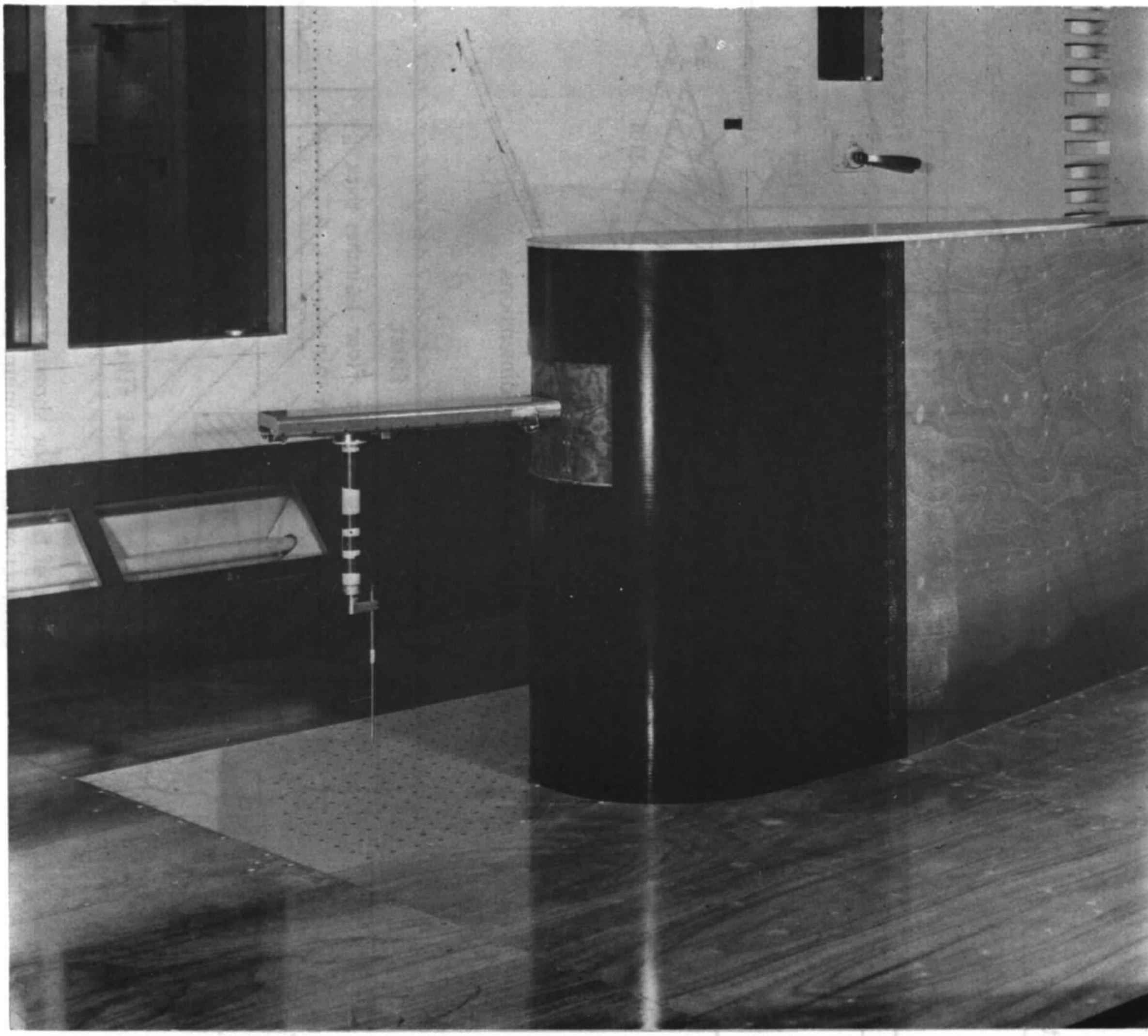

FIG. 1. Apparatus mounted in the 13ft $\times$ 9ft low-speed wind tunnel, showing the flow obstruction, the traverse gear arm and probe, and the false floor.

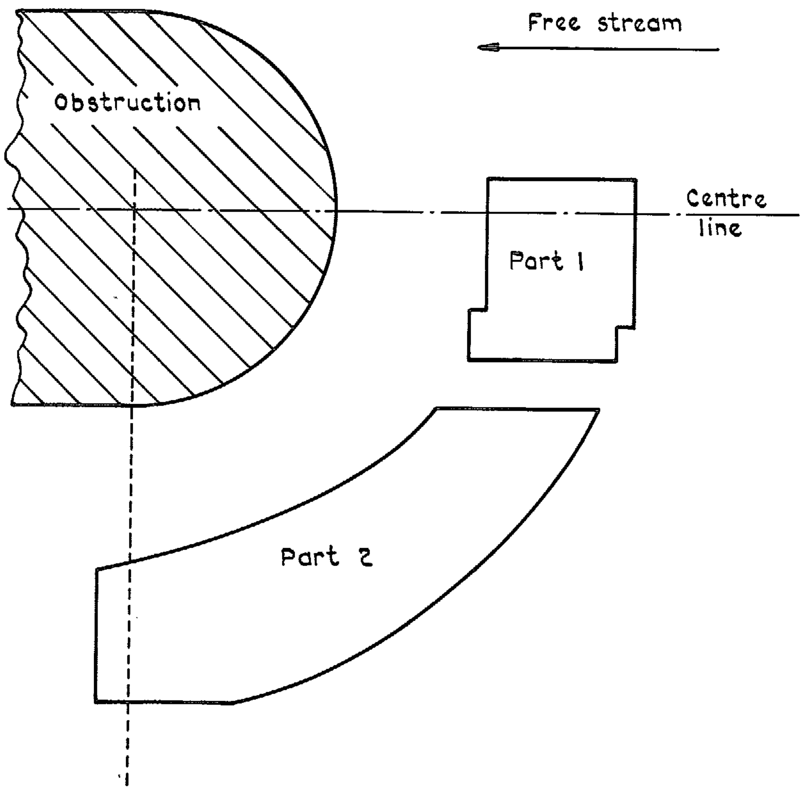

FIG. 2. Sketch showing approximate areas of measurements in each part of the experiment.

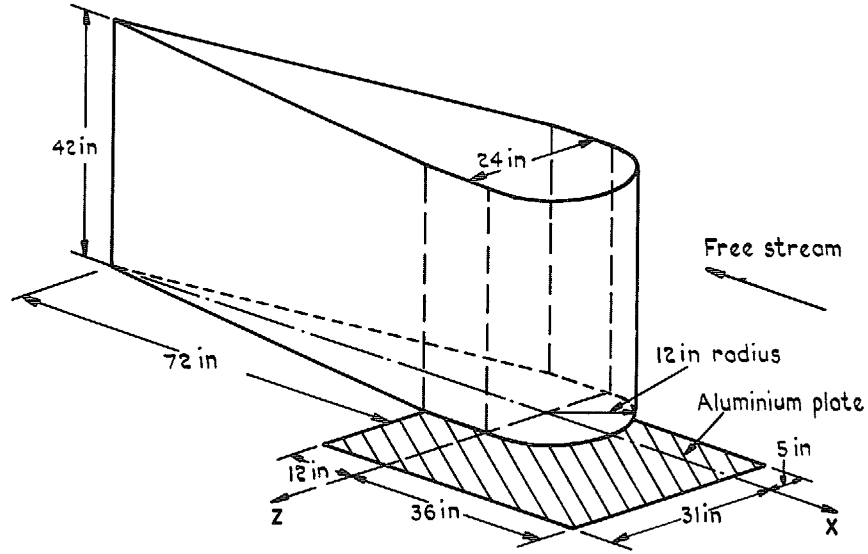

FIG. 3. Sketch of the obstruction and the aluminium plate showing leading dimensions.

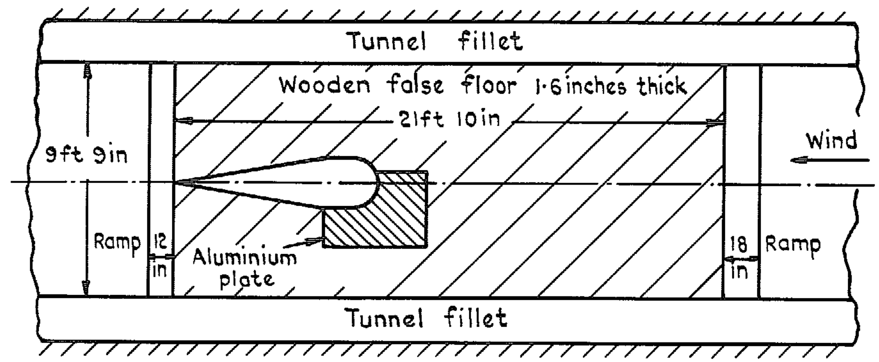

FIG. 4. Plan of false floor showing positions of obstruction and aluminium plate.

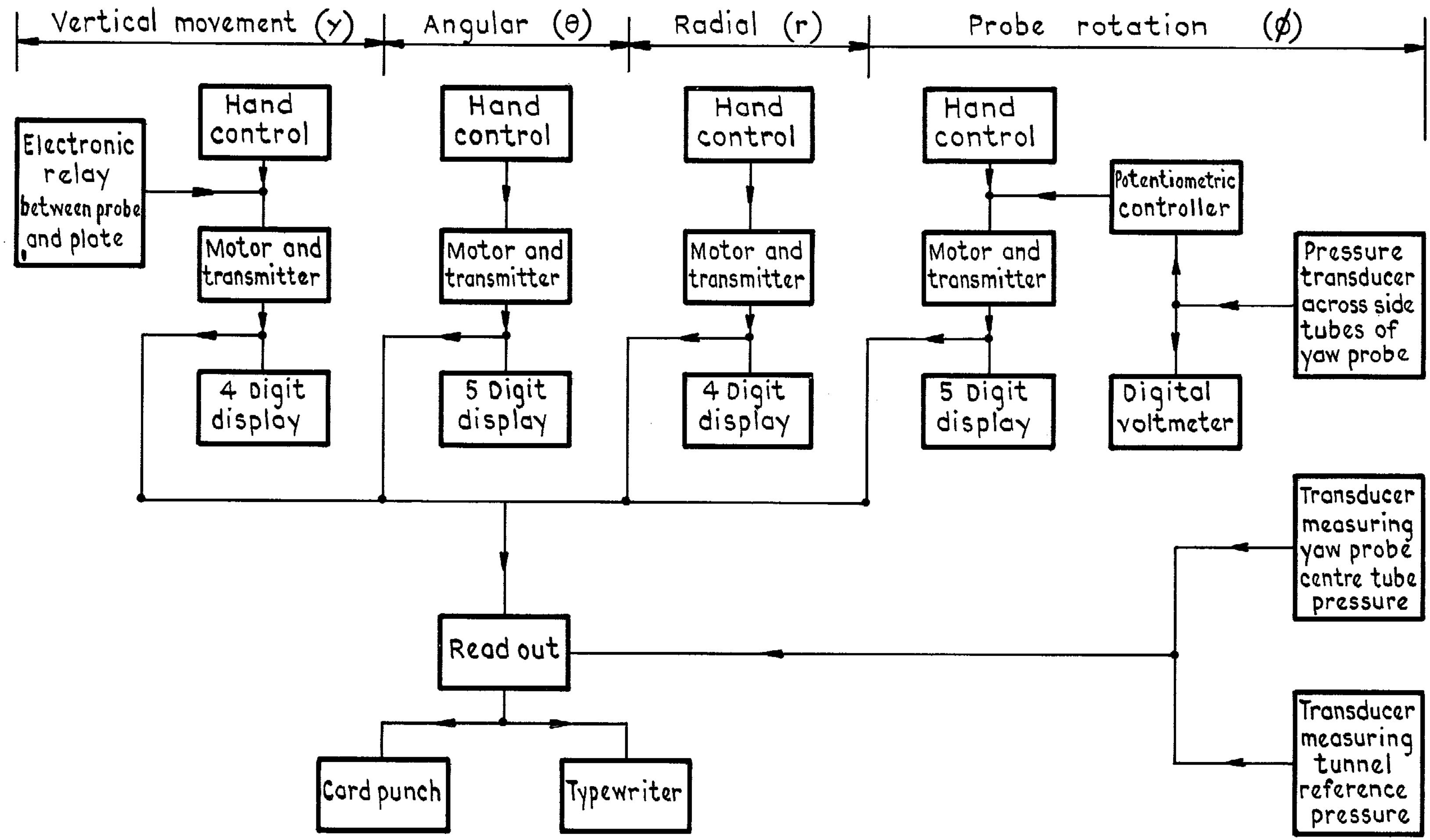

FIG. 5. Block diagram of traverse gear control and data handling.

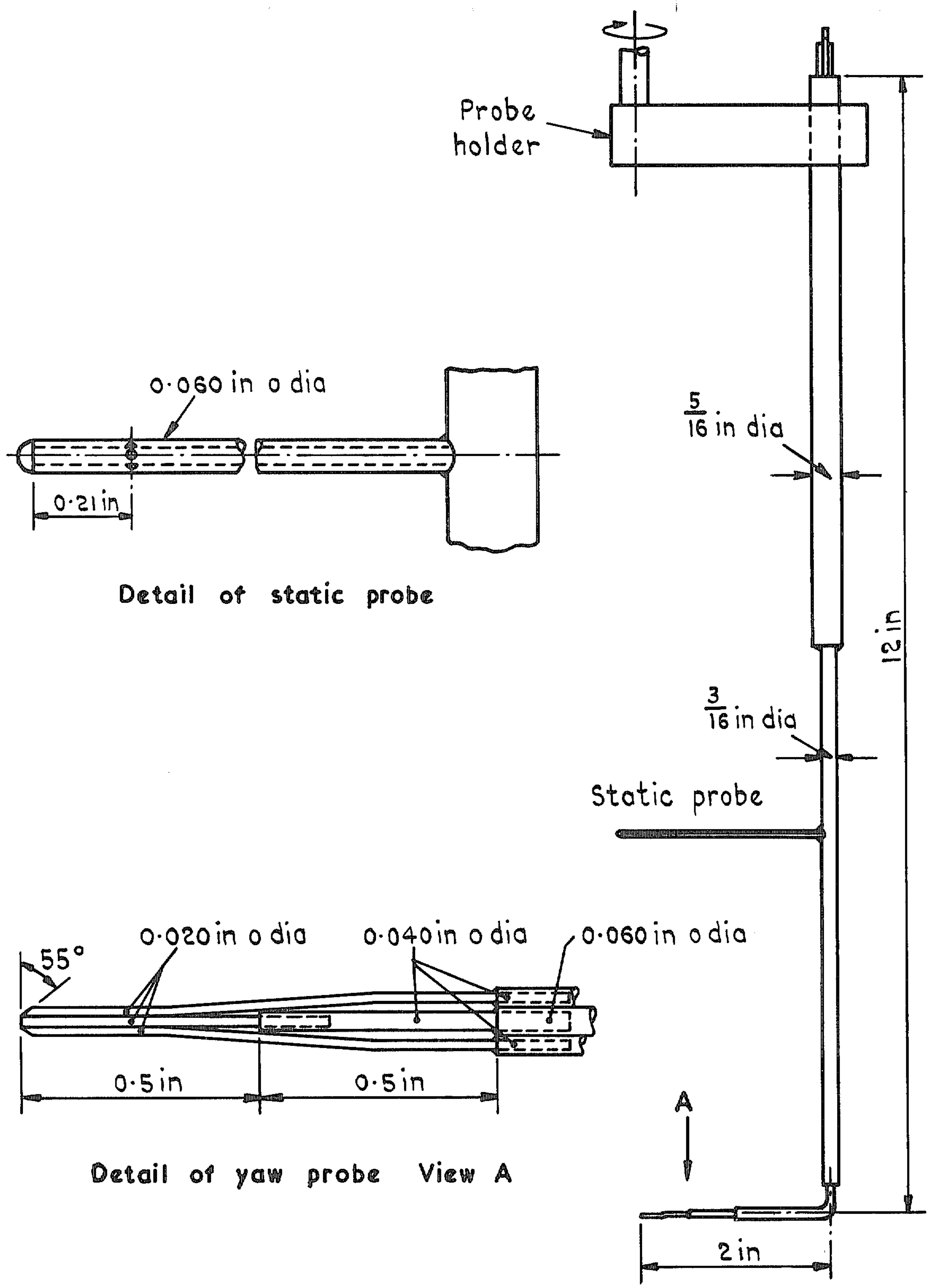

FIG. 6. Standard yaw probe.

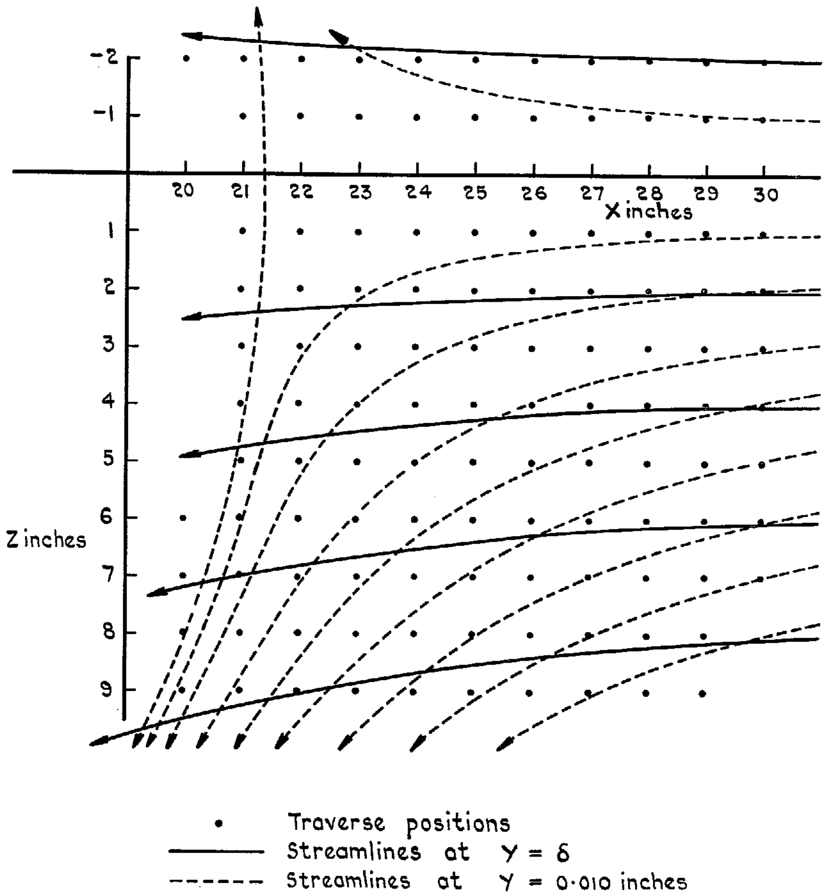

FIG. 7. Diagram showing the positions of the traverses and streamline patterns deduced from the flow measurements.

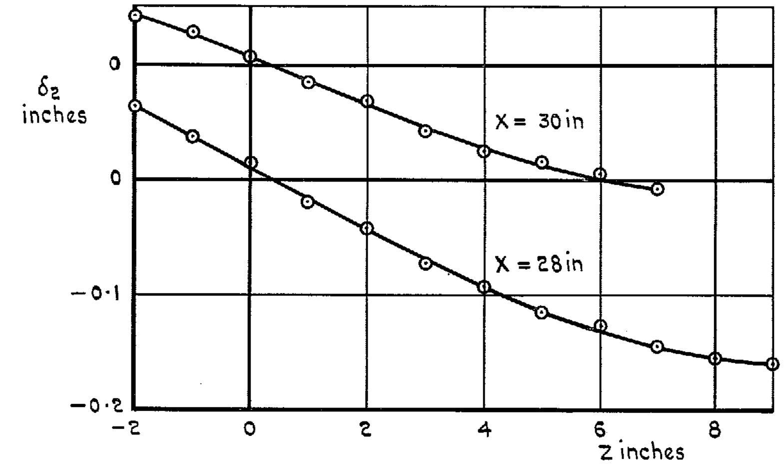

FIG. 8. Transverse velocity integral (δ_2) at X = 28 and 30in.

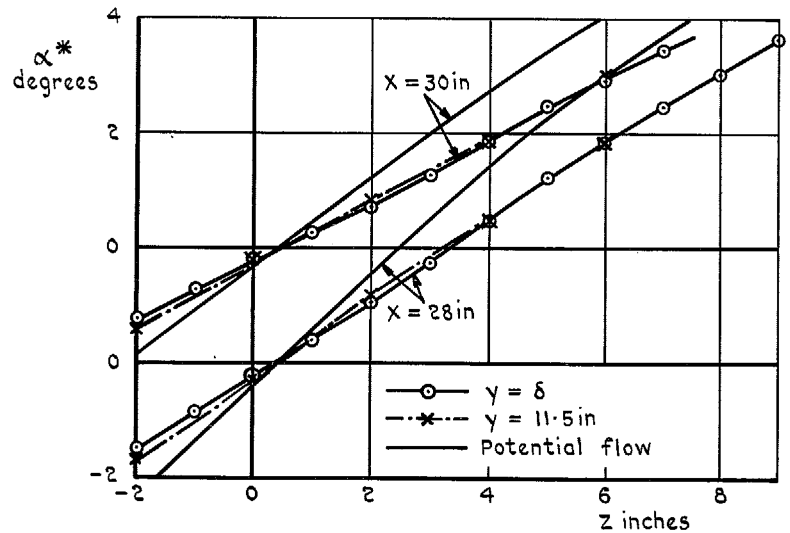

FIG. 9. Freestream flow direction at X = 28 and 30in.

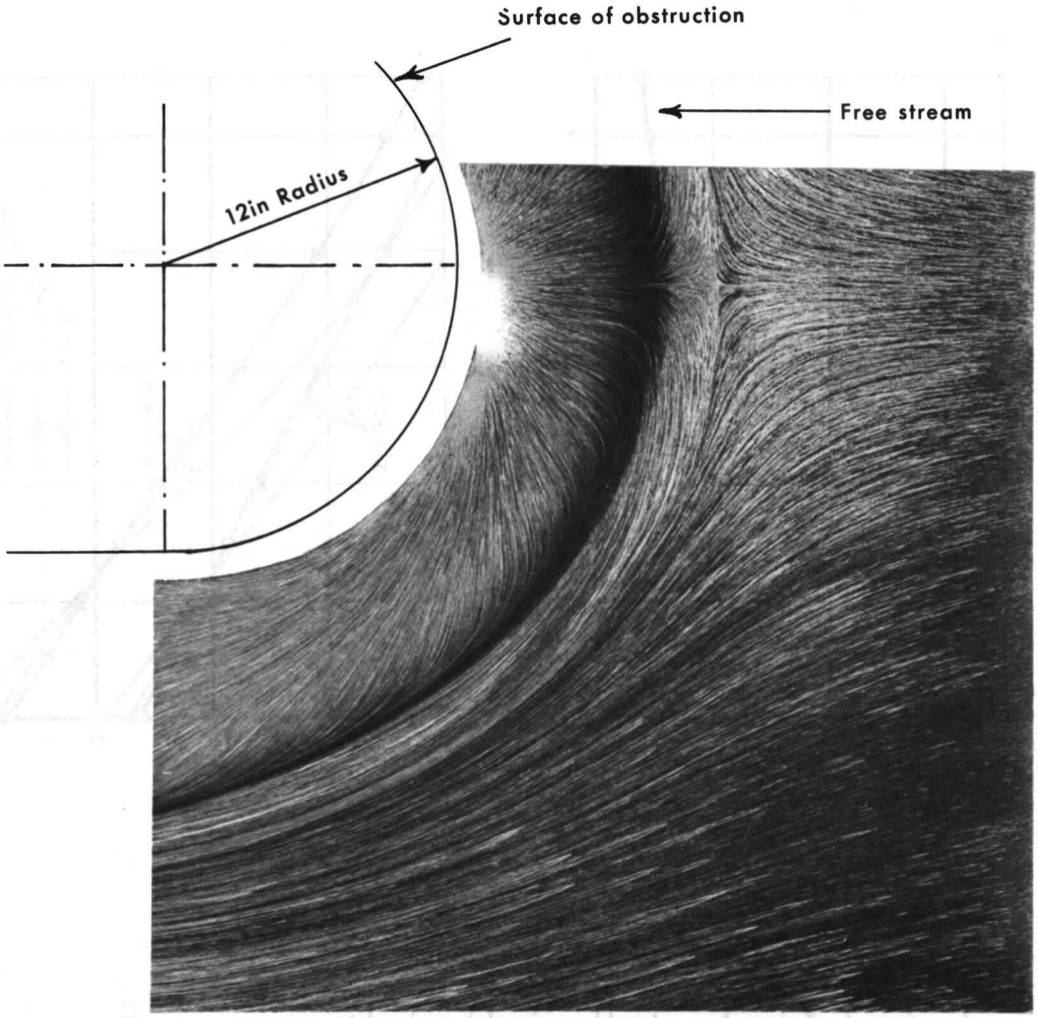

FIG. 10. Oil flow pattern ahead of obstruction. Free stream velocity 200ft/s.

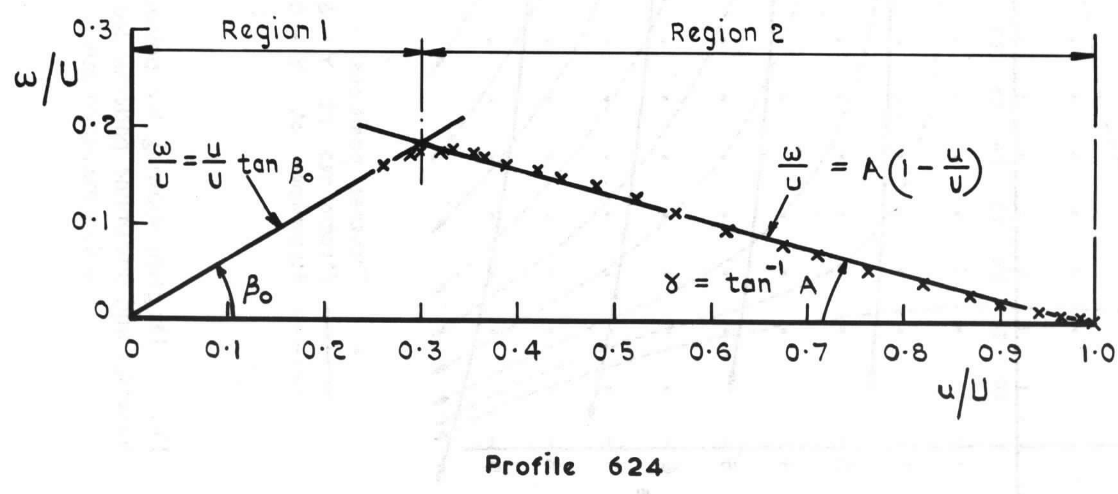

FIG. 11. Characteristic features of the triangular model of Johnson.

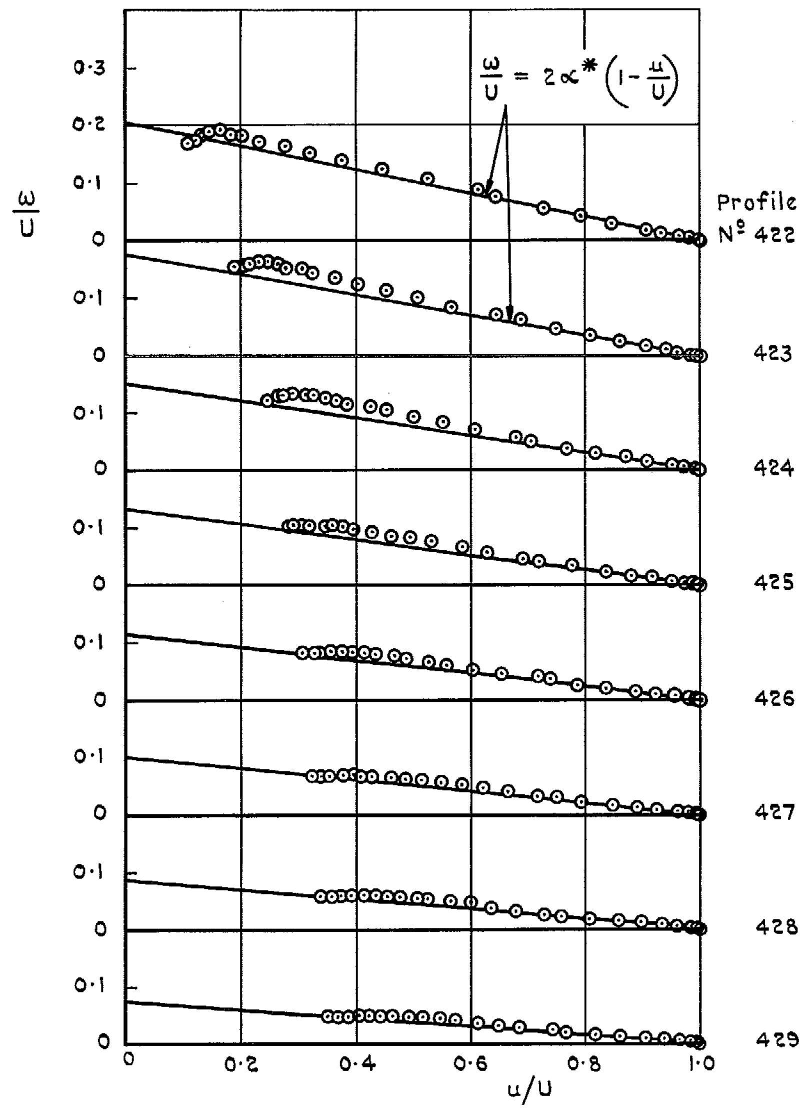

FIG. 12. Johnston plots of a selection of profiles Z = 4 inches.

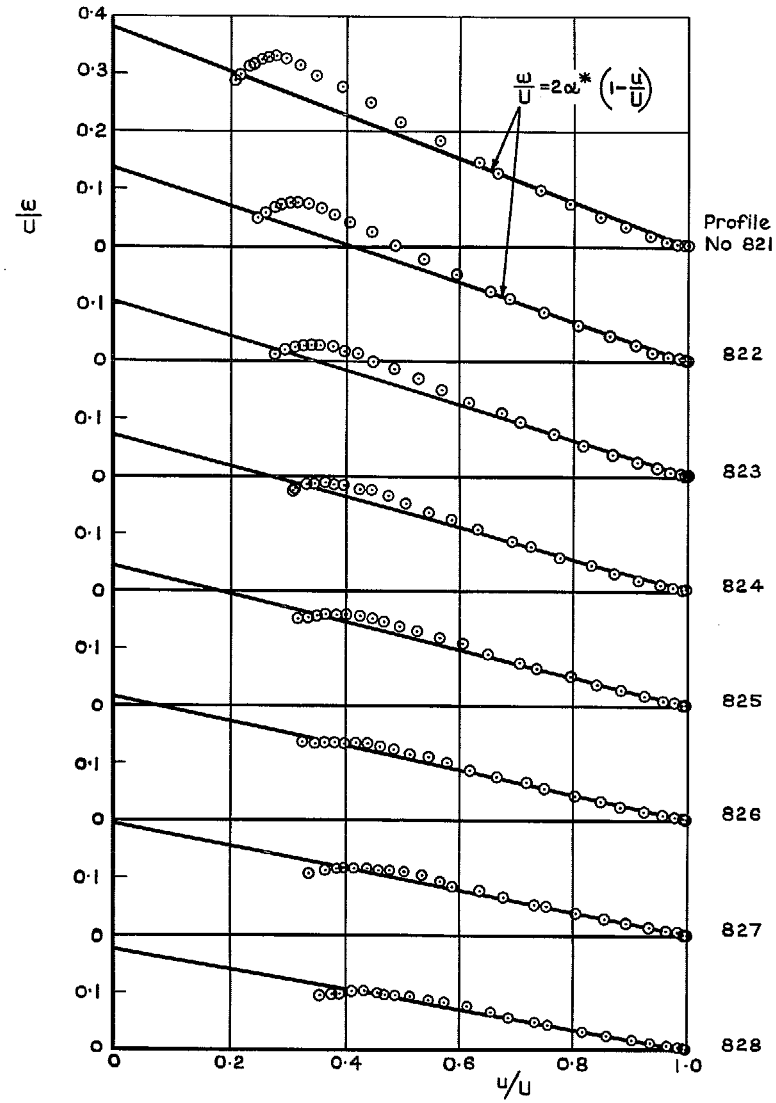

FIG. 12 *contd.* Johnston plots of a selection of profiles. Z = 8 inches.

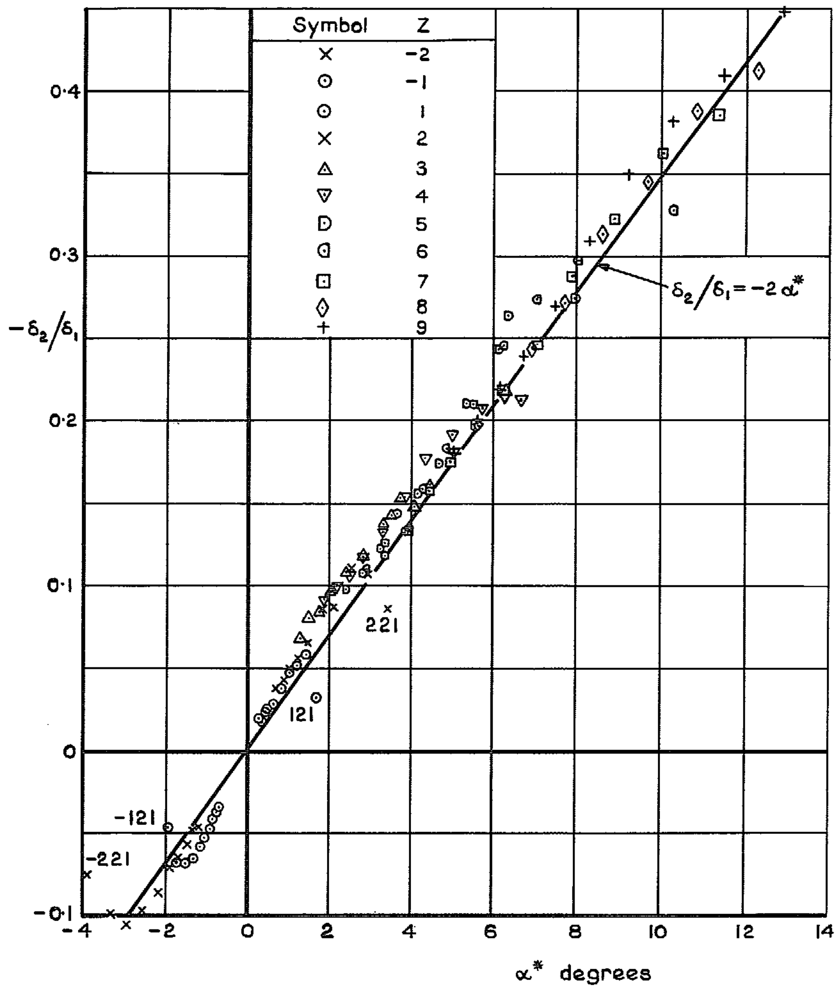

FIG. 13. Plot of ratio of displacement thicknesses against smoothed free stream angle.

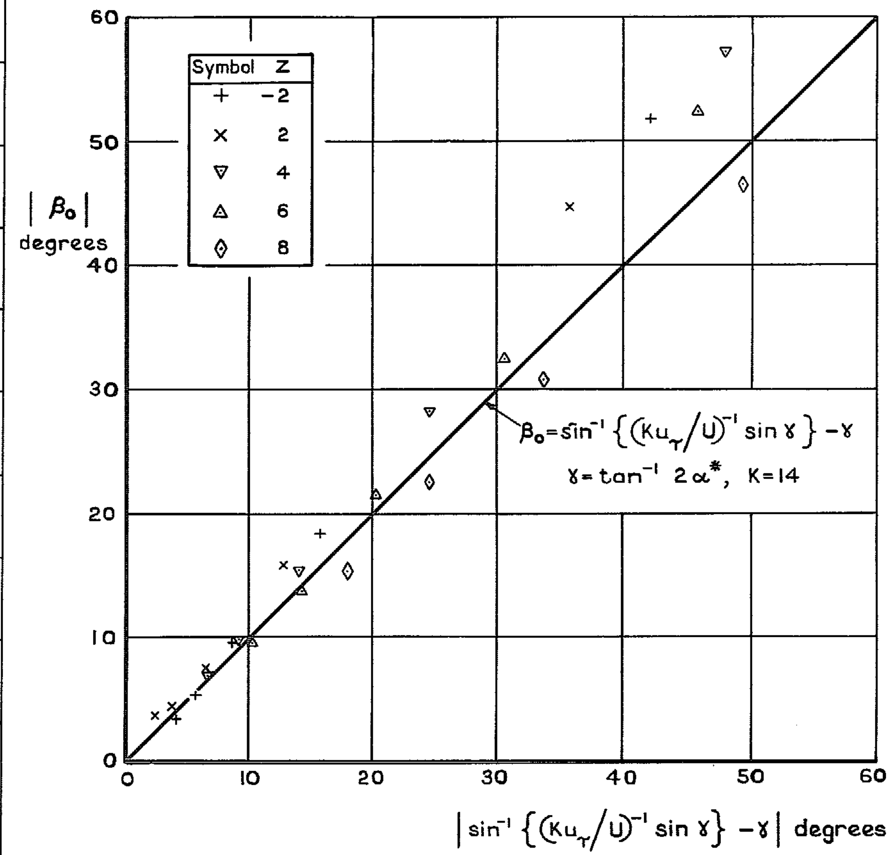

FIG. 14. Surface-flow direction given by equation 8 compared with data.

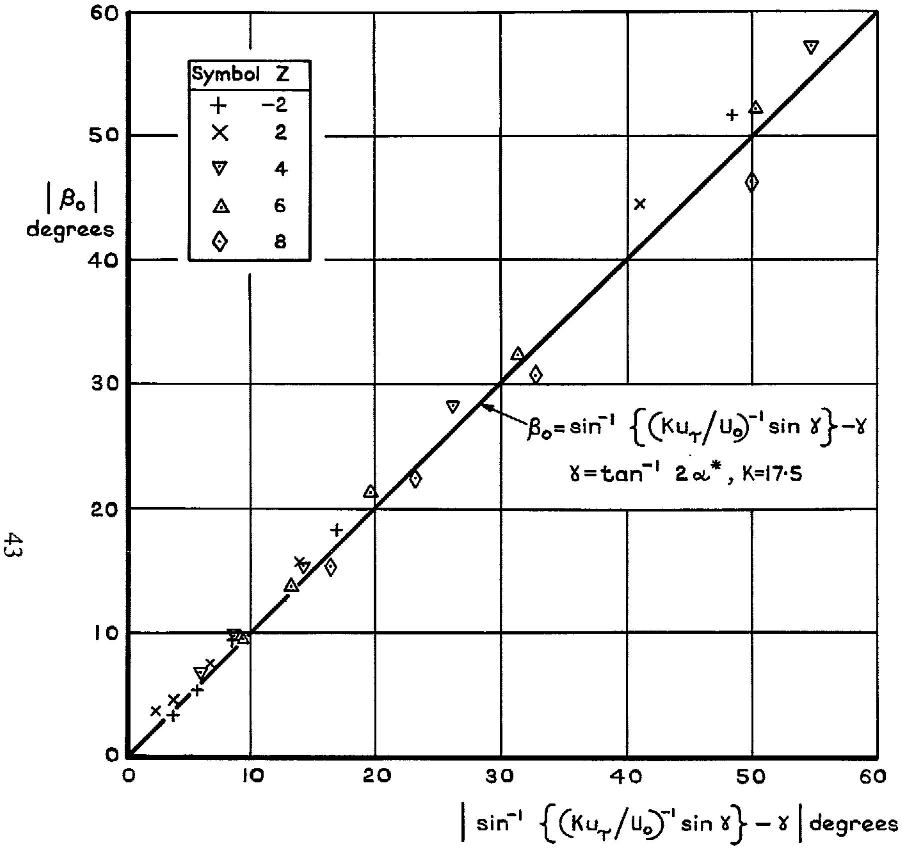

FIG. 15. Surface-flow direction given by equation 9 compared with data.

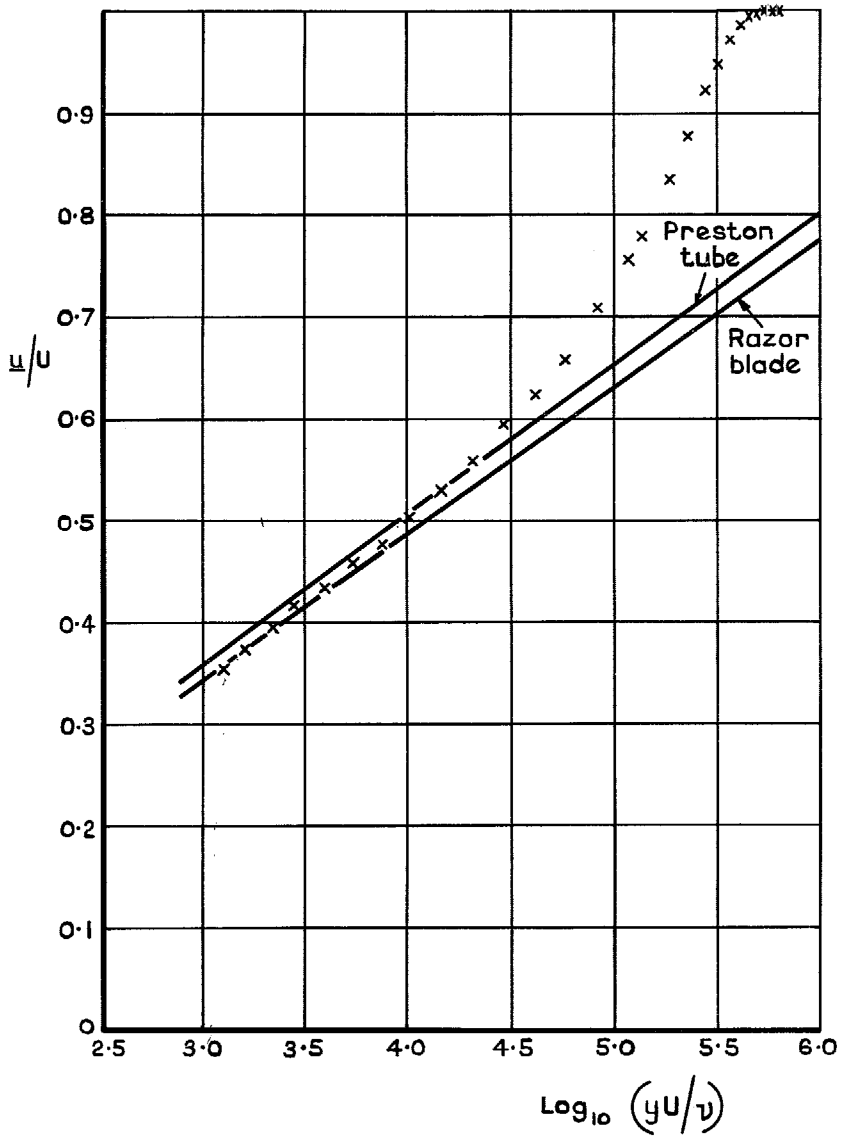

FIG. 16. Logarithmic plots. Profile No. 30.

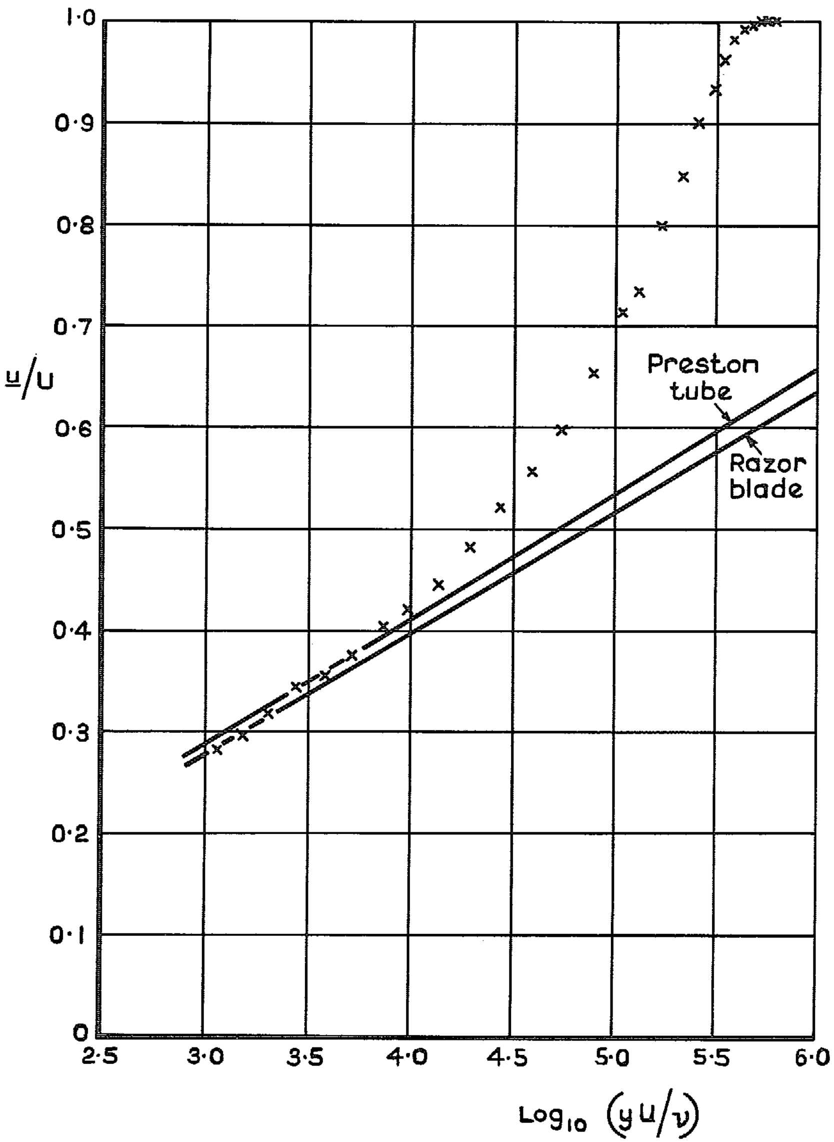

FIG. 16 *contd.* Logarithmic plots. Profile No. 26.

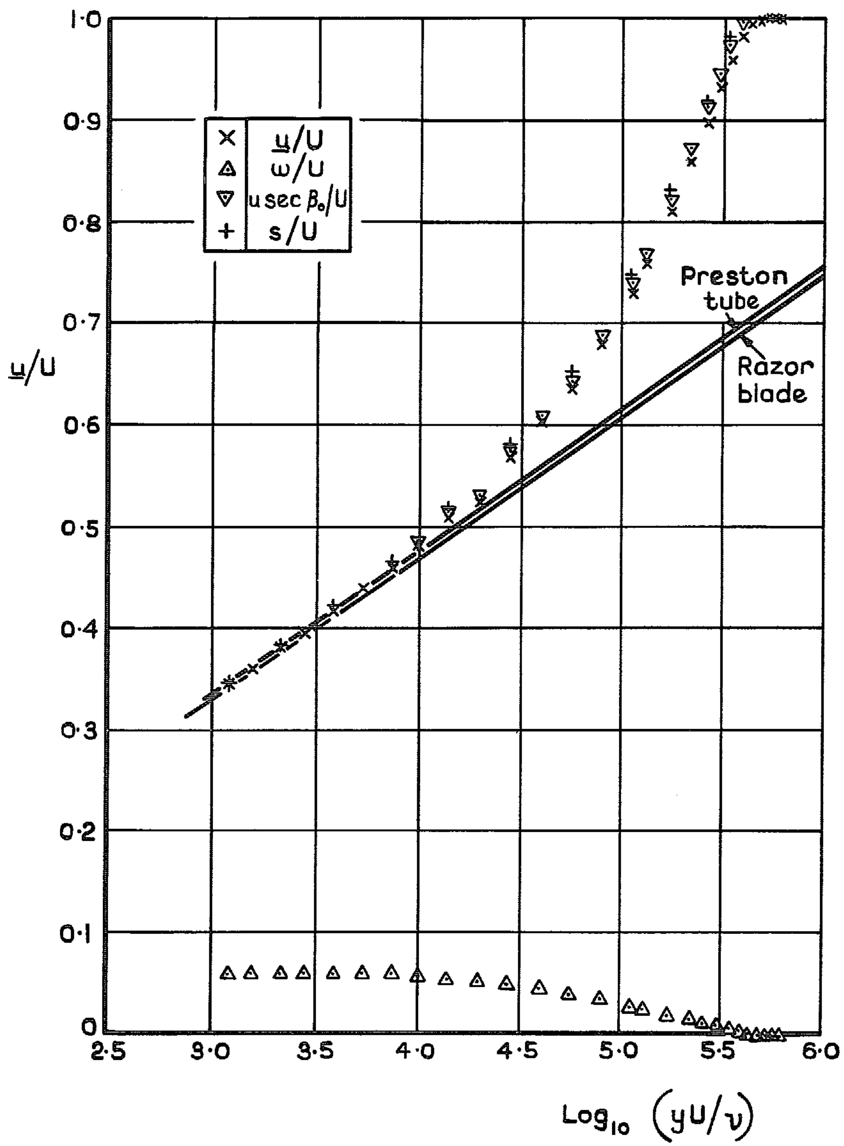

FIG. 16 *contd.* Logarithmic plots. Profile No. 428.

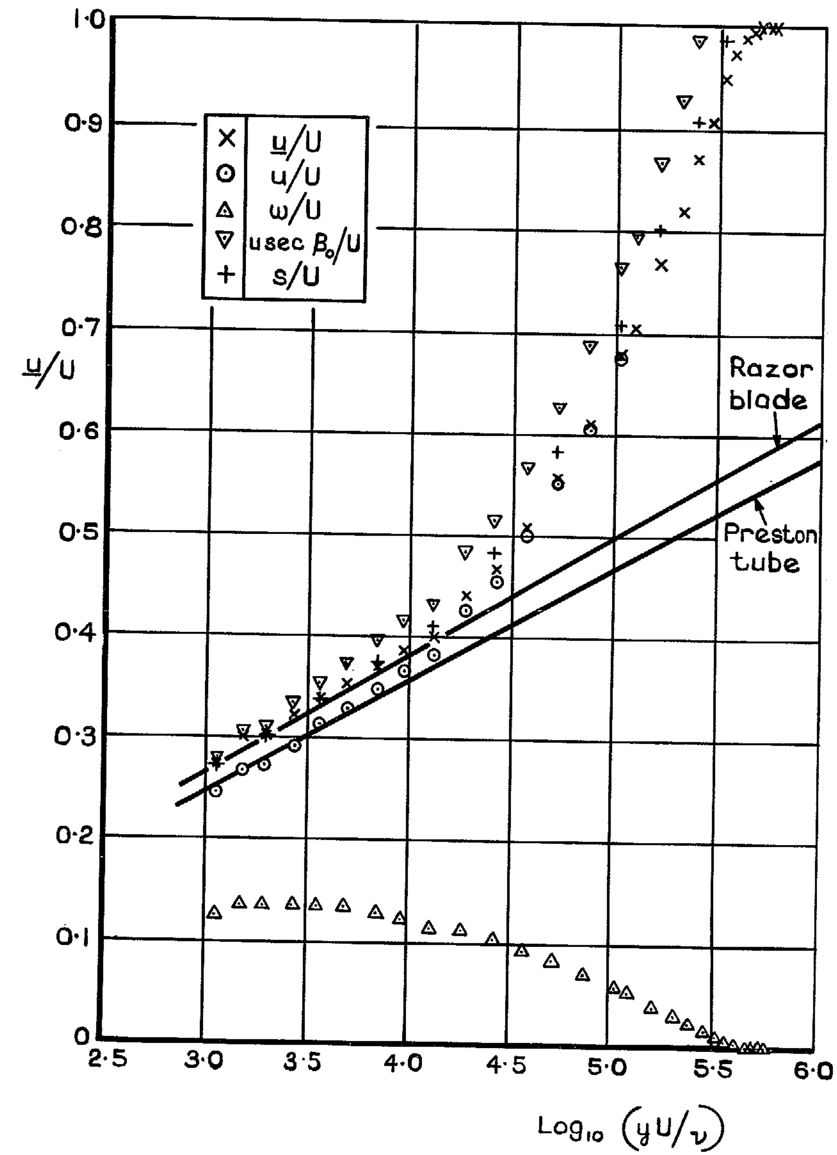

FIG. 16 *contd.* Logarithmic plots. Profile No. 424.

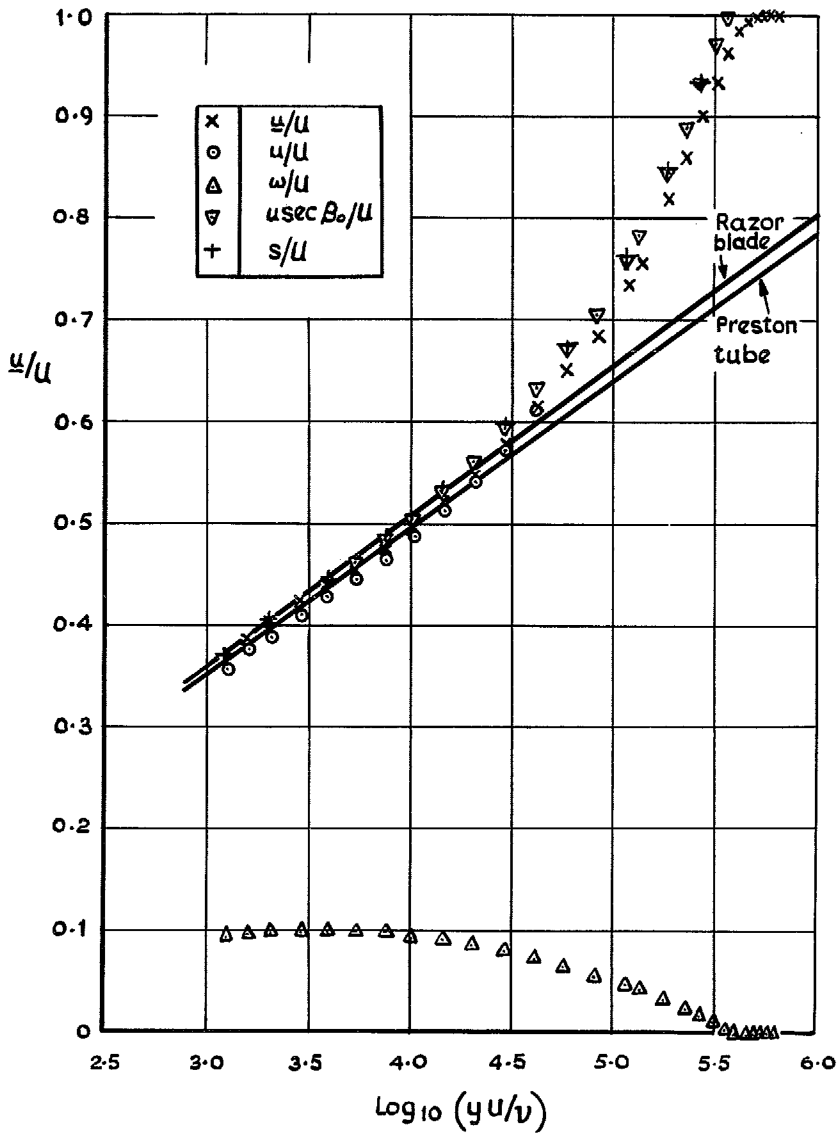

FIG. 16 *contd.* Logarithmic plots. Profile No. 828.

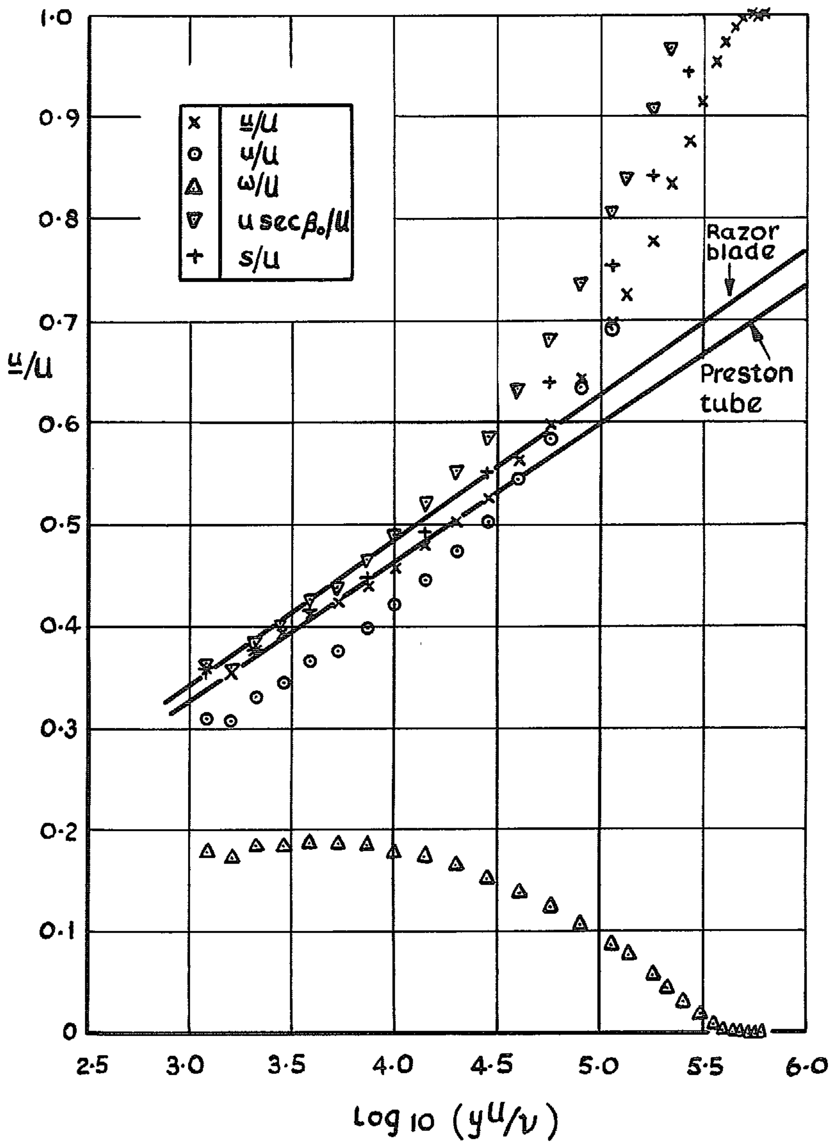

FIG. 16 *contd.* Logarithmic plots. Profile No. 824.

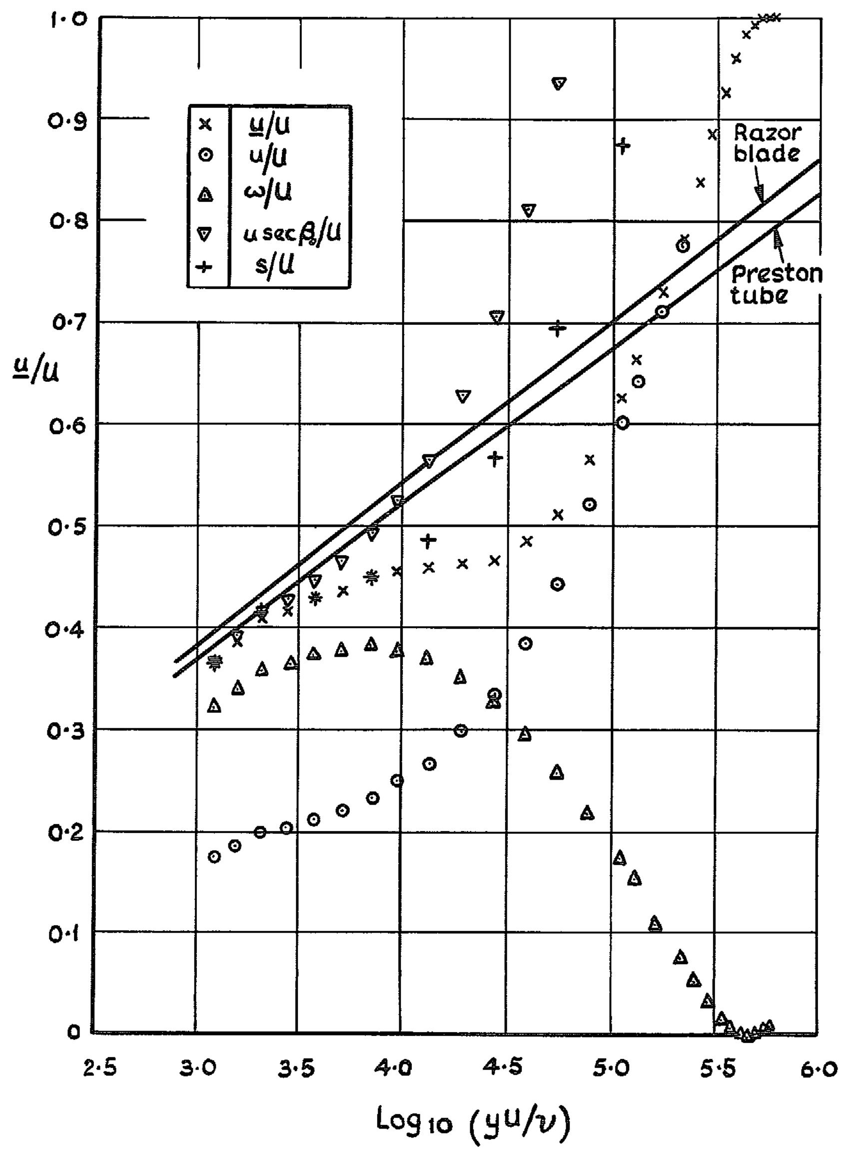

FIG. 16 *concld.* Logarithmic plots. Profile No. 820.

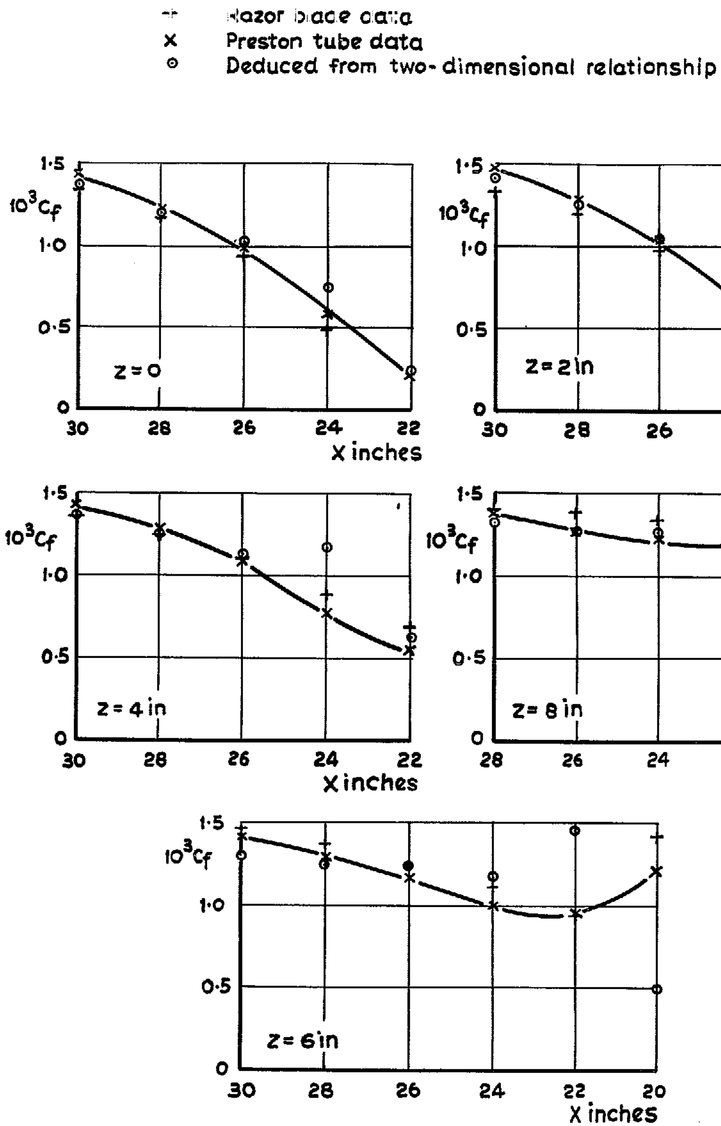

FIG. 17. Skin friction measured by the Preston tube, razor blades and deduced from two-dimensional relationship.

Symbol	Profile number
×	430
+	424
⊙	824
λ	820

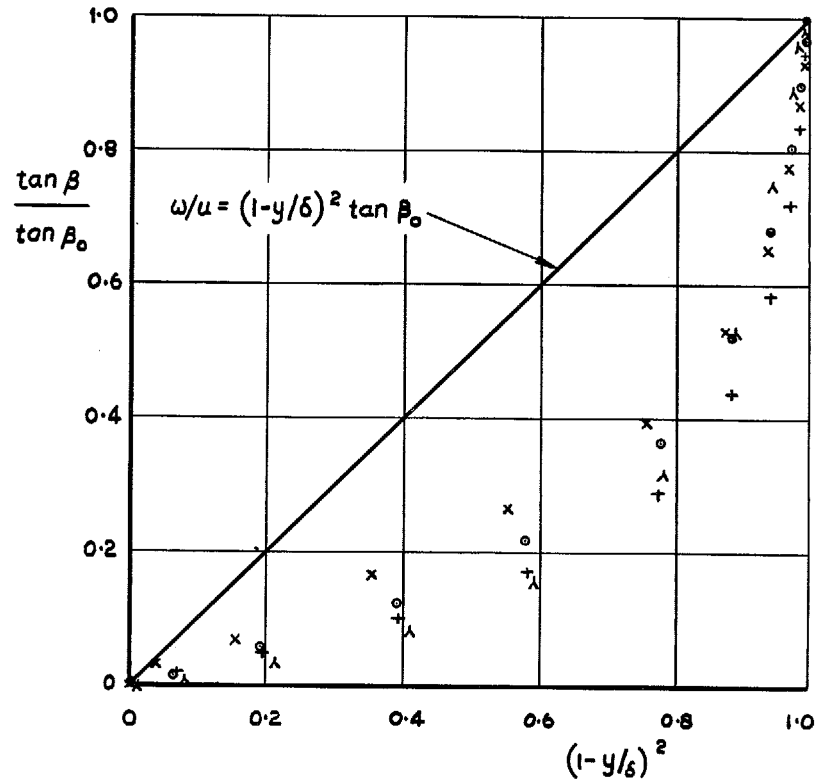

FIG. 18. Test of Mager's cross flow equation.

Symbol	Profile number
+	226
⊙	222
x	430
△	426
▽	422
⊡	828
◇	824
⌓	820

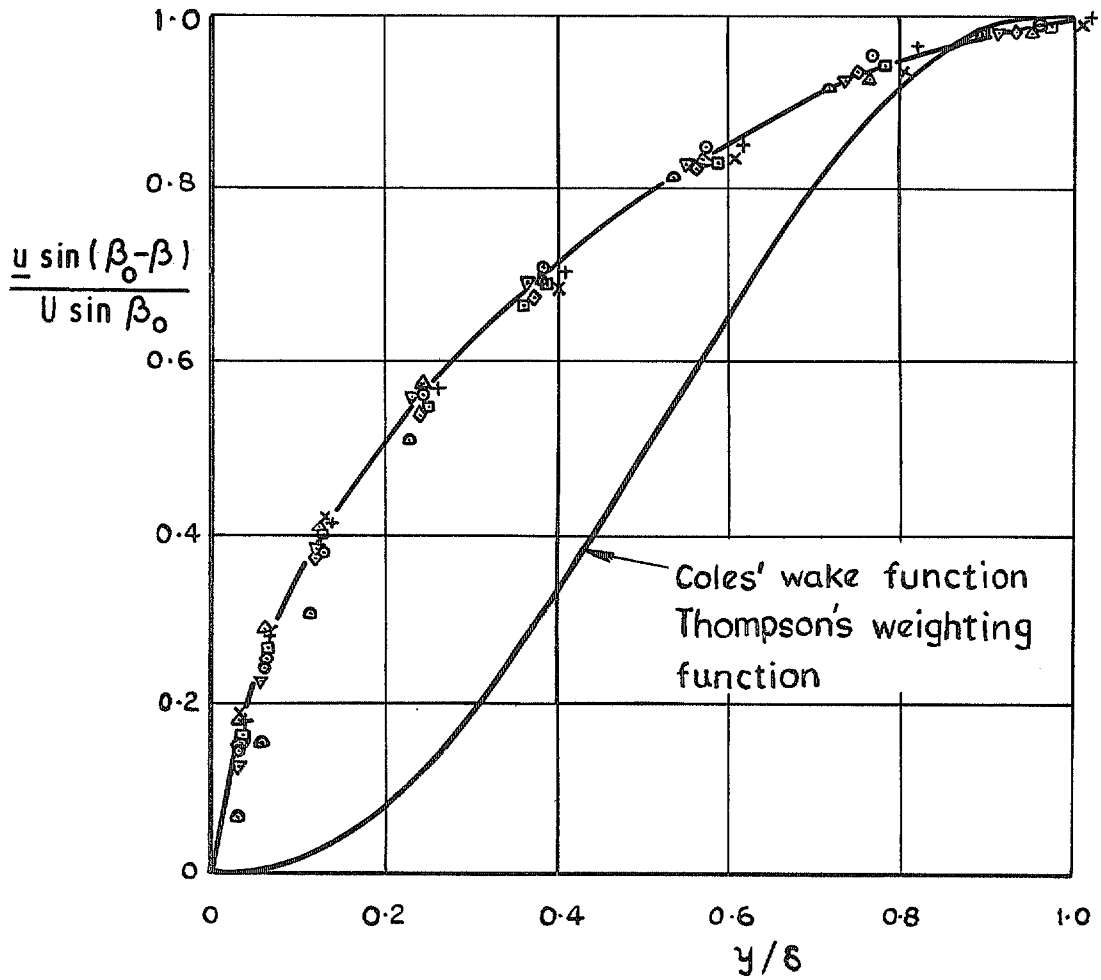

FIG. 19. Velocity profiles normal to surface shear-stress vector compared with Cole's wake function and Thompson's weighting function.

Low-Speed Three-Dimensional Turbulent Boundary-Layer Data
Part 2

Summary.

A comprehensive low speed three-dimensional turbulent boundary layer experiment is described and the results are presented in detail. The flow caused by an obstruction placed in a thick two-dimensional boundary layer is investigated at a free-stream velocity of 200 ft/sec. A typical Reynolds number based on the boundary layer momentum thickness and local free-stream velocity is 50 000.

Profiles obtained upstream of the free-stream inflexion are well represented by Johnston's triangular model. Polar profiles further downstream become more curved and are not well represented by a triangle, though the change from an inner region to an outer region is clear. The method discussed in Part 1 for deducing the skin friction from the three-dimensional profile by using a modified law of the wall is shown to be equally applicable to the present data. Mager's cross-flow profile and simple extensions to three dimensions of existing methods of representing two-dimensional profiles, using Cole's wake function and Thompson's weighting function, are all shown not to fit the data.

This part is concerned with the flow to one side of the obstruction and the main characteristic of this region is that it contains a free-stream inflexion.

LIST OF CONTENTS

1. *Introduction.*

This second part of the Report is written to be read in conjunction with Part 1, where a full description of the experiment is given.

The regions of the flow studied in the two parts of the experiment are illustrated in Fig. 2 of Part 1. In the first part, the decelerating and diverging flow directly upstream of the obstruction was studied. In this part, the flow to one side of the obstruction is investigated and, as shown in Fig. 1, the flow contains a free-stream inflexion. The significance of a free-stream inflexion is that it indicates that the pressure gradient normal to the free-stream streamline changes sign. This change in the transverse pressure gradient can be expected to have a significant effect on the transverse mass flow within the boundary layer and on the detailed shape of the velocity profiles.

The data obtained in the second part of the experiment are presented and an analysis of the characteristics of the profiles is given which is similar to that given in Part 1.

The experimental results given were obtained in the 13ft × 9ft low-speed tunnel at R.A.E. Bedford in the period October to December, 1967.

2. *Experimental Details.*

The equipment used in the experiment was the same as that described in detail in Part 1, except that the operation of the traverse gear was improved by two minor modifications. The two angular motions of the traverse gear were improved by the replacement and addition of parts so that they maintained their reliability over the larger ranges required for this part of the experiment. The measurement of the angular position of the traverse gear arm was improved by the addition of a Bendix Electronics 1000 step Rotapulse geared directly to the arm. The probe rotating mechanism was improved by replacing a slightly damaged 3000:1 gear box by a new and superior 1000:1 gear box. This change improved the linearity of the mechanism although the resolution was reduced from 0·01° to 0·03°. An incidental result of this change was that the hysterisis was greatly reduced because the new gear box was reversible which enabled the anti-backlash spring to take up all the hysterisis between the probe and the transmitter.

The experimental procedure was the same as described in Part 1. Eighty-three traverses were made from $y = 0$ to $y = 7{\cdot}000$ inches on a 2·0 inch grid at the positions shown in Fig. 1. Six traverses were repeated. A two inch grid was used in place of the one inch grid used in Part 1 partly to enable a much larger area of the flow to be covered but also because the gradients of the flow quantities in the X and Z directions were, in general, less than in the flow immediately upstream of the obstruction (Part 1). At a reduced number of positions the velocity traverses were extended into the freestream up to $y = 11{\cdot}5$ inches and static pressure traverses were made within the boundary layer. Finally, indirect measurements of skin friction were made at all eighty-three positions using a Preston[1] tube mounted on the traverse gear and at about half the positions using small segments of razor blade attached magnetically to the surface[2]. In Part 1 a Betz water monometer was used in conjunction with the razor blades but because of the very small orifice beneath the sharp edge of the razor blades the response of the manometer was very slow. A considerable saving in time was achieved in the present part by using a Texas fused-quartz precision pressure gauge.

3. *Experimental Results.*

The experimental data are given in Tables 1 to 5 and are deduced directly from the measurements with no smoothing applied. In Table 1 the displacement and momentum integrals are given together with the free-stream direction and static pressure. The two measured values of skin friction are listed in Table 2 and the detailed velocity profiles are given in Table 3. As in Part 1, the profiles are referred to by a number obtained by combining the Z and X co-ordinates. These profile numbers are listed in Table 3 together with the co-ordinates (note profile at $Z = 30$ inches, $X = -2$ inches is number 2998 etc.). The values of the static-pressure coefficient obtained from the traverses of the static probe across the boundary layer are listed in Table 4 and in general the static gradients are small. Close to separation a small reduction in pressure occurs which is centred at between 10 and 20 per cent of the boundary layer thickness from the surface. The reduction of pressure, which increases as the separation line is crossed and the separated region entered, is associated with the region of comparatively high suction that occurs within the separated region and which suggests a large concentration of vorticity[3].

The extended velocity profiles are given in Table 5 and the data show that the variations of the flow angle in the free-stream is small except near and above the separated region.

The region of the flow investigated is illustrated in Fig. 1 together with the positions of the traverses. Using the measured flow directions free-hand streamlines have been drawn which give approximately the streamline patterns very close to the surface and at the outer edge of the boundary layer. The flow pattern close to the surface is in close visual agreement with the pattern obtained by the oil flow visualisation technique as shown in Fig. 10 of Part 1. The pattern at the outer edge of the boundary layer is compared with the computed potential flow in Section 4. Fig. 1 shows that the free-stream streamlines pass through inflexions and consequently the lateral pressure gradient acting upon the boundary layer changes sign as the flow progresses.

In Fig. 2 the skin-friction field is depicted for the whole region studied in both parts of the experiment. In addition to the free-hand surface streamline pattern, contours of constant skin friction are shown. On the axis of symmetry ($Z = 0$) the skin friction falls to zero at the separation point. Two similar separation lines emanate from the saddle point[4] and Fig. 2 shows that the magnitude of the skin friction exhibits no peculiarities on crossing the separation line, nor is it zero at any point other than the saddle point. Rather the skin friction on the separation line rises rapidly under the influence of the strong favourable pressure gradient acting in the same direction as the sub-layer flow. Maximum skin friction is reached on the separation line just ahead of the Z axis and thereafter a more gradual fall in skin friction is to be expected under the influence of a moderate adverse pressure gradient. The level of skin friction in the separated region is high and probably reaches a maximum beneath the concentrated vorticity[3]. No measurements are avilable to confirm this but the oil flow (Fig. 10, Part 1) indicates a high level of skin friction throughout the separated region and measurements[5,6] on the lifting surface of a slender wing showed that there was a large increase in skin friction beneath the leading-edge vortex.

4. *Freestream.*

The two-dimensional flow around a cylinder with the same section as the obstruction is now compared with the measured flow field outside the boundary layer. Data from both Parts 1 and 2 are used.

The potential flow field was obtained by representing the body by a distribution of source elements and the strength of these elements was determined by satisfying the solid boundary condition[7]. The tunnel walls were represented by computing the flow through an infinite cascade of bodies. The computation was made both with an infinite flow and with tunnel walls at 13ft spacing, but as the difference between the computed results was small, only the solution with the walls represented is used in this Report.

Fig. 3 shows that the measured velocity was less than the calculated value over most of the flow field but was greater than the calculated value near the axis of symmetry directly upstream of the obstruction. Fig. 4a shows that the measured flow angle at the edge of the boundary layer was less than the two-dimensional calculated value and that the difference increased to about 4° as the flow approached and crossed the separation line. Fig. 4b shows that a broadly similar pattern existed at $y = 11{\cdot}5$ inches (approximately 2δ) but that the extent of the maximum difference was reduced to 2·5°.

It is suggested that these differences are caused by the three-dimensionality of the actual flow resulting from the limited height of the obstruction, which did not span the tunnel, and the variation of the displacement thickness of the floor boundary layer. The limited height of the obstruction will result in the flow ahead of it diverging in the $X-y$ plane, that is $\partial v/\partial y$ will be positive, where v is the velocity in the y direction. This is consistent with the measured divergence of the $X-Z$ plane being about 25 per cent less than the two-dimensional potential-flow solution while the measured velocity is only about 2 per cent high. As a result of this vertical divergence ahead of the obstruction the velocity to the side of it will be low (Fig. 3). The changes to the flow field near the floor boundary layer resulting from the limited height of the model can be expected to vary in the X, y and Z directions with a length scale the same order as the height of the obstruction. The rapid increase, in the $X-Z$ plane, of the difference between the measured and calculated values of α, shown in Fig. 4a, as the separation line is crossed and the appreciable reduction in the y direction of this difference, shown by comparing Fig. 4a and Fig. 4b, are likely to be due to the displacement effect of the floor boundary layer. The differences are certainly consistent with the induced flow that would be caused by a vortex extending around the front of the obstruction in the separated region. The oil-flow pattern and the measurements in the separated region[3] suggest the presence of a vortex-like flow. However, it cannot be stated with certainty that the major effect of the boundary layer displacement distribution is the same as this clearly visible vortex flow and some doubt must remain.

It is concluded that the relatively small differences between the measured free-stream field and the two-dimensional potential-flow solutions are qualitatively consistent with the three-dimensional effects likely to be caused by the limited height of the obstruction and the displacement thickness of the floor boundary layer.

5. *Profile Analysis.*

5.1. *Polar Plot.*

A selection of profiles is shown in Fig. 5. In this figure profiles 1614, 2204 and 2206 are within the separated region as shown in Fig. 1. Considerable deviation from the simple triangular model proposed by Johnston[8] will be seen. The triangular model was shown to fit the data of Part 1 well but amongst the present data a reasonable fit is only obtained for the most upstream profiles (e.g. profile 1626). Elsewhere the outer region of the boundary layer becomes progressively more curved on the polar plot with distance downstream. Nevertheless two regions are distinguishable and are separated by a clearly defined apex. It can also be seen in Fig. 5 that after the free-stream has passed through its inflexion point and the lateral pressure gradient has changed sign, which occurs at approximately profile 2214 and slightly upstream of profile 2812, the reduction of the transverse velocity (w) is greatest in the outermost region of the boundary layer (say $u/U > 0{\cdot}9$) and that the corresponding change in the middle region in the vicinity of the apex lags behind. This deduction can be made from Fig. 5 although the sets of profiles shown are at constant Z and not along streamlines. For any particular profile shown in Fig. 5 the profiles on the same free-stream streamline upstream of the inflexion will be in close agreement with the simple triangular model so that the qualitative change that the profile has undergone since the inflexion can be deduced directly from its shape. Even for this complex flow the equation

$$\underset{u \to U}{Lt} \left(\frac{w}{U-u} \right) = 2\alpha^*, \tag{1}$$

where α^* is the corrected angular displacement of the free-stream, is quite closely followed. This is shown in Fig. 5 by the agreement, as $u/U \to 1$, between the data and the lines representing

$$w/U = 2\alpha^*(1-u/U). \tag{2}$$

The position of the apex is appreciably further out in the boundary layer than in the data of Part 1 and the inner region extends up to $y/\delta \doteqdot 0{\cdot}1$. Also the inner region is not always linear. Upstream profiles such as 1626, 1624 and 1622 appear to exhibit a mildly curved inner region such that $\partial^2 w/\partial u^2$ is negative. Further downstream profiles such as 1616, 2214 and 2812 have inner regions which are closely linear ($\partial^2 w/\partial u^2 \doteqdot 0$) and still further downstream profiles such as 2802, 2800 and 2798 appear to be curved such that $\partial^2 w/\partial u^2$ is positive. This behaviour is more closely demonstrated in Fig. 6 in which the cross-flow angle β is plotted against the y co-ordinate. In this figure y is corrected for probe displacement effects by $+0{\cdot}004$ inch: this correction is the same as applied in Part 1. It will be seen in Fig. 6 that over the innermost region ($y < 0{\cdot}1$ inch), the slope of the β against y curves change in going from profile 2218 to profile 2210. This change of slope is identifiable with the change of sign of the pressure gradient normal to the surface shear stress. It is straightforward to show directly from the boundary layer momentum equations that in the limit as the surface is approached

$$\underset{y \to 0}{Lt} \, \partial\beta/\partial y = -(2\, C_{f_0})^{-1} (\partial C_p/\partial n), \tag{3}$$

where n is taken normal to the surface shear stress.

The curves through the experimental points in Fig. 6 have therefore been extrapolated to the wall in such a way that at the wall they have the limiting slope given by equation (3). Provided the points at $y = 0{\cdot}014$ inch are ignored and it is appreciated that equation (3) can at the most be applied throughout the laminar sub-layer which is about 0·002 inch thick, the calculated limiting slopes seem consistent with the data. The data at $y = 0{\cdot}014$ inch were obtained with the probe touching the surface and so are likely to be in error.

Further evidence of the response of the boundary layer as a whole to changes of the transverse pressure gradient is shown in Fig. 7 where $(-\delta_2/\delta_1)$ is plotted against α^*. Points relating to profiles having the same value of Z have the same symbol and points corresponding to constant values of X are connected by dotted lines. These symbols and dotted lines show a clear pattern. Also shown in Fig. 7 are the loci of the free-stream streamlines drawn in Fig. 1 and labelled with the letters A to E, and the locus of the separation line. Also shown is the line $\delta_2/\delta_1 = -2\alpha^*$ which would hold if equation (2) applied to the complete boundary layer. The data in Part 1, which are well represented by the triangular model, also fit this line closely. The present data (Fig. 7) clearly do not fit and, as expected from the shape of the polar plots in Fig. 5, $(-\delta_2/\delta_1)$ is in many cases much greater than $2\alpha^*$. The upstream ends of the streamlines appear to be tending to $\delta_2/\delta_1 = -2\alpha^*$ which agrees with Part 1 in that the upstream ends of these streamlines are all subjected to a monotonic transverse pressure field and a starting value of α^* of zero. However as the inflexion point of the free-stream streamline is approached $(-\delta_2/\delta_1)$ rises more rapidly than $2\alpha^*$. $(-\delta_2/\delta_1)$ continues to increase as the inflexion point is passed, at which α^* reaches its maximum, and throughout an appreciable distance downstream during which α^* is falling. Finally after $(-\delta_2/\delta_1)$ has reached a maximum it decreases with further reductions of α^*. Fig. 7 also appears to show that the separation line follows quite closely the locus of the maximum of $(-\delta_2/\delta_1)$. This conclusion must be treated with caution since in the immediate vicinity of separation and particularly in the separated region the value of $(-\delta_2/\delta_1)$ may be in significant error due to the static pressure gradients through the boundary layer.

Two equations were proposed in Part 1 relating the magnitude and direction of the skin-friction vector to the free-stream conditions. These equations are

$$\beta_0 = \sin^{-1}\{(Ku_\tau/U)^{-1}\sin\gamma\} - \gamma\,, \tag{4}$$

which was derived directly from the triangular model, and

$$\beta_0 = \sin^{-1}\{(Ku_\tau/U_0)^{-1}\sin\gamma\} - \gamma \tag{5}$$

which was found to give better agreement with the data. γ is the included angle between the side of the polar triangle representing the outer region of the boundary layer and the u/U axis (*see* Fig. 11 of Part 1). For the data in Part 1, equation (2) represented this side of the polar triangle closely so that γ could be written as

$$\gamma = \tan^{-1} 2\alpha^*\,. \tag{6}$$

Equation (5) with γ given by equation (6) is applied to the present data in Fig. 8 and good agreement is not obtained. However a qualitative similarity can be seen between Fig. 7 and Fig. 8, which suggests that α^* is not the proper independent variable to use in equation (6). An alternative form, which reduces to equation (6) for the data of Part 1 for which $\delta_2/\delta_1 = -2\alpha^*$, is

$$\gamma = -\tan^{-1}(\delta_2/\delta_1)\,. \tag{7}$$

The use of equation (7) implies that the side of the polar triangle which represents the outer region of the boundary layer is a weighted mean of the actual profile data. Equation (7) is not related directly to free-stream conditions but rather infers the existence of an equivalent polar triangle for profiles which do not fit the triangular model closely. Equation (4) with γ given by equation (7) is applied to the data in Fig. 9 and equation (5) with γ given by equation (7) is used in Fig. 10. These figures include all the data from Parts 1 and 2 for which Preston tube measurements were made with the exception of profiles which are either within the separated region or on the separation line. This last group of profiles have experimental values of β_0 greatly in excess of the calculated values. The values of K used in Figs. 9 and 10 were obtained by writing equations (4) and (7) in the form

$$U/u_\tau = K\,(\cos\beta_0 - (\delta_1/\delta_2)\sin\beta_0) \tag{8}$$

and equations (5) and (7) in the form

$$U_0/u_\tau = K\,(\cos\beta_0 - (\delta_1/\delta_2)\sin\beta_0) \tag{9}$$

and in each case taking the mean value of K for all the data shown in Figs. 9 and 10. Fig. 9 shows a wide and fairly systematic spread of the data which is very much reduced in Fig. 10. The standard deviation of the individual values of K using equation (9) is 1·07 which is 5·5 per cent of the mean. A slight trend is discernable in the individual values of K throughout the data and can also be seen in Fig. 10. This trend may be a genuine limitation of equation (9) or it may be a systematic error in the value of skin friction deduced from the Preston tube caused by the change from strong adverse pressure gradient to strong favourable pressure gradient in the data. From a consideration of the data it appears that the form of equation (9) is such that it gives a more accurate evaluation of u_τ/U_0 than of β_0 when compared on a percentage basis.

Equation (9) is of course entirely empirical but its derivation is such that it holds exactly for any profile which, when plotted in a polar plot of $\mathbf{u}/U$, takes the form of a triangle complying with the following two conditions.

(1) The magnitude of the velocity at the apex of the triangle is given by

$$(\mathbf{u}/U)_{\text{apex}} = K\,u_\tau/U_0\,.$$

(2) The inner region of the boundary layer up to the apex is sufficiently thin for the cross-flow integral (δ_2) to be obtained by assuming that the outer region extends over the whole boundary layer.

The above conditions are in general satisfied by a pair of triangles but the data suggest that, for unseparated boundary layers at least, the definition can be made unique by adding the restriction that the included angle at the apex should be obtuse.

An example of the many profiles that fit this equivalent triangle closely is profile 1228 shown in Fig. 11. Such profiles are confined to the region of the flow upstream of the free-stream inflexion point. Profile 2598 in Fig. 11 is an example of those profiles which are quite well correlated by equation (9) although they are not well represented by a triangle on the polar plot.

Also shown in Fig. 11 are two profiles which are not so well correlated by equation (9). Profile 2998 is representative of these profiles on $Z = 28$ and 30 inches for which, as shown in Fig. 10, measured values of β_0 are less than given by equation (7). These are decaying profiles in which the inner region appears to be decaying more rapidly than the rest of the profile. If this trend is continued a profile will be reached having $\beta_0 = 0$ but $\delta_2 \neq 0$, which is a condition that cannot be represented by an equivalent triangle. It must be assumed therefore that, for a free-stream flow that undergoes one or more inflexions, as soon as β_0 passes through zero for the first time equation (9) and the equivalent triangle concept in its present form cannot be applied to the flow thereafter.

Profile 2198 shown in Fig. 11 is quite clearly not represented by its equivalent triangle and in common with other profiles through the separated region the value of β_0 is much greater than the value given by equation (9). These are the profiles which have been excluded from Figs. 9 and 10. Profile 2198 could be described as a 'cross-over' profile though it should be appreciated that the twist of the velocity vector ($\partial\beta/\partial y$) in the outer region ($u/U > 0{\cdot}8$) is qualitatively the same as would occur in the potential flow around the obstruction with the floor boundary layer represented by its displacement thickness. Profile

2198 also exhibits quite clearly the characteristics of a 'double' boundary layer in which the inner and outer layers are displaced by about 35° and have quite different upstream histories.

It is concluded that equation (9) with a constant value of $K = 19{\cdot}45$ correlates the unseparated boundary layer data obtained in this experiment, although many of the profiles do not fit Johnston's triangular model well.

5.2. *Logarithmic Plots.*

Examples of the present data are shown in Fig. 12 plotted as $\mathbf{u}/U$ against $\log_{10}(y\,U/\nu)$. Also shown are the components of velocity, u/U and w/U, and the function $u \sec \beta_0/U$. As in Fig. 6 the values of y used in this figure are corrected for displacement effects by $+0{\cdot}004$ inch. The function $u \sec \beta_0/U$ was used in Part 1 because it generally exhibited a linear logarithmic region which, it was suggested, gave the best estimate of the skin friction by the method proposed by Clauser[9] for two-dimensional flows. These plots are compared in Fig. 12 with the 'Clauser' lines corresponding to the values of skin friction deduced from the Preston tube and razor blade measurements. As mentioned in Section 3 the inner region of most of the profiles is thick (up to $0{\cdot}1\,\delta$) and so covers much the same portion of the boundary layer as does the logarithmic law in two-dimensional boundary layers. In this region $\mathbf{u}/U$ and $u \sec \beta_0/U$ are very nearly equal, and as shown in Fig. 12, they both exhibit a linear logarithmic region which is in close agreement with the Preston tube and razor blade lines. The best examples shown are profiles 2416, 2808 and 2800. For some profiles, for which the inner region is thinner (e.g. profile 1624), $u \sec \beta_0/U$ produces a longer logarithmic region than $\mathbf{u}/U$ whereas for other profiles (e.g. 2008 and to a very small extent 2400) the opposite effect is produced. Profiles in the last group are either within the separated region or very close to the separation line and should probably be corrected for vertical static pressure gradients which will tend to increase the velocity in the region of $\log_{10}(y\,U/\nu)$ equal to about 4·5 and so improve the agreement between the data and the 'Clauser' lines.

It is concluded that the use of the function ($u \sec \beta_0/U$) to predict the skin friction in a three-dimensional boundary layer by the method proposed by Clauser for two-dimensional flows is satisfactory for all the data given in both parts of this Report with the possible exception of profiles within the separated region.

The proposal discussed in Part 1 that the $u \sec \beta_0/U$ profile might be treated as a two-dimensional equivalent of the actual three-dimensional boundary layer for the purpose of making use of existing two-dimensional skin-friction laws has not been tested with the present data owing to the lack of a two-dimensional skin-friction law applicable to the present pressure gradients.

5.3. *Mager's Cross-Flow Profiles.*

In Part 1 it was shown that Mager's cross-flow profile[10]

$$w/u = (1 - y/\delta)^2 \tan \beta_0 \qquad (10)$$

did not fit the data presented. Nine profiles from the present data are compared in Fig. 13 with equation (10) and it is readily seen that there is little agreement. The data are scattered widely about the line representing equation (10) which is inevitable in view of the wide variations of $\partial\beta/\partial y$ in the inner region and in the limit as $y \to 0$ in particular (*see* Section 5.1). By comparison equation (10) restricts the limiting twist to

$$\underset{y \to 0}{Lt}\,(\partial\beta/\partial y) = -\sin 2\,\beta_0/\delta\,.$$

Further support is therefore given to the conclusion of Part 1 that this type of representation is too simple and restrictive.

5.4. *Coles's and Thompson's Profiles.*

Fig. 14 shows a comparison between selected profiles from the present data and simple extensions of Coles's[11] and Thompson's[12] two-dimensional profiles to three dimensions. These extensions, which are discussed in Part 1 result in profiles in the direction normal to the surface shear stress having the shape of Coles's wake function and one minus Thompson's weighting function, and are both represented by one curve on Fig. 14. The data do not fit the curve (Fig. 14) and produce much wider variations than were found in Part 1. The reason for these wide variations of the present data is the same as given in Section 5.3 for similar variations about Mager's cross-flow profile.

6. *Conclusions.*

Extensive information is given of a turbulent three-dimensional boundary layer produced by an obstruction placed in a two-dimensional boundary layer flow. The flow is dominated by the large pressure gradients produced by the obstruction and the influence of the shear stress is restricted to the region of the flow close to the surface. Also, in the region of the separation line, the measurements show that the normal boundary layer approximations are invalidated by significant pressure gradients through to layer.

The analysis presented in the Report suggests that the experimental data have been obtained with an acceptable accuracy and the data have been compared with several existing theories of two and three-dimensional boundary layers.

The greater part of the data in this part of the Report relates to the flow downstream of a free-stream inflexion and the velocity profiles do not fit in closely with Johnston's triangular model. Data obtained ahead of the inflexion point do fit the triangular model quite closely, as did the data of Part 1. In spite of these limitations the triangular model has been used to derive an equation relating the skin-friction vector to other boundary layer parameters and this equation correlates all the unseparated boundary layer data. The equation will fail in separated regions and sufficiently far downstream of an inflexion point that the cross-flow angle at the surface has returned to zero.

The method described in Part 1 for deducing the skin friction in three-dimensional boundary layers using the logarithmic plot is found to be equally satisfactory for the data given in this part.

Mager's cross-flow profile and simple extensions to three dimensions of existing methods of representing two-dimensional profiles, using Coles's wake function and Thompson's weighting function, are all shown not to fit the data and in particular they are shown to be too restrictive to describe adequately the more complicated profile shapes that occur downstream of a free-stream inflexion.

LIST OF SYMBOLS

C_{f_0}	Skin-friction coefficient based on tunnel reference kinetic pressure
C_p	Static-pressure coefficient based on tunnel reference kinetic pressure
K	Constant (*see* equation (4))
n	Axis in the plane of the surface and normal to the skin-friction vector
U	Free-stream velocity
$\mathbf{u}$	Local velocity vector within boundary layer
u	Component of $\mathbf{u}$ parallel to $\mathbf{U}$
u_τ	Skin-friction velocity defined by $u_\tau = \sqrt{\tau/\rho}$
v	Component of velocity in y direction
w	Component of $\mathbf{u}$ normal to $\mathbf{U}$
X	Cartesian co-ordinate (*see* Fig. 2)
y	Displacement of probe centre from surface
Z	Cartesian co-ordinate (*see* Fig. 2)
α	Angular displacement of free-stream (uncorrected)
α^*	Corrected value of α, $\alpha^* = \alpha - 0{\cdot}1$ degree
β	Boundary-layer cross-flow angle. The angle between $\mathbf{u}$ and $\mathbf{U}$
β_0	Value of β in the limit as y tends to zero
γ	Defined by equations (5) and (6)
δ	Boundary-layer thickness $y = \delta$ at $\mathbf{u}/U = 0{\cdot}995$
δ_1	$\int_0^\delta (1-u/U)\,dy$
δ_2	$-\int_0^\delta (w/U)\,dy$
ν	Kinematic viscosity of fluid
ρ	Density of fluid
τ	Skin friction

REFERENCES

No.	*Author(s)*	*Title, etc.*
1	V. C. Patel	Calibration of the Preston tube and limitations of its use in pressure gradients. *J. Fluid Mech.* **23**, 185–208 (1965).
2	L. F. East	Measurement of skin friction at low subsonic speeds by the razor-blade technique. A.R.C. R. & M. 3525 (1966).
3	L. F. East and R. P. Hoxey ..	Boundary layer effects in an idealized wing-body junction at low speed. R.A.E. Technical Report 68161 (1968). A.R.C. 31028.
4	L. Rosenhead	*Laminar Boundary Layers*, Chapter 2. Oxford University Press (1963).
5	L. A. Wyatt and L. F. East ..	Low-speed measurements of skin friction on a slender wing. A.R.C. R. & M. 3499 (1966).
6	L. A. Wyatt and L. F. East ..	Low-speed measurements of skin friction on a large half-model slender wing. A.R.C. C.P. 1007 (1967).
7	A. M. O. Smith and J. L. Hess	Calculations of potential flow about arbitrary bodies. *Progress in Aeronautical Sciences*, Vol. 8 (1966).
8	J. P. Johnston	On the three-dimensional turbulent boundary layer generated by secondary flow. *Journal of Basic Engineering*, Trans. ASME Series D, **82** (1960).
9	F. H. Clauser	Turbulent boundary layers in adverse pressure gradients. *J. Aeronaut. Sci.*, **21**, No. 2 (1954).
10	A. Mager	Generalization of boundary layer momentum-integral equations to three-dimensional flows including those of rotating systems. NACA Technical Note 2310 (1951).
11	D. Coles	The law of the wake in the turbulent boundary layer. *J. Fluid Mech.* **1** (1956).
12	B. G. J. Thompson	A new two-parameter family of mean velocity profiles for incompressible turbulent boundary layers on smooth walls. A.R.C. R. & M. 3463 (1965).

TABLE 1

Boundary-Layer Displacement and Momentum Thickness.

Profile No.	Z	X	α	C_p	δ	δ_1	δ_2	θ_{11}	θ_{12}	θ_{22}	H
	inches	inches	degrees		inches	inches	inches	inches	inches	inches	
1228	12	28	6·82	0·226	5·21	0·7517	−0·1955	0·5570	0·0495	−0·0129	1·3496
1226	12	26	8·27	0·235	5·09	0·7808	−0·2458	0·5762	0·0644	−0·0208	1·3551
1224	12	24	9·80	0·243	5·29	0·8069	−0·3121	0·5865	0·0843	−0·0330	1·3756
1222	12	22	11·51	0·242	5·31	0·8423	−0·4028	0·6035	0·1151	−0·0567	1·3959
1220	12	20	13·42	0·230	5·27	0·9116	−0·5181	0·6307	0·1641	−0·0978	1·4453
1218	12	18	15·33	0·201	5·35	1·0110	−0·6594	0·6676	0·2376	−0·1678	1·5144
1426	14	26	8·42	0·201	5·30	0·7801	−0·2451	0·5822	0·0619	−0·0199	1·3400
1424	14	24	9·81	0·201	5·32	0·7894	−0·3048	0·5889	0·0777	−0·0310	1·3404
1422	14	22	11·37	0·192	5·29	0·7931	−0·3808	0·5877	0·0989	−0·0489	1·3494
1420	14	20	13·10	0·172	5·32	0·8272	−0·4718	0·6050	0·1299	−0·0781	1·3671
1418	14	18	14·49	0·137	5·42	0·8774	−0·5954	0·6247	0·1781	−0·1288	1·4046
1416	14	16	15·78	0·077	5·40	0·9590	−0·7312	0·6673	0·2391	−0·2027	1·4373
1626	16	26	8·42	0·166	5·18	0·7417	−0·2269	0·5601	0·0559	−0·0177	1·3243
1624	16	24	9·71	0·162	5·23	0·7608	−0·2783	0·5724	0·0690	−0·0261	1·3291
1622	16	22	11·03	0·148	5·25	0·7667	−0·3395	0·5776	0·0848	−0·0393	1·3274
1620	16	20	12·32	0·125	5·31	0·7806	−0·4192	0·5879	0·1059	−0·0601	1·3278
1618	16	18	13·56	0·087	5·37	0·7998	−0·5164	0·5983	0·1342	−0·0926	1·3367
1616	16	16	14·47	0·032	5·49	0·8242	−0·6206	0·6111	0·1687	−0·1389	1·3487
1614	16	14	14·88	−0·047	5·52	0·8709	−0·7154	0·6407	0·2060	−0·1938	1·3593
1824	18	24	9·16	0·126	5·09	0·7102	−0·2593	0·5412	0·0606	−0·0225	1·3123
1822	18	22	10·38	0·111	5·19	0·7180	−0·3051	0·5488	0·0715	−0·0313	1·3083
1820	18	20	11·53	0·087	5·19	0·7173	−0·3625	0·5506	0·0845	−0·0444	1·3028
1818	18	18	12·54	0·051	5·27	0·7210	−0·4322	0·5552	0·1009	−0·0639	1·2986
1816	18	16	13·22	−0·001	5·29	0·7256	−0·5100	0·5584	0·1207	−0·0911	1·2995
1814	18	14	13·53	−0·068	5·34	0·7369	−0·5845	0·5667	0·1413	−0·1234	1·3004
1812	18	12	13·23	−0·154	5·34	0·7592	−0·6616	0·5841	0·1637	−0·1624	1·2997
1810	18	10	12·44	−0·250	5·38	0·8602	−0·6803	0·6257	0·2171	−0·2249	1·3747
2022	20	22	9·64	0·079	4·98	0·6654	−0·2709	0·5145	0·0604	−0·0252	1·2932
2020	20	20	10·56	0·055	5·14	0·6665	−0·3185	0·5184	0·0699	−0·0344	1·2857
2018	20	18	11·39	0·021	5·14	0·6674	−0·3666	0·5220	0·0795	−0·0456	1·2784
2016	20	16	12·00	−0·023	5·23	0·6642	−0·4223	0·5216	0·0908	−0·0610	1·2734
2014	20	14	12·22	−0·079	5·16	0·6624	−0·4819	0·5217	0·1032	−0·0800	1·2696
2012	20	12	12·06	−0·150	5·27	0·6638	−0·5309	0·5246	0·1146	−0·1006	1·2654
2010	20	10	11·26	−0·225	5·32	0·6727	−0·5955	0·5354	0·1266	−0·1250	1·2564
2008	20	8	10·23	−0·309	5·28	0·7346	−0·6155	0·5722	0·1500	−0·1537	1·2839
2006	20	6	8·40	−0·385	5·34	0·8461	−0·6226	0·6222	0·2012	−0·2218	1·3599
2004	20	4	6·64	−0·450	5·31	0·9068	−0·5877	0·6490	0·2181	−0·2682	1·3973
2220	22	20	9·72	0·031	5·07	0·6090	−0·2764	0·4788	0·0568	−0·0260	1·2720
2218	22	18	10·51	−0·001	4·98	0·6038	−0·3075	0·4763	0·0627	−0·0326	1·2677
2216	22	16	11·01	−0·041	4·93	0·6020	−0·3466	0·4777	0·0695	−0·0412	1·2604
2214	22	14	11·33	−0·088	5·01	0·6012	−0·3797	0·4802	0·0755	−0·0502	1·2518
2212	22	12	11·08	−0·143	5·07	0·5995	−0·4236	0·4807	0·0830	−0·0622	1·2471

TABLE 1—*continued*

Boundary Layer Displacement and Momentum Thickness

Profile No.	Z	X	α	C_p	δ	δ_1	δ_2	θ_{11}	θ_{12}	θ_{22}	H
	inches	inches	degrees		inches	inches	inches	inches	inches	inches	
2210	22	10	10·48	−0·206	5·24	0·6038	−0·4675	0·4862	0·0912	−0·0763	1·2418
2208	22	8	9·56	−0·268	5·24	0·6092	−0·5018	0·4937	0·0971	−0·0889	1·2339
2206	22	6	8·12	−0·330	5·41	0·6285	−0·5426	0·5108	0·1047	−0·1020	1·2304
2204	22	4	6·56	−0·378	5·31	0·6897	−0·5560	0·5494	0·1219	−0·1198	1·2555
2202	22	2	4·96	−0·434	5·31	0·7709	−0·5567	0·5954	0·1498	−0·1585	1·2947
2200	22	0	3·38	−0·461	5·42	0·8499	−0·5434	0·6401	0·1700	−0·1998	1·3278
2198	22	−2	2·17	−0·449	5·47	0·8909	−0·5218	0·6654	0·1689	−0·2099	1·3389
2418	24	18	9·39	−0·020	5·20	0·5968	−0·2770	0·4777	0·0536	−0·0256	1·2495
2416	24	16	9·90	−0·052	5·12	0·5841	−0·3026	0·4697	0·0569	−0·0303	1·2435
2414	24	14	10·05	−0·093	5·17	0·5745	−0·3273	0·4644	0·0605	−0·0357	1·2372
2412	24	12	9·98	−0·139	5·21	0·5709	−0·3514	0·4636	0·0638	−0·0409	1·2314
2410	24	10	9·73	−0·188	5·08	0·5654	−0·3661	0·4603	0·0664	−0·0456	1·2283
2408	24	8	9·03	−0·237	5·17	0·5675	−0·3899	0·4630	0·0707	−0·0528	1·2257
2406	24	6	7·97	−0·284	5·34	0·5786	−0·4248	0·4739	0·0761	−0·0612	1·2208
2404	24	4	6·88	−0·325	5·33	0·5818	−0·4458	0·4792	0·0785	−0·0667	1·2143
2402	24	2	5·45	−0·374	5·46	0·5935	−0·4685	0·4911	0·0812	−0·0717	1·2085
2400	24	0	4·14	−0·383	5·51	0·6457	−0·4778	0·5277	0·0892	−0·0760	1·2236
2398	24	−2	3·04	−0·395	5·47	0·6892	−0·4594	0·5548	0·0947	−0·0777	1·2423
2616	26	16	8·95	−0·061	5·24	0·6090	−0·2548	0·4909	0·0490	−0·0218	1·2406
2614	26	14	8·99	−0·094	5·28	0·5927	−0·2794	0·4818	0·0514	−0·0257	1·2302
2612	26	12	8·96	−0·132	5·29	0·5770	−0·2967	0·4717	0·0527	−0·0286	1·2232
2610	26	10	8·74	−0·174	5·30	0·5786	−0·3048	0·4748	0·0539	−0·0307	1·2186
2608	26	8	8·14	−0·210	5·39	0·5716	−0·3273	0·4708	0·0566	−0·0353	1·2141
2606	26	6	7·49	−0·251	5·41	0·5653	−0·3421	0·4668	0·0582	−0·0385	1·2110
2604	26	4	6·71	−0·290	5·51	0·5700	−0·3520	0·4719	0·0596	−0·0410	1·2079
2602	26	2	5·70	−0·319	5·54	0·5713	−0·3657	0·4725	0·0618	−0·0439	1·2090
2600	26	0	4·74	−0·354	5·48	0·5708	−0·3701	0·4742	0·0615	−0·0448	1·2038
2598	26	−2	3·78	−0·349	5·68	0·5924	−0·3745	0·4924	0·0620	−0·0440	1·2030
2812	28	12	8·27	−0·131	5·09	0·5665	−0·2347	0·4603	0·0424	−0·0184	1·2305
2810	28	10	8·12	−0·161	5·13	0·5592	−0·2407	0·4572	0·0428	−0·0197	1·2230
2808	28	8	7·62	−0·194	5·18	0·5532	−0·2587	0·4549	0·0442	−0·0221	1·2160
2806	28	6	7·03	−0·227	5·20	0·5523	−0·2685	0·4565	0·0450	−0·0238	1·2098
2804	28	4	6·41	−0·256	5·32	0·5457	−0·2724	0·4523	0·0447	−0·0244	1·2063
2802	28	2	5·62	−0·295	5·42	0·5409	−0·2836	0·4499	0·0453	−0·0260	1·2023
2800	28	0	4·88	−0·315	5·52	0·5616	−0·2831	0·4663	0·0464	−0·0264	1·2043
2798	28	−2	4·06	−0·312	5·53	0·5817	−0·2827	0·4812	0·0469	−0·0258	1·2088
3006	30	6	6·68	−0·209	4·87	0·5167	−0·2077	0·4236	0·0346	−0·0145	1·2197
3004	30	4	6·19	−0·233	5·01	0·5261	−0·2087	0·4327	0·0345	−0·0145	1·2158
3002	30	2	5·57	−0·263	5·09	0·5253	−0·2117	0·4336	0·0345	−0·0149	1·2115
3000	30	0	4·83	−0·285	5·26	0·5318	−0·2150	0·4404	0·0343	−0·0151	1·2077
2998	30	−2	4·20	−0·283	5·26	0·5367	−0·2103	0·4425	0·0336	−0·0142	1·2131

TABLE 2

Skin Friction.

Profile No.	Preston tube U/u_τ	Preston tube $C_f \times 10^3$	Razor blade U/u_τ	Razor blade $C_f \times 10^3$
1228	35·19	1·615	35·49	1·588
1226	35·19	1·615		
1224	35·20	1·614	35·31	1·604
1222	34·59	1·671		
1220	33·97	1·733	34·74	1·657
1218	30·60	2·136		
1426	34·57	1·673		
1424	34·66	1·665	35·72	1·567
1422	33·29	1·804		
1420	32·60	1·882	34·49	1·681
1418	30·88	2·098		
1416	28·15	2·525	28·22	2·511
1626	33·73	1·758		
1624	32·91	1·847	30·60	2·136
1622	32·94	1·843		
1620	32·07	1·945	30·03	2·218
1618	31·03	2·077		
1616	29·20	2·345	29·86	2·243
1614	26·98	2·747		
1824	32·80	1·859	30·48	2·153
1822	32·43	1·901		
1820	31·74	1·985	31·11	2·067
1818	30·65	2·129		
1816	29·38	2·317	30·30	2·178
1814	28·40	2·479		
1812	26·64	2·818	27·24	2·696
1810	27·44	2·657		
2022	32·01	1·952		
2020	31·55	2·010	30·53	2·146
2018	30·73	2·118		
2016	29·84	2·246	31·24	2·049
2014	29·08	2·366		
2012	28·23	2·510	28·60	2·445
2010	26·78	2·789		
2008	26·88	2·768	26·83	2·779
2006	27·60	2·625		
2004	25·08	3·180		
2220	31·24	2·050	30·05	2·214
2218	30·51	2·148		
2216	30·12	2·205	30·11	2·205
2214	29·57	2·288		
2212	29·06	2·368	28·13	2·527

Profile No.	Preston tube U/u_τ	Preston tube $C_f \times 10^3$	Razor blade U/u_τ	Razor blade $C_f \times 10^3$
2210	28·36	2·486		
2208	27·37	2·671	27·83	2·582
2206	26·61	2·825		
2204	27·45	2·654	27·34	2·676
2202	28·62	2·442		
2200	27·43	2·658	26·82	2·780
2198	26·12	2·932		
2418	30·08	2·211		
2416	30·11	2·206	29·39	2·316
2414	29·68	2·270		
2412	29·41	2·313	29·11	2·360
2410	29·04	2·371		
2408	28·52	2·459	28·34	2·490
2406	28·20	2·515		
2404	27·87	2·576	26·99	2·746
2402	27·43	2·658		
2400	27·55	2·635	27·79	2·590
2398	28·37	2·486		
2616	30·15	2·200	29·25	2·338
2614	29·62	2·280		
2612	29·40	2·314	27·90	2·569
2610	29·28	2·333		
2608	29·16	2·352	28·68	2·432
2606	28·98	2·382		
2604	28·83	2·406	27·79	2·589
2602	28·94	2·388		
2600	28·68	2·431	28·84	2·405
2598	28·52	2·459		
2812	29·71	2·266	38·31	2·495
2810	29·47	2·303		
2808	29·14	2·355	28·66	2·435
2806	29·13	2·357		
2804	29·42	2·310	29·17	2·350
2802	29·30	2·329		
2800	29·29	2·331	27·85	2·579
2798	29·45	2·307		
3006	29·46	2·305		
3004	29·63	2·278	29·77	2·257
3002	29·47	2·303		
3000	29·52	2·295	28·62	2·442
2998	29·66	2·274		

TABLE 3

Velocity Profiles.

Profile No	1228		1225		1224		1222		1220		1218	
y	u/U	beta	u/U	beta	u/U	beta	u/U	beta	u/U	beta	u/U	beta
0.010	0.403	15.80	0.414	20.05	0.421	25.24	0.433	32.66	0.451	41.22	0.507	47.26
0.014	0.426	15.32	0.436	19.45	0.443	24.64	0.453	31.94	0.470	40.62	0.526	46.94
0.020	0.458	14.81	0.452	19.15	0.461	24.37	0.475	31.52	0.494	40.45	0.539	47.08
0.028	0.469	14.70	0.471	18.55	0.483	23.71	0.492	31.12	0.510	40.33	0.554	46.91
0.040	0.495	14.16	0.500	17.99	0.498	22.98	0.509	30.52	0.523	39.82	0.573	46.85
0.057	0.515	13.65	0.516	17.48	0.519	22.26	0.529	29.38	0.541	39.55	0.586	46.64
0.080	0.545	12.82	0.537	16.56	0.534	21.39	0.544	28.72	0.554	38.39	0.598	46.40
0.113	0.558	12.22	0.561	15.57	0.558	20.16	0.564	27.06	0.568	37.08	0.608	45.66
0.160	0.579	11.26	0.582	14.53	0.580	18.64	0.583	25.13	0.582	35.20	0.613	44.23
0.226	0.605	10.37	0.608	13.33	0.598	16.94	0.601	23.02	0.596	32.49	0.619	42.09
0.320	0.632	9.24	0.636	11.81	0.628	15.15	0.625	20.56	0.610	28.97	0.624	38.81
0.453	0.659	8.01	0.660	10.23	0.653	13.21	0.647	17.63	0.640	24.72	0.628	34.53
0.640	0.702	6.83	0.687	8.80	0.685	11.24	0.679	14.98	0.663	20.54	0.645	29.57
0.905	0.730	5.77	0.731	7.16	0.720	9.16	0.715	12.11	0.705	16.14	0.680	23.25
1.280	0.772	4.41	0.773	5.67	0.765	7.25	0.752	9.34	0.746	12.03	0.725	16.89
1.500	0.802	3.84	0.794	4.92	0.781	6.20	0.782	7.97	0.767	10.36	0.753	14.00
2.000	0.852	2.75	0.837	3.59	0.832	4.38	0.829	5.73	0.817	7.19	0.807	9.12
2.500	0.881	2.00	0.880	2.50	0.873	3.19	0.868	4.00	0.868	4.96	0.854	5.93
3.000	0.912	1.36	0.908	1.68	0.907	2.12	0.906	2.63	0.900	3.34	0.889	3.60
3.500	0.942	0.82	0.941	1.05	0.945	1.42	0.937	1.64	0.932	2.00	0.928	1.96
4.000	0.970	0.49	0.962	0.60	0.968	0.79	0.962	0.96	0.957	1.05	0.955	0.89
4.500	0.986	0.28	0.982	0.20	0.982	0.39	0.981	0.45	0.978	0.45	0.973	0.35
5.000	0.993	0.03	0.994	0.02	0.992	0.18	0.991	0.15	0.990	0.12	0.988	0.11
5.500	0.998	-0.03	0.998	-0.10	0.996	-0.09	0.997	-0.06	0.997	-0.06	0.997	-0.01
6.000	1.000	-0.09	1.000	-0.19	1.000	-0.09	1.000	-0.09	0.999	-0.06	0.999	0.11
6.500	1.000	-0.09	1.000	-0.19	1.000	-0.18	1.000	-0.09	1.001	-0.06	1.000	0.20
7.000	1.000	-0.09	1.000	-0.22	1.000	-0.18	1.000	-0.09	1.000	-0.03	1.000	0.29

Profile No	1425		1424		1422		1420		1418		1415	
y	u/U	beta	u/U	beta	u/U	beta	u/U	beta	u/U	beta	u/U	beta
0.010	0.444	19.50	0.433	22.38	0.452	27.42	0.472	33.26	0.498	39.09	0.542	37.97
0.014	0.455	18.43	0.459	21.87	0.475	26.76	0.503	32.69	0.521	38.86	0.569	37.79
0.020	0.467	17.77	0.480	21.57	0.503	26.40	0.516	32.60	0.550	39.03	0.596	38.03
0.028	0.489	17.42	0.500	21.23	0.515	26.07	0.538	32.42	0.566	38.65	0.618	38.03
0.040	0.512	16.88	0.525	20.63	0.539	25.58	0.560	31.97	0.585	38.92	0.638	37.91
0.057	0.533	16.25	0.544	20.09	0.560	24.83	0.574	31.55	0.602	38.65	0.654	37.97
0.080	0.557	15.48	0.562	19.16	0.577	24.05	0.590	30.92	0.616	38.47	0.667	38.03
0.113	0.574	14.64	0.582	18.19	0.594	23.11	0.611	29.26	0.630	37.76	0.679	37.73
0.160	0.594	13.66	0.604	16.96	0.608	21.55	0.622	27.97	0.643	36.62	0.686	37.29
0.226	0.624	12.55	0.632	15.59	0.634	19.74	0.641	25.80	0.652	34.45	0.686	36.87
0.320	0.644	11.27	0.648	14.07	0.654	17.88	0.656	23.39	0.660	31.66	0.690	35.95
0.453	0.675	9.87	0.673	12.34	0.679	15.59	0.677	20.32	0.673	27.61	0.689	34.34
0.640	0.696	8.41	0.702	10.40	0.705	13.15	0.701	17.13	0.691	22.85	0.696	31.87
0.905	0.740	7.03	0.740	8.79	0.736	10.92	0.732	13.85	0.728	18.00	0.714	27.17
1.280	0.774	5.57	0.773	6.91	0.779	8.59	0.773	10.69	0.761	13.54	0.745	20.20
1.500	0.789	4.80	0.792	5.96	0.794	7.43	0.785	9.18	0.785	11.50	0.764	16.59
2.000	0.832	3.48	0.836	4.37	0.831	5.49	0.835	6.59	0.832	8.15	0.810	10.20
2.500	0.871	2.53	0.865	3.12	0.873	3.94	0.866	4.68	0.863	5.71	0.846	6.11
3.000	0.907	1.78	0.905	2.20	0.906	2.71	0.903	3.19	0.900	3.80	0.893	3.61
3.500	0.937	1.21	0.932	1.42	0.941	1.73	0.935	1.96	0.926	2.37	0.923	2.10
4.000	0.962	0.67	0.958	0.82	0.961	0.98	0.957	1.13	0.959	1.30	0.954	1.05
4.500	0.981	0.33	0.979	0.44	0.979	0.47	0.975	0.53	0.973	0.58	0.973	0.48
5.000	0.991	0.09	0.991	0.11	0.990	0.12	0.990	0.11	0.989	0.10	0.989	0.12
5.500	0.997	-0.06	0.996	-0.04	0.998	-0.06	0.997	-0.07	0.996	-0.02	0.996	0.00
6.000	0.999	-0.18	0.999	-0.13	1.000	-0.18	1.000	-0.27	0.999	-0.14	0.998	0.15
6.500	1.000	-0.15	1.000	-0.16	1.000	-0.21	1.000	-0.24	1.001	-0.02	1.000	0.27
7.000	1.001	-0.15	1.000	-0.16	1.000	-0.24	1.000	-0.24	1.000	0.01	1.000	0.54

Profile No	1526		1624		1622		1620		1618		1516	
y	u/U	beta	u/U	beta	u/U	beta	u/U	beta	u/U	beta	u/U	beta
0.010	0.456	16.79	0.444	19.19	0.465	23.15	0.485	27.39	0.509	31.72	0.529	34.46
0.014	0.467	16.40	0.467	18.86	0.488	22.67	0.506	27.03	0.531	31.24	0.556	34.40
0.020	0.486	16.08	0.488	18.53	0.504	22.46	0.533	26.64	0.552	31.03	0.580	34.37
0.028	0.502	15.66	0.509	18.35	0.530	22.10	0.547	26.52	0.570	30.92	0.606	34.73
0.040	0.529	15.15	0.528	18.05	0.551	21.80	0.573	26.13	0.595	30.83	0.630	34.85
0.057	0.549	14.82	0.552	17.59	0.570	21.32	0.592	25.71	0.617	30.59	0.649	34.88
0.080	0.571	14.29	0.578	16.96	0.594	20.66	0.611	24.95	0.631	30.17	0.667	34.88
0.113	0.589	13.42	0.597	16.24	0.610	19.69	0.629	23.87	0.646	29.61	0.682	34.43
0.160	0.617	12.61	0.617	15.34	0.631	18.55	0.646	22.82	0.664	28.39	0.696	33.75
0.226	0.638	11.66	0.640	14.10	0.651	17.10	0.664	21.28	0.679	26.57	0.705	32.59
0.320	0.657	10.44	0.659	12.73	0.670	15.45	0.679	19.29	0.695	24.51	0.712	30.36
0.453	0.685	9.24	0.687	11.12	0.693	13.73	0.702	17.06	0.704	21.56	0.718	27.00
0.640	0.710	7.90	0.710	9.63	0.716	11.71	0.723	14.54	0.727	18.16	0.732	22.80
0.905	0.744	6.56	0.738	7.96	0.743	9.79	0.746	11.96	0.748	14.94	0.750	18.52
1.280	0.780	5.19	0.773	6.26	0.778	7.67	0.781	9.36	0.781	11.44	0.782	14.00
1.500	0.803	4.50	0.799	5.51	0.799	6.69	0.797	8.15	0.800	9.88	0.797	12.04
2.000	0.842	3.25	0.842	4.05	0.835	4.90	0.834	5.99	0.835	7.08	0.837	8.55
2.500	0.881	2.32	0.875	2.89	0.873	3.44	0.872	4.32	0.871	5.09	0.869	5.87
3.000	0.914	1.58	0.909	1.99	0.908	2.39	0.905	2.92	0.901	3.55	0.901	3.82
3.500	0.942	0.92	0.937	1.27	0.936	1.53	0.934	1.87	0.929	2.29	0.928	2.38
4.000	0.965	0.47	0.962	0.65	0.961	0.81	0.957	1.04	0.957	1.28	0.954	1.35
4.500	0.981	0.23	0.981	0.32	0.980	0.30	0.978	0.47	0.976	0.62	0.973	0.60
5.000	0.992	0.05	0.992	0.08	0.992	0.10	0.990	0.08	0.989	0.17	0.988	0.18
5.500	0.998	-0.06	0.997	-0.07	0.997	-0.08	0.997	-0.04	0.996	-0.04	0.995	-0.00
6.000	0.999	-0.09	0.999	-0.13	1.000	-0.17	0.999	-0.16	0.999	-0.10	0.999	-0.00
6.500	1.000	-0.12	1.000	-0.19	1.000	-0.23	1.001	-0.22	1.000	-0.10	1.000	0.03
7.000	1.000	-0.18	1.001	-0.25	1.000	-0.29	0.999	-0.25	1.000	-0.10	1.000	0.15

TABLE 3—*continued*
Velocity Profiles.

Profile No	1614		1824		1822		1820		1818		1815	
y	u/U	beta	u/U	beta	u/U	beta	u/U	beta	u/U	beta	u/U	beta
0.010	0.574	30.57	0.458	17.32	0.467	19.80	0.493	22.51	0.515	24.99	0.533	27.16
0.014	0.596	30.48	0.479	17.08	0.487	19.50	0.513	22.05	0.533	24.82	0.553	27.22
0.020	0.628	30.66	0.500	16.93	0.509	19.28	0.533	21.81	0.552	24.70	0.582	27.37
0.028	0.652	30.84	0.522	16.57	0.533	18.98	0.554	21.72	0.576	24.76	0.598	27.40
0.040	0.670	30.87	0.542	16.24	0.553	18.74	0.578	21.39	0.596	24.52	0.621	27.49
0.057	0.691	31.13	0.567	15.79	0.579	18.23	0.601	20.94	0.620	24.31	0.647	27.61
0.080	0.705	31.31	0.590	15.19	0.603	17.57	0.624	20.37	0.642	23.92	0.666	27.40
0.113	0.718	31.49	0.609	14.64	0.623	17.00	0.640	19.74	0.661	23.36	0.683	27.01
0.160	0.731	31.58	0.629	13.74	0.640	15.94	0.659	18.74	0.679	22.31	0.701	26.24
0.226	0.732	31.55	0.655	12.69	0.662	14.80	0.677	17.51	0.693	21.11	0.713	25.05
0.320	0.733	31.49	0.677	11.51	0.684	13.50	0.692	16.06	0.707	19.24	0.724	23.26
0.453	0.735	30.93	0.699	10.23	0.708	11.94	0.714	14.20	0.725	17.07	0.736	20.71
0.640	0.739	29.53	0.726	8.74	0.729	10.28	0.735	12.18	0.744	14.66	0.751	17.81
0.905	0.751	26.17	0.748	7.22	0.751	8.65	0.759	10.13	0.768	12.16	0.771	14.47
1.280	0.769	19.71	0.793	5.70	0.789	6.80	0.795	8.02	0.798	9.51	0.802	11.00
1.500	0.783	16.53	0.812	5.04	0.810	5.99	0.814	7.00	0.813	8.25	0.819	9.59
2.000	0.823	10.05	0.850	3.73	0.853	4.32	0.850	5.19	0.851	5.99	0.850	7.00
2.500	0.863	5.96	0.887	2.71	0.884	3.16	0.883	3.72	0.882	4.30	0.883	4.95
3.000	0.896	3.43	0.916	1.88	0.914	2.12	0.912	2.56	0.913	2.92	0.912	3.36
3.500	0.927	1.92	0.946	1.19	0.942	1.40	0.942	1.63	0.941	1.80	0.941	2.12
4.000	0.952	0.96	0.968	0.68	0.966	0.77	0.964	0.86	0.961	1.11	0.961	1.19
4.500	0.972	0.32	0.984	0.24	0.981	0.36	0.981	0.41	0.977	0.51	0.977	0.53
5.000	0.988	-0.01	0.994	0.03	0.992	0.06	0.992	0.11	0.991	0.12	0.990	0.16
5.500	0.995	-0.01	0.998	-0.06	0.998	-0.03	0.998	-0.13	0.997	-0.06	0.997	-0.08
6.000	0.999	0.17	1.000	-0.00	0.999	-0.03	1.000	-0.19	0.999	-0.12	0.999	-0.14
6.500	1.000	0.29	1.000	-0.00	1.000	-0.12	1.000	-0.22	1.000	-0.12	1.000	-0.17
7.000	1.001	0.57	1.000	-0.03	1.001	-0.21	1.000	-0.28	1.000	-0.12	1.000	-0.11

Profile No	1814		1812		1810		2022		2020		2018	
y	u/U	beta	u/U	beta	u/U	beta	u/U	beta	u/U	beta	u/U	beta
0.010	0.546	28.56	0.585	25.76	0.539	26.22	0.476	17.16	0.488	18.80	0.501	20.63
0.014	0.571	28.68	0.618	25.85	0.568	25.98	0.494	16.86	0.510	18.59	0.525	20.30
0.020	0.600	28.92	0.638	26.17	0.592	26.28	0.519	16.68	0.534	18.53	0.545	20.24
0.028	0.627	29.34	0.667	26.29	0.623	26.70	0.537	16.44	0.554	18.35	0.569	20.30
0.040	0.649	29.37	0.692	26.59	0.651	27.32	0.562	16.14	0.578	18.14	0.592	20.09
0.057	0.675	29.75	0.717	26.71	0.681	27.80	0.586	15.87	0.603	17.87	0.618	19.91
0.080	0.694	29.75	0.735	27.04	0.704	29.17	0.610	15.45	0.625	17.36	0.642	19.55
0.113	0.713	29.84	0.747	27.01	0.726	30.59	0.634	14.76	0.646	16.78	0.662	18.91
0.160	0.727	29.66	0.756	27.10	0.744	32.77	0.655	14.03	0.667	16.03	0.682	18.10
0.226	0.738	28.71	0.765	27.10	0.759	34.40	0.675	13.04	0.686	14.98	0.701	17.11
0.320	0.745	27.16	0.766	26.98	0.773	36.07	0.698	11.86	0.706	13.71	0.719	15.69
0.453	0.752	24.55	0.768	26.63	0.777	36.87	0.720	10.57	0.728	12.30	0.737	13.97
0.640	0.759	20.83	0.769	25.28	0.771	35.71	0.742	9.06	0.750	10.55	0.756	12.20
0.905	0.773	16.93	0.779	22.63	0.756	30.06	0.769	7.68	0.775	8.89	0.781	10.15
1.280	0.801	13.07	0.797	17.87	0.760	19.56	0.804	6.05	0.805	6.94	0.810	8.10
1.500	0.817	11.21	0.809	14.69	0.776	14.14	0.820	5.30	0.823	6.15	0.826	7.02
2.000	0.854	7.89	0.843	9.47	0.824	6.76	0.859	3.84	0.860	4.53	0.860	5.15
2.500	0.883	5.46	0.876	5.67	0.865	3.18	0.893	2.74	0.893	3.26	0.892	3.71
3.000	0.911	3.65	0.908	3.23	0.904	1.58	0.922	1.87	0.921	2.27	0.919	2.53
3.500	0.936	2.20	0.935	1.82	0.933	0.62	0.950	1.10	0.948	1.40	0.946	1.60
4.000	0.959	1.24	0.959	0.92	0.958	0.14	0.973	0.56	0.970	0.72	0.966	0.88
4.500	0.976	0.46	0.976	0.34	0.975	0.05	0.986	0.23	0.985	0.27	0.982	0.39
5.000	0.988	0.09	0.988	0.04	0.989	-0.07	0.995	-0.01	0.993	0.03	0.993	0.06
5.500	0.997	-0.03	0.997	0.01	0.996	0.05	0.999	-0.07	0.998	-0.06	0.998	-0.09
6.000	0.999	-0.06	0.999	0.13	0.999	0.32	1.000	-0.07	1.000	-0.12	1.000	-0.09
6.500	1.000	0.00	1.000	0.31	1.000	0.65	1.000	-0.04	1.000	-0.03	1.000	-0.09
7.000	1.000	0.09	1.001	0.52	1.000	0.86	1.000	-0.04	1.000	-0.03	1.000	-0.06

Profile No	2015		2014		2012		2010		2008		2006	
y	u/U	beta	u/U	beta	u/U	beta	u/U	beta	u/U	beta	u/U	beta
0.010	0.512	21.99	0.531	22.65	0.551	23.72	0.572	22.27	0.557	17.68	0.512	28.86
0.014	0.529	21.81	0.554	22.77	0.571	23.64	0.601	22.24	0.584	17.98	0.548	28.98
0.020	0.556	21.78	0.580	23.04	0.599	23.87	0.631	22.62	0.613	18.48	0.581	28.68
0.028	0.586	21.87	0.604	23.25	0.626	24.08	0.658	22.92	0.648	18.80	0.613	29.52
0.040	0.610	21.93	0.632	23.40	0.654	24.26	0.689	23.25	0.679	19.34	0.648	30.14
0.057	0.634	21.75	0.657	23.60	0.682	24.71	0.720	23.54	0.706	19.85	0.682	31.07
0.080	0.660	21.63	0.681	23.69	0.705	25.00	0.741	23.66	0.731	20.34	0.714	31.87
0.113	0.681	21.25	0.702	23.60	0.727	25.36	0.759	23.99	0.750	20.92	0.748	33.21
0.160	0.701	20.59	0.720	23.34	0.744	25.21	0.773	24.11	0.760	22.14	0.778	34.10
0.226	0.716	19.55	0.735	22.44	0.756	24.91	0.782	23.90	0.773	22.68	0.799	35.08
0.320	0.732	18.06	0.748	20.96	0.767	23.70	0.786	23.46	0.776	24.49	0.809	35.83
0.453	0.747	16.33	0.759	18.87	0.774	21.58	0.789	22.44	0.784	25.50	0.811	35.80
0.640	0.764	14.22	0.774	16.17	0.781	18.67	0.793	20.75	0.789	26.19	0.795	33.98
0.905	0.787	11.66	0.790	13.34	0.794	14.92	0.802	18.25	0.792	23.99	0.764	29.19
1.280	0.814	9.19	0.818	10.39	0.818	11.38	0.818	14.68	0.803	18.36	0.745	18.57
1.500	0.829	7.96	0.834	8.98	0.834	9.95	0.828	12.54	0.813	14.61	0.755	12.56
2.000	0.863	5.94	0.863	6.54	0.864	7.16	0.858	8.40	0.842	8.16	0.814	3.96
2.500	0.893	4.23	0.893	4.64	0.893	4.99	0.888	5.48	0.876	4.29	0.863	1.40
3.000	0.918	2.84	0.918	3.23	0.917	3.33	0.915	3.50	0.907	2.27	0.905	0.48
3.500	0.944	1.79	0.943	2.14	0.943	2.04	0.941	2.08	0.938	1.13	0.934	0.06
4.000	0.965	1.00	0.965	1.21	0.964	1.17	0.962	1.12	0.960	0.53	0.959	-0.09
4.500	0.983	0.43	0.981	0.55	0.980	0.47	0.980	0.46	0.976	0.10	0.977	-0.14
5.000	0.992	0.10	0.992	0.09	0.991	0.08	0.990	0.06	0.991	-0.02	0.990	-0.09
5.500	0.997	-0.08	0.998	-0.09	0.997	-0.04	0.997	0.00	0.997	0.04	0.997	0.08
6.000	0.999	-0.14	0.999	-0.03	1.000	-0.07	1.000	0.09	0.999	0.22	0.999	0.33
6.500	1.000	-0.11	1.000	-0.03	1.000	0.05	1.000	0.27	1.000	0.50	1.000	0.60
7.000	1.000	-0.08	1.000	0.06	1.000	0.17	1.000	0.43	1.000	0.68	1.000	0.96

TABLE 3—*continued*

Velocity Profiles.

Profile No	2004		2220		2218		2216		2214		2212	
y	u/U	beta	u/U	beta	u/U	beta	u/U	beta	u/U	beta	u/U	beta
0.010	0.562	41.09	0.489	16.01	0.500	17.13	0.513	17.89	0.522	18.53	0.530	18.81
0.014	0.605	40.82	0.517	15.71	0.519	16.98	0.531	17.65	0.547	18.41	0.555	18.64
0.020	0.660	40.76	0.531	15.68	0.550	16.80	0.561	17.74	0.570	18.41	0.581	18.72
0.028	0.697	40.55	0.559	15.62	0.571	16.74	0.581	17.59	0.596	18.47	0.604	18.96
0.040	0.743	40.91	0.581	15.32	0.593	16.65	0.609	17.65	0.623	18.53	0.634	19.20
0.057	0.770	40.73	0.607	15.14	0.621	16.41	0.634	17.47	0.649	18.59	0.661	19.38
0.080	0.809	40.82	0.631	14.84	0.644	16.19	0.657	17.41	0.673	18.59	0.687	19.58
0.113	0.840	40.64	0.654	14.21	0.670	15.65	0.683	16.96	0.697	18.38	0.711	19.73
0.160	0.868	40.28	0.676	13.64	0.691	15.08	0.703	16.49	0.719	17.96	0.731	19.64
0.226	0.875	40.25	0.698	12.79	0.709	14.27	0.721	15.69	0.737	17.22	0.751	18.99
0.320	0.867	39.84	0.716	11.77	0.728	13.03	0.738	14.64	0.752	16.03	0.764	18.04
0.453	0.837	38.23	0.740	10.56	0.744	11.74	0.755	13.22	0.767	14.48	0.776	16.46
0.640	0.793	36.00	0.760	9.12	0.768	10.14	0.775	11.50	0.782	12.61	0.789	14.20
0.905	0.735	31.03	0.786	7.55	0.791	8.52	0.797	9.49	0.802	10.57	0.805	11.58
1.280	0.687	18.39	0.820	6.08	0.819	6.77	0.825	7.53	0.827	8.29	0.832	8.99
1.500	0.701	10.41	0.839	5.29	0.837	5.90	0.838	6.54	0.840	7.23	0.844	7.83
2.000	0.792	0.39	0.875	3.85	0.874	4.30	0.875	4.79	0.874	5.24	0.875	5.79
2.500	0.858	-1.19	0.905	2.76	0.904	3.01	0.902	3.49	0.903	3.74	0.903	4.16
3.000	0.899	-1.07	0.933	1.89	0.934	2.01	0.930	2.35	0.928	2.44	0.928	2.80
3.500	0.935	-0.86	0.957	1.17	0.957	1.26	0.955	1.48	0.954	1.54	0.952	1.75
4.000	0.959	-0.63	0.976	0.63	0.975	0.66	0.974	0.75	0.972	0.82	0.971	1.00
4.500	0.978	-0.39	0.990	0.27	0.989	0.27	0.988	0.27	0.986	0.34	0.986	0.40
5.000	0.990	-0.18	0.994	0.02	0.995	-0.01	0.996	-0.03	0.995	0.01	0.994	0.03
5.500	0.997	0.12	0.999	-0.10	0.999	-0.10	0.999	-0.15	0.999	-0.15	0.998	-0.15
6.000	1.000	0.44	1.000	-0.10	1.000	-0.16	1.000	-0.18	1.000	-0.18	1.000	-0.18
6.500	1.000	0.83	1.000	-0.10	1.001	-0.13	1.000	-0.18	1.000	-0.18	1.000	-0.18
7.000	1.000	1.10	1.000	-0.10	0.999	-0.19	1.000	-0.18	1.000	-0.15	1.000	-0.12

Profile No	2210		2208		2206		2204		2202		2200	
y	u/U	beta	u/U	beta	u/U	beta	u/U	beta	u/U	beta	u/U	beta
0.010	0.544	19.08	0.558	18.96	0.561	15.50	0.555	15.02	0.526	20.67	0.541	29.56
0.014	0.569	18.87	0.582	18.87	0.590	15.73	0.577	14.87	0.555	20.58	0.564	29.35
0.020	0.596	19.22	0.611	19.08	0.626	16.39	0.607	15.08	0.579	20.64	0.600	29.50
0.028	0.623	19.37	0.638	19.35	0.659	16.92	0.636	15.23	0.608	21.06	0.630	29.95
0.040	0.652	19.73	0.670	19.64	0.688	17.22	0.667	15.64	0.639	21.68	0.661	30.39
0.057	0.680	20.12	0.701	19.97	0.722	17.61	0.696	16.00	0.669	22.19	0.701	30.72
0.080	0.703	20.33	0.727	20.39	0.745	17.97	0.721	16.33	0.696	22.55	0.732	30.96
0.113	0.727	20.80	0.749	20.77	0.766	18.26	0.743	16.98	0.729	23.56	0.771	31.49
0.160	0.745	21.01	0.767	21.01	0.785	18.71	0.761	17.61	0.755	24.72	0.802	32.15
0.226	0.764	20.89	0.783	20.98	0.793	18.74	0.777	18.53	0.779	25.73	0.829	32.24
0.320	0.777	20.15	0.795	20.57	0.801	18.89	0.788	19.99	0.799	27.04	0.838	32.27
0.453	0.789	18.48	0.802	19.35	0.803	18.92	0.793	21.30	0.809	27.81	0.835	31.70
0.640	0.796	16.04	0.806	17.23	0.809	18.32	0.800	21.95	0.809	27.48	0.817	30.54
0.905	0.808	13.07	0.813	14.50	0.816	17.01	0.806	20.73	0.796	24.63	0.778	27.03
1.280	0.832	9.79	0.831	11.28	0.827	14.22	0.813	16.63	0.781	17.64	0.740	18.37
1.500	0.843	8.48	0.841	9.80	0.838	12.28	0.824	13.68	0.787	13.08	0.743	12.16
2.000	0.876	6.13	0.870	6.91	0.863	8.21	0.845	7.91	0.824	5.29	0.792	2.37
2.500	0.904	4.35	0.898	4.68	0.891	5.14	0.879	4.43	0.861	1.99	0.841	-0.79
3.000	0.927	3.06	0.924	3.07	0.918	3.12	0.909	2.29	0.898	0.59	0.888	-1.02
3.500	0.948	1.97	0.946	1.85	0.941	1.72	0.938	1.15	0.931	0.17	0.925	-0.67
4.000	0.968	1.13	0.966	0.96	0.963	0.86	0.959	0.50	0.956	-0.10	0.954	-0.49
4.500	0.984	0.50	0.981	0.42	0.980	0.38	0.978	0.17	0.975	-0.16	0.973	-0.34
5.000	0.993	0.10	0.992	0.09	0.990	0.09	0.990	0.02	0.990	-0.13	0.988	-0.19
5.500	0.997	-0.08	0.997	-0.06	0.996	-0.00	0.997	0.02	0.997	0.08	0.996	0.05
6.000	0.999	-0.14	0.999	-0.09	0.999	0.06	0.999	0.20	0.999	0.26	0.999	0.37
6.500	1.000	-0.08	1.000	-0.03	1.000	0.23	1.000	0.38	1.000	0.50	1.000	0.64
7.000	1.000	-0.08	1.000	0.09	1.000	0.38	1.000	0.59	1.000	0.71	1.000	0.88

Profile No	2198		2418		2416		2414		2412		2410	
y	u/U	beta	u/U	beta	u/U	beta	u/U	beta	u/U	beta	u/U	beta
0.010	0.565	32.72	0.509	14.50	0.512	14.81	0.522	15.05	0.532	15.15	0.532	14.82
0.014	0.595	32.84	0.531	14.32	0.532	14.72	0.544	14.96	0.550	15.15	0.554	14.79
0.020	0.633	32.78	0.549	14.32	0.556	14.72	0.569	15.05	0.578	15.18	0.580	14.94
0.028	0.668	33.02	0.576	14.32	0.577	14.75	0.589	15.05	0.600	15.36	0.605	15.18
0.040	0.703	33.08	0.599	14.20	0.607	14.69	0.618	15.14	0.625	15.48	0.633	15.36
0.057	0.741	33.05	0.625	14.05	0.632	14.60	0.643	15.17	0.656	15.57	0.660	15.57
0.080	0.777	33.17	0.650	13.75	0.658	14.42	0.668	15.05	0.680	15.66	0.688	15.83
0.113	0.814	33.32	0.674	13.39	0.682	14.18	0.693	14.87	0.705	15.60	0.713	16.10
0.160	0.843	33.23	0.696	12.88	0.705	13.70	0.717	14.57	0.727	15.42	0.736	16.07
0.226	0.864	33.08	0.718	12.18	0.727	13.13	0.737	13.95	0.746	14.97	0.756	15.75
0.320	0.868	32.45	0.737	11.28	0.746	12.29	0.754	13.08	0.764	14.08	0.774	15.09
0.453	0.852	31.81	0.757	10.14	0.763	11.05	0.771	11.86	0.780	12.83	0.788	13.84
0.640	0.818	30.24	0.776	8.84	0.784	9.58	0.791	10.44	0.796	11.11	0.800	12.15
0.905	0.771	27.16	0.801	7.49	0.805	8.10	0.812	8.87	0.815	9.29	0.816	9.91
1.280	0.716	19.03	0.827	6.01	0.833	6.44	0.837	7.03	0.839	7.39	0.840	7.71
1.500	0.709	12.37	0.843	5.35	0.848	5.69	0.853	6.16	0.854	6.55	0.854	6.73
2.000	0.764	1.30	0.875	3.87	0.880	4.19	0.879	4.59	0.882	4.95	0.881	4.95
2.500	0.833	-1.85	0.903	2.79	0.909	3.04	0.907	3.33	0.909	3.57	0.909	3.46
3.000	0.880	-1.64	0.928	1.89	0.929	2.14	0.935	2.25	0.929	2.46	0.933	2.50
3.500	0.919	-1.23	0.954	1.22	0.954	1.36	0.954	1.43	0.953	1.58	0.953	1.66
4.000	0.949	-0.93	0.972	0.71	0.972	0.84	0.970	0.83	0.970	0.89	0.970	0.93
4.500	0.971	-0.54	0.985	0.29	0.983	0.36	0.983	0.32	0.984	0.41	0.982	0.39
5.000	0.987	-0.36	0.992	0.05	0.994	0.03	0.993	0.05	0.993	0.08	0.994	0.03
5.500	0.995	0.02	0.998	-0.04	0.998	-0.06	0.998	-0.07	0.997	-0.07	0.998	-0.09
6.000	0.999	0.32	0.999	-0.07	0.999	-0.15	1.000	-0.16	0.999	-0.16	0.999	-0.18
6.500	1.000	0.62	1.000	-0.07	1.000	-0.12	1.000	-0.13	1.000	-0.19	1.000	-0.21
7.000	1.000	0.89	1.001	-0.07	1.000	-0.12	1.000	-0.13	1.001	-0.19	1.000	-0.18

TABLE 3—*continued*

Velocity Profiles.

Profile No	2408		2406		2404		2402		2400	
y	u/U	beta	u/U	beta	u/U	beta	u/U	beta	u/U	beta
0.010	0.518	13.68	0.544	14.58	0.547	14.38	0.569	12.96	0.549	11.39
0.014	0.545	13.89	0.563	14.49	0.569	14.38	0.590	12.93	0.575	11.36
0.020	0.576	14.40	0.592	14.82	0.600	14.50	0.621	13.29	0.600	11.51
0.028	0.608	14.90	0.621	15.12	0.629	14.71	0.646	13.29	0.632	11.75
0.040	0.636	15.20	0.648	15.33	0.659	15.06	0.678	13.68	0.662	11.99
0.057	0.667	15.56	0.676	15.71	0.689	15.33	0.708	13.92	0.690	12.23
0.080	0.696	15.98	0.706	16.19	0.718	15.87	0.734	14.18	0.723	12.44
0.113	0.721	16.39	0.732	16.70	0.744	16.28	0.759	14.63	0.748	12.85
0.160	0.743	16.75	0.754	17.14	0.767	16.67	0.782	14.99	0.768	13.21
0.226	0.765	16.72	0.774	17.50	0.786	17.06	0.797	15.22	0.783	13.72
0.320	0.782	16.30	0.790	17.32	0.800	16.91	0.808	15.34	0.796	14.31
0.453	0.793	15.29	0.803	16.37	0.811	[illegible]	0.817	15.31	0.803	14.96
0.640	0.806	13.36	0.811	14.55	0.818	14.94	0.819	14.81	0.807	15.50
0.905	0.819	0.89	0.821	11.82	0.825	12.65	0.826	13.68	0.815	15.29
1.280	0.841	8.30	0.839	8.93	0.840	9.92	0.838	11.84	0.827	13.24
1.500	0.853	7.14	0.851	7.68	0.849	8.61	0.847	10.41	0.834	11.63
2.000	0.882	5.15	0.879	5.66	0.876	6.28	0.871	7.37	0.854	7.88
2.500	0.908	3.69	0.904	4.02	0.902	4.35	0.894	4.84	0.881	5.03
3.000	0.931	2.53	0.927	2.80	0.926	[illegible]	0.918	3.00	0.908	2.92
3.500	0.952	1.63	0.950	1.85	0.945	1.82	0.944	1.81	0.935	1.61
4.000	0.967	0.89	0.964	1.11	0.961	1.02	0.959	0.94	0.955	0.83
4.500	0.984	0.41	0.981	0.54	0.978	0.45	0.976	0.47	0.975	0.39
5.000	0.993	0.09	0.990	0.18	0.990	0.16	0.988	0.17	0.988	0.12
5.500	0.998	-0.12	0.997	-0.05	0.997	-0.05	0.995	-0.01	0.995	-0.00
6.000	0.999	-0.18	0.999	-0.08	1.000	-0.08	0.999	-0.01	0.999	0.12
6.500	1.001	-0.21	1.000	-0.05	1.000	-0.05	1.000	0.11	1.000	0.18
7.000	1.000	-0.21	1.000	-0.02	1.000	-0.02	1.001	0.17	1.001	0.30

Profile No.	2398		2616		2614		2612		2610	
y	u/U	beta	u/U	beta	u/U	beta	u/U	beta	u/U	beta
0.010	0.519	11.31	0.504	12.69	0.515	12.71	0.522	12.65	0.525	12.33
0.014	0.543	11.28	0.528	12.51	0.538	12.62	0.545	12.53	0.545	12.18
0.020	0.572	11.34	0.552	12.54	0.562	12.65	0.568	12.59	0.575	12.24
0.028	0.603	11.52	0.576	12.48	0.589	12.59	0.592	12.65	0.598	12.42
0.040	0.630	11.66	0.600	12.48	0.613	12.65	0.620	12.71	0.626	12.54
0.057	0.666	11.84	0.632	12.39	0.642	12.65	0.650	12.71	0.655	12.69
0.080	0.696	12.17	0.657	12.24	0.666	12.62	0.676	12.80	0.681	12.78
0.113	0.729	12.59	0.681	12.03	0.692	12.41	0.701	12.74	0.707	12.87
0.160	0.747	12.97	0.703	11.76	0.716	12.18	0.726	12.56	0.731	12.96
0.226	0.767	13.99	0.727	11.22	0.737	11.67	0.747	12.20	0.753	12.66
0.320	0.782	15.03	0.745	10.43	0.756	10.99	0.764	11.52	0.774	12.09
0.453	0.792	15.98	0.766	9.41	0.774	10.03	0.783	10.51	0.788	11.20
0.640	0.800	16.60	0.777	8.23	0.791	8.84	0.799	9.26	0.803	9.71
0.905	0.807	16.43	0.800	6.97	0.809	7.57	0.815	7.80	0.820	8.17
1.280	0.812	14.07	0.829	5.49	0.834	6.04	0.842	6.19	0.842	6.47
1.500	0.819	11.96	0.841	4.77	0.847	5.34	0.851	5.59	0.855	5.70
2.000	0.842	7.26	0.868	3.51	0.877	3.93	0.880	4.27	0.876	4.18
2.500	0.872	4.11	0.898	2.54	0.899	2.84	0.900	3.06	0.900	2.99
3.000	0.900	2.20	0.925	1.79	0.923	1.97	0.925	2.13	0.922	2.09
3.500	0.928	1.10	0.948	1.16	0.945	1.25	0.946	1.38	0.944	1.40
4.000	0.955	0.48	0.963	0.65	0.964	0.71	0.965	0.81	0.963	0.86
4.500	0.973	0.12	0.981	0.28	0.979	0.28	0.981	0.35	0.979	0.41
5.000	0.988	0.03	0.991	0.04	0.992	0.10	0.991	0.08	0.991	0.10
5.500	0.995	0.00	0.998	-0.02	0.997	-0.05	0.997	-0.04	0.997	-0.05
6.000	0.999	0.12	0.999	-0.02	1.000	-0.02	0.999	-0.07	0.999	-0.08
6.500	1.000	0.24	1.000	0.01	1.000	0.01	1.000	-0.07	1.000	-0.02
7.000	1.001	0.36	1.000	0.01	1.000	-0.05	1.000	-0.07	1.000	-0.05

Profile No	2608		2606		2604		2602		2600	
y	u/U	beta	u/U	beta	u/U	beta	u/U	beta	u/U	beta
0.010	0.527	12.12	0.528	11.59	0.530	11.04	0.530	10.54	0.538	10.11
0.014	0.549	12.06	0.549	11.62	0.551	10.95	0.550	10.54	0.560	10.05
0.020	0.575	12.18	0.574	11.68	0.576	11.16	0.575	10.57	0.582	10.20
0.028	0.600	12.24	0.602	11.89	0.603	11.34	0.602	10.78	0.610	10.47
0.040	0.629	12.47	0.630	12.18	0.632	11.55	0.632	11.13	0.640	10.80
0.057	0.658	12.71	0.660	12.51	0.661	11.93	0.662	11.55	0.672	11.21
0.080	0.685	12.95	0.687	12.84	0.692	12.41	0.692	12.02	0.697	11.60
0.113	0.712	13.19	0.716	13.19	0.718	12.88	0.720	12.50	0.728	12.10
0.160	0.738	13.34	0.742	13.52	0.744	13.36	0.746	13.21	0.754	12.76
0.226	0.760	13.28	0.764	13.70	0.765	13.75	0.768	13.66	0.776	13.30
0.320	0.780	12.74	0.784	13.46	0.786	13.87	0.789	13.96	0.797	13.65
0.453	0.796	11.91	0.800	12.66	0.804	13.18	0.806	13.60	0.813	13.35
0.640	0.809	10.48	0.812	11.20	0.816	11.75	0.818	12.35	0.823	12.43
0.905	0.825	8.84	0.828	9.21	0.828	9.79	0.829	10.39	0.833	10.56
1.280	0.847	7.00	0.847	7.18	0.847	7.44	0.844	7.86	0.846	8.24
1.500	0.857	6.14	0.860	6.26	0.859	6.46	0.856	6.79	0.855	7.11
2.000	0.879	4.53	0.883	4.69	0.886	4.76	0.883	4.91	0.879	5.11
2.500	0.903	3.25	0.905	3.41	0.907	3.42	0.904	3.66	0.901	3.66
3.000	0.922	2.27	0.928	2.39	0.921	2.38	0.922	2.50	0.924	2.50
3.500	0.945	1.47	0.942	1.56	0.941	1.61	0.948	1.64	0.942	1.63
4.000	0.962	0.87	0.961	0.94	0.960	1.01	0.962	1.02	0.960	1.04
4.500	0.979	0.42	0.977	0.46	0.975	0.48	0.976	0.54	0.972	0.53
5.000	0.990	0.13	0.989	0.13	0.987	0.16	0.988	0.15	0.986	0.14
5.500	0.996	-0.02	0.996	-0.02	0.995	0.00	0.995	0.01	0.995	-0.00
6.000	0.999	-0.05	0.999	-0.04	0.999	-0.06	0.999	-0.02	0.998	-0.06
6.500	1.000	-0.02	1.000	-0.04	1.000	-0.12	1.000	-0.02	1.001	-0.06
7.000	1.000	-0.05	1.000	-0.07	1.000	-0.09	1.000	-0.02	1.000	-0.06

TABLE 3—*concluded*

Velocity Profiles.

Profile No	2598		2812		2810		2808		2806	
y	u/U	beta	u/U	beta	u/U	beta	u/U	beta	u/U	beta
0.010	0.525	9.61	0.514	10.35	0.519	10.03	0.513	9.34	0.520	9.34
0.014	0.550	9.58	0.533	10.23	0.543	9.94	0.537	9.25	0.542	9.22
0.020	0.577	9.73	0.558	10.20	0.570	10.09	0.562	9.40	0.568	9.37
0.028	0.603	9.85	0.586	10.26	0.591	10.09	0.590	9.67	0.593	9.49
0.040	0.635	10.21	0.611	10.35	0.616	10.15	0.619	9.90	0.622	9.64
0.057	0.666	10.48	0.637	10.41	0.647	10.36	0.649	10.17	0.651	9.88
0.080	0.696	10.95	0.667	10.41	0.671	10.44	0.676	10.38	0.681	10.15
0.113	0.726	11.40	0.691	10.38	0.701	10.50	0.705	10.53	0.710	10.38
0.160	0.752	11.91	0.717	10.26	0.726	10.50	0.732	10.59	0.736	10.62
0.226	0.779	12.32	0.738	9.93	0.746	10.24	0.757	10.53	0.760	10.62
0.320	0.797	12.65	0.757	9.42	0.767	9.76	0.776	10.08	0.782	10.44
0.453	0.812	12.59	0.776	8.53	0.784	8.93	0.792	9.34	0.798	9.70
0.640	0.820	11.88	0.793	7.55	0.798	7.86	0.806	8.30	0.814	8.89
0.905	0.831	10.54	0.810	6.30	0.815	6.58	0.824	7.05	0.830	7.29
1.280	0.842	8.54	0.837	5.05	0.838	5.18	0.844	5.59	0.847	5.74
1.500	0.851	7.56	0.849	4.48	0.852	4.55	0.855	4.85	0.859	5.06
2.000	0.875	5.54	0.876	3.33	0.880	3.33	0.882	3.60	0.881	3.72
2.500	0.898	3.99	0.905	2.43	0.905	2.35	0.904	2.61	0.904	2.68
3.000	0.916	2.74	0.930	1.65	0.930	1.64	0.926	1.81	0.925	1.90
3.500	0.938	1.82	0.953	1.08	0.952	1.03	0.951	1.19	0.950	1.25
4.000	0.956	1.02	0.972	0.53	0.970	0.55	0.969	0.65	0.964	0.69
4.500	0.970	0.51	0.987	0.20	0.984	0.22	0.985	0.29	0.981	0.33
5.000	0.983	0.15	0.994	0.02	0.993	0.04	0.993	0.06	0.992	0.06
5.500	0.992	0.03	0.998	-0.07	0.998	-0.08	0.998	-0.06	0.998	-0.06
6.000	0.998	-0.05	1.000	-0.10	0.999	-0.11	1.000	-0.09	0.999	-0.12
6.500	1.000	-0.02	1.000	-0.10	1.000	-0.11	1.000	-0.12	1.000	-0.12
7.000	1.001	0.00	1.000	-0.13	1.000	-0.17	1.000	-0.15	1.000	-0.15

Profile No	2804		2802		2800		2798		3006	
y	u/U	beta	u/U	beta	u/U	beta	u/U	beta	u/U	beta
0.010	0.515	8.80	0.524	8.08	0.526	7.35	0.505	6.11	0.513	6.42
0.014	0.538	8.62	0.548	7.96	0.547	7.29	0.528	6.25	0.534	6.69
0.020	0.563	8.74	0.571	8.11	0.573	7.44	0.554	6.46	0.562	7.16
0.028	0.589	8.89	0.595	8.29	0.596	7.56	0.579	6.67	0.583	7.43
0.040	0.622	9.13	0.622	8.53	0.622	7.80	0.607	7.00	0.612	7.64
0.057	0.648	9.31	0.655	8.86	0.651	8.18	0.641	7.50	0.643	7.85
0.080	0.679	9.72	0.681	9.24	0.680	8.60	0.668	7.92	0.670	8.11
0.113	0.709	10.05	0.710	9.68	0.709	9.17	0.699	8.55	0.696	8.23
0.160	0.736	10.41	0.740	10.08	0.736	9.64	0.729	9.20	0.723	8.41
0.226	0.762	10.59	0.765	10.52	0.763	10.36	0.755	9.82	0.750	8.41
0.320	0.784	10.53	0.787	10.55	0.784	10.65	0.780	10.30	0.770	8.20
0.453	0.801	9.93	0.808	10.22	0.804	10.50	0.802	10.39	0.791	7.67
0.640	0.818	8.92	0.821	9.24	0.820	9.64	0.817	9.76	0.808	6.80
0.905	0.833	7.46	0.837	7.84	0.834	8.09	0.828	8.31	0.825	5.67
1.280	0.852	5.86	0.856	6.12	0.847	6.34	0.845	6.28	0.849	4.57
1.500	0.861	5.08	0.865	5.34	0.858	5.45	0.853	5.36	0.859	3.98
2.000	0.885	3.74	0.888	3.95	0.880	3.84	0.878	3.81	0.889	2.91
2.500	0.906	2.67	0.907	2.82	0.901	2.80	0.898	2.80	0.915	2.10
3.000	0.928	1.87	0.925	2.01	0.921	1.97	0.918	2.00	0.938	1.39
3.500	0.946	1.27	0.945	1.27	0.946	1.25	0.940	1.35	0.960	0.88
4.000	0.965	0.77	0.966	0.79	0.962	0.75	0.957	0.81	0.978	0.47
4.500	0.979	0.32	0.979	0.41	0.976	0.39	0.974	0.48	0.989	0.17
5.000	0.990	0.08	0.989	0.11	0.987	0.12	0.986	0.18	0.996	-0.04
5.500	0.997	-0.04	0.996	-0.01	0.995	0.00	0.995	0.01	0.999	-0.13
6.000	0.999	-0.09	0.999	-0.04	0.999	-0.06	0.999	-0.05	1.000	-0.19
6.500	1.001	-0.09	1.000	-0.07	1.000	-0.06	1.000	-0.05	1.000	-0.25
7.000	1.000	-0.15	1.001	-0.10	1.000	-0.09	1.001	-0.05	1.000	-0.34

Profile No	3004		3002		3000		2998	
y	u/U	beta	u/U	beta	u/U	beta	u/U	beta
0.010	0.513	6.46	0.516	6.37	0.515	5.52	0.498	4.72
0.014	0.535	6.40	0.537	6.22	0.529	5.46	0.521	4.69
0.020	0.559	6.64	0.559	6.28	0.557	5.70	0.549	4.87
0.028	0.582	6.85	0.584	6.43	0.582	5.88	0.571	5.02
0.040	0.609	7.05	0.615	6.67	0.611	6.03	0.600	5.29
0.057	0.642	7.29	0.643	6.88	0.641	6.36	0.629	5.59
0.080	0.668	7.56	0.670	7.20	0.672	6.80	0.661	5.94
0.113	0.696	7.89	0.699	7.53	0.698	7.07	0.690	6.42
0.160	0.726	8.10	0.730	7.92	0.730	7.52	0.722	6.93
0.226	0.750	8.30	0.754	8.12	0.755	7.93	0.750	7.40
0.320	0.774	8.13	0.778	8.18	0.778	8.08	0.773	7.70
0.453	0.793	7.71	0.797	7.83	0.801	7.90	0.796	7.61
0.640	0.810	6.91	0.816	7.05	0.816	7.19	0.815	7.10
0.905	0.826	5.78	0.830	5.95	0.834	6.00	0.830	5.97
1.280	0.846	4.53	0.850	4.61	0.852	4.72	0.846	4.66
1.500	0.860	3.96	0.861	4.02	0.863	4.10	0.859	4.04
2.000	0.886	2.92	0.887	2.98	0.885	2.97	0.887	2.97
2.500	0.911	2.06	0.908	2.14	0.909	2.19	0.908	2.19
3.000	0.938	1.49	0.933	1.49	0.930	1.51	0.931	1.51
3.500	0.958	0.93	0.956	0.95	0.949	1.00	0.951	1.00
4.000	0.972	0.51	0.973	0.48	0.970	0.58	0.971	0.59
4.500	0.986	0.21	0.986	0.18	0.984	0.26	0.983	0.26
5.000	0.995	0.00	0.994	0.03	0.992	0.08	0.992	0.08
5.500	0.999	-0.09	0.999	-0.12	0.997	-0.04	0.997	-0.07
6.000	1.000	-0.15	1.000	-0.15	1.000	-0.04	0.999	-0.16
6.500	1.000	-0.23	1.000	-0.21	1.000	-0.13	1.000	-0.19
7.000	1.000	-0.32	1.000	-0.30	1.000	-0.19	1.000	-0.25

TABLE 4

Static-Pressure Distribution through the Boundary Layer.

Profile	3000	3004	2600	2604	2608	2612	2616	2200	2204	2208
y	C_p	C_p	C_p	C_p	C_p	C_p	C_p	C_p	C_p	C_p
0	−0·258	−0·217	−0·325	−0·273	−0·196	−0·120	−0·050	−0·460	−0·378	−0·251
0·08	−0·271	−0·232	−0·345	−0·286	−0·206	−0·128	−0·058	−0·512	−0·408	−0·275
0·16	−0·271	−0·234	−0·347	−0·288	−0·207	−0·129	−0·059	−0·520	−0·420	−0·278
0·32	−0·272	−0·234	−0·351	−0·291	−0·209	−0·131	−0·060	−0·538	−0·434	−0·283
0·64	−0·274	−0·235	−0·353	−0·294	−0·211	−0·131	−0·062	−0·579	−0·449	−0·285
1·28	−0·272	−0·235	−0·348	−0·291	−0·211	−0·132	−0·060	−0·687	−0·455	−0·280
2·00	−0·272	−0·232	−0·343	−0·288	−0·209	−0·131	−0·060	−0·624	−0·442	−0·272
3·00	−0·271	−0·231	−0·339	−0·285	−0·207	−0·131	−0·059	−0·534	−0·410	−0·268
4·00	−0·268	−0·229	−0·337	−0·285	−0·207	−0·129	−0·059	−0·490	−0·390	−0·270
5·00	−0·268	−0·227	−0·337	−0·283	−0·207	−0·131	−0·059	−0·474	−0·384	−0·268
6·00	−0·268	−0·229	−0·337	−0·285	−0·207	−0·129	−0·059	−0·464	−0·381	−0·267
7·00	−0·271	−0·232	−0·340	−0·288	−0·209	−0·131	−0·059	−0·459	−0·382	−0·267

Profile	2212	2216	2220	1812	1816	1820	1824	1416	1420	1424
y	C_p	C_p	C_p	C_p	C_p	C_p	C_p	C_p	C_p	C_p
0	−0·120	−0·021	0·040	−0·152	0·014	0·095	0·122	0·064	0·186	0·204
0·08	−0·134	−0·029	0·036	−0·173	0·011	0·100	0·130	0·052	0·189	0·210
0·16	−0·134	−0·029	0·035	−0·180	0·009	0·099	0·130	0·047	0·188	0·210
0·32	−0·138	−0·030	0·033	−0·192	0·008	0·098	0·129	0·038	0·186	0·207
0·64	−0·138	−0·031	0·032	−0·202	0·006	0·096	0·128	0·032	0·185	0·207
1·28	−0·138	−0·031	0·032	−0·192	0·006	0·095	0·128	0·039	0·183	0·207
2·00	−0·138	−0·031	0·033	−0·175	0·005	0·095	0·129	0·048	0·180	0·207
3·00	−0·138	−0·033	0·033	−0·173	0·002	0·095	0·130	0·049	0·178	0·207
4·00	−0·140	−0·033	0·035	−0·169	−0·001	0·094	0·131	0·052	0·174	0·206
5·00	−0·143	−0·034	0·035	−0·163	−0·001	0·093	0·131	0·061	0·174	0·205
6·00	−0·141	−0·035	0·033	−0·159	0·001	0·093	0·130	0·072	0·174	0·205
7·00	−0·141	−0·035	0·033	−0·154	0·001	0·093	0·130	0·080	0·177	0·203

TABLE 5

Cross-Flow Angles in the Free-stream (degrees).

Profile	3000	3004	2600	2604	2608	2612	2616	2200	2204	2208
y	β	β	β	β	β	β	β	β	β	β
7·0	−0·19	−0·32	−0·06	−0·09	−0·05	−0·07	0·01	0·88	0·59	0·09
7·5	−0·31	−0·38	−0·09	−0·06	−0·08	−0·10	−0·05	1·09	0·77	0·21
8·0	−0·34	−0·53	−0·03	−0·06	−0·11	−0·13	−0·08	1·26	0·92	0·30
8·5	−0·46	−0·59	−0·03	−0·06	−0·17	−0·19	−0·14	1·39	1·04	0·36
9·0	−0·52	−0·67	0·00	−0·09	−0·20	−0·22	−0·20	1·54	1·16	0·39
9·5	−0·55	−0·70	0·00	−0·09	−0·17	−0·28	−0·20	1·60	1·22	0·45
10·0	−0·61	−0·73	0·00	−0·09	−0·20	−0·28	−0·23	1·69	1·31	0·48
10·5	−0·61	−0·73	0·03	−0·09	−0·20	−0·28	−0·29	1·74	1·37	0·54
11·0	−0·64	−0·73	0·03	−0·06	−0·20	−0·25	−0·29	1·80	1·46	0·60
11·5	−0·64	−0·76	0·03	−0·03	−0·14	−0·28	−0·29	1·92	1·52	0·63

Profile	2212	2216	2220	1812	1816	1820	1824	1416	1420	1424
y	β	β	β	β	β	β	β	β	β	β
7·0	−0·12	−0·18	−0·10	0·52	−0·11	−0·28	−0·03	0·54	−0·24	−0·16
7·5	−0·09	−0·18	−0·10	0·70	−0·08	−0·31	−0·03	0·75	−0·24	−0·22
8·0	−0·06	−0·18	−0·13	0·82	−0·08	−0·34	−0·03	0·84	−0·24	−0·28
8·5	−0·06	−0·18	−0·16	0·97	−0·05	−0·31	−0·06	0·99	−0·24	−0·34
9·0	−0·03	−0·18	−0·19	1·09	0·07	−0·28	−0·06	1·11	−0·24	−0·34
9·5	0·00	−0·21	−0·25	1·18	0·13	−0·22	0·00	1·20	−0·27	−0·34
10·0	0·00	−0·21	−0·25	1·33	0·16	−0·22	−0·03	1·32	−0·15	−0·34
10·5	0·03	−0·21	−0·25	1·39	0·25	−0·22	−0·03	1·50	−0·09	−0·31
11·0	0·06	−0·21	−0·28	1·48	0·28	−0·19	−0·06	1·62	−0·06	−0·31
11·5	0·09	−0·18	−0·22	1·60	0·40	−0·19	−0·09	1·78	−0·01	−0·25

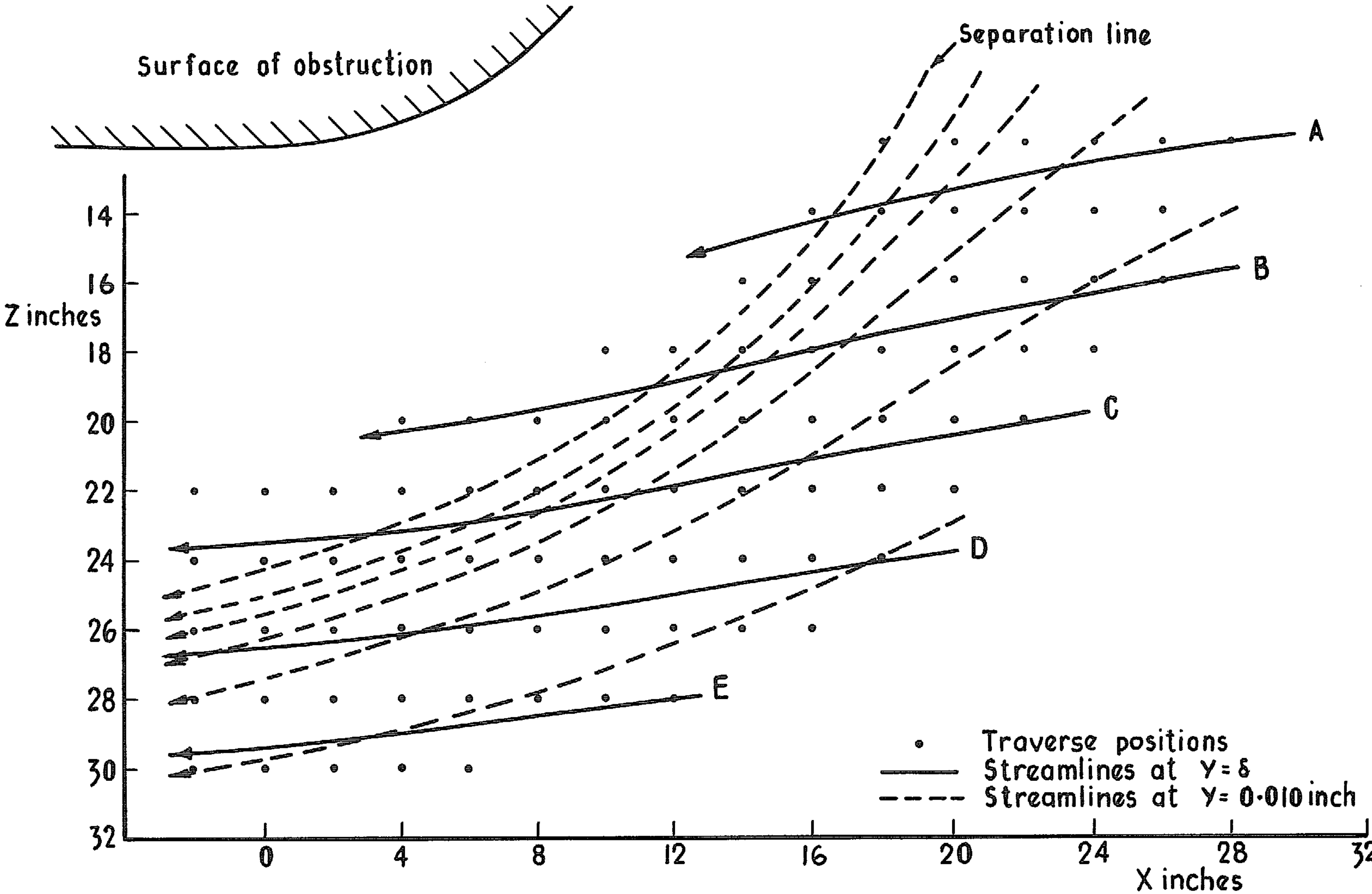

FIG. 1. Diagram showing the positions of the traverses and streamline patterns deduced from the flow measurements.

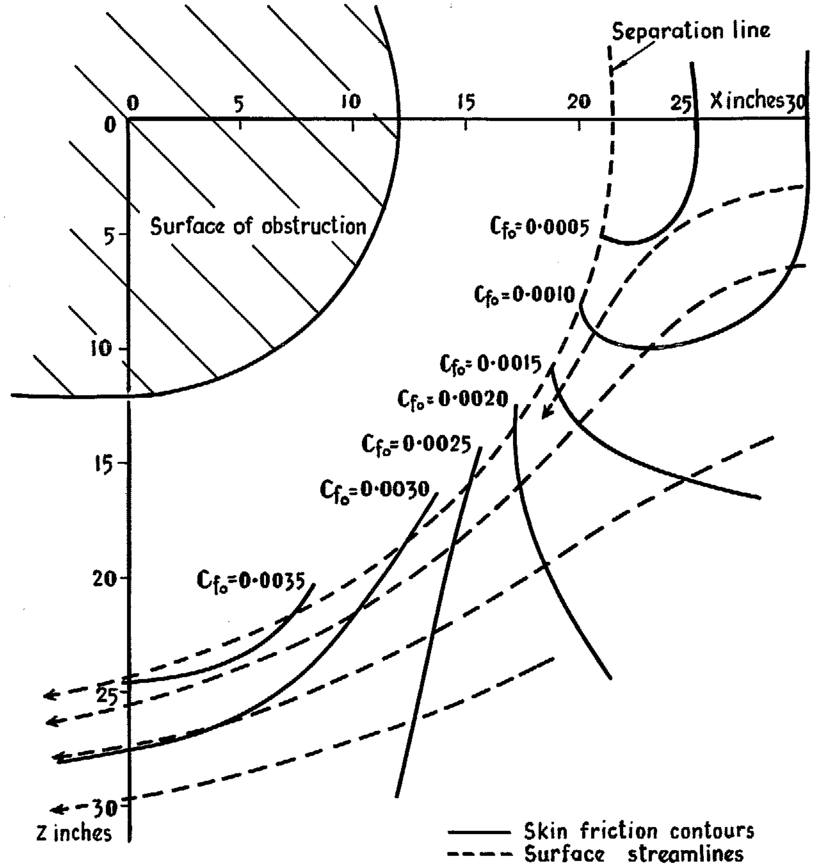

FIG. 2. Skin-friction contours, deduced from Preston tube measurements and surface streamlines.

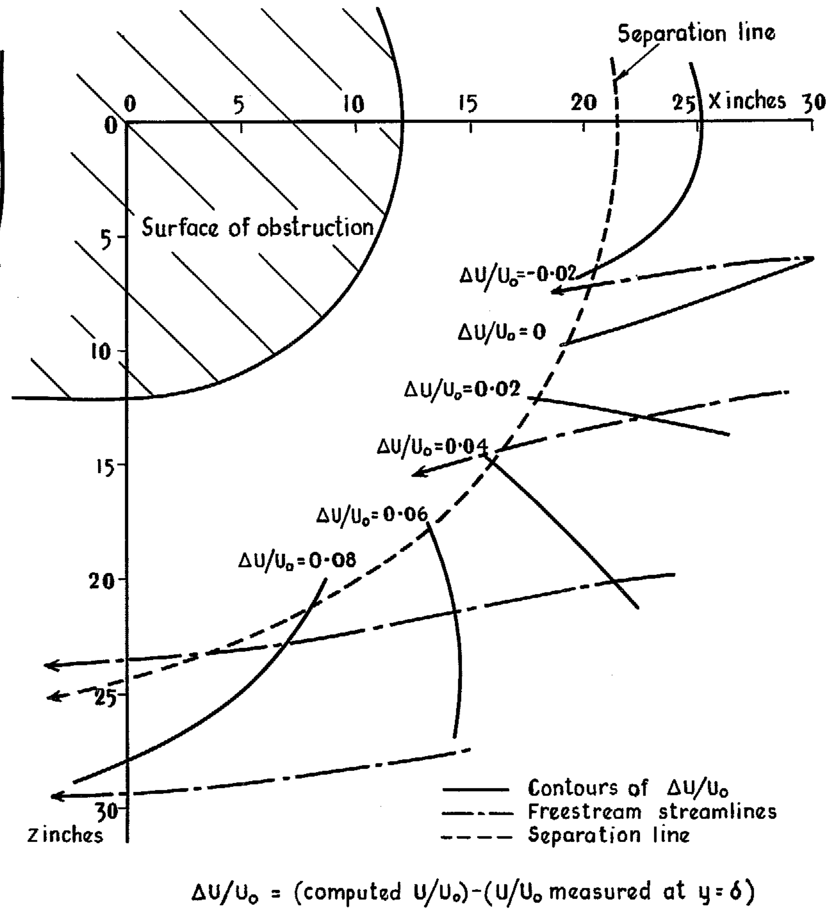

FIG. 3. Comparison between measured and computed free-stream velocity.

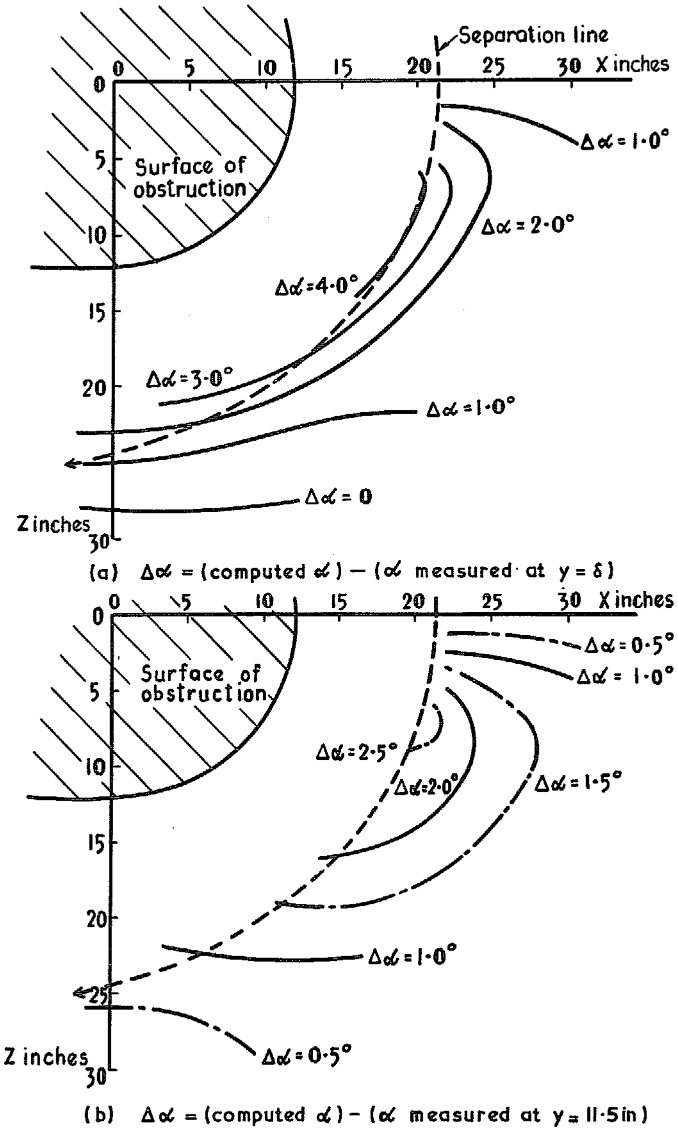

FIG. 4 a & b. Comparison between measured and computed free-stream flow angle.

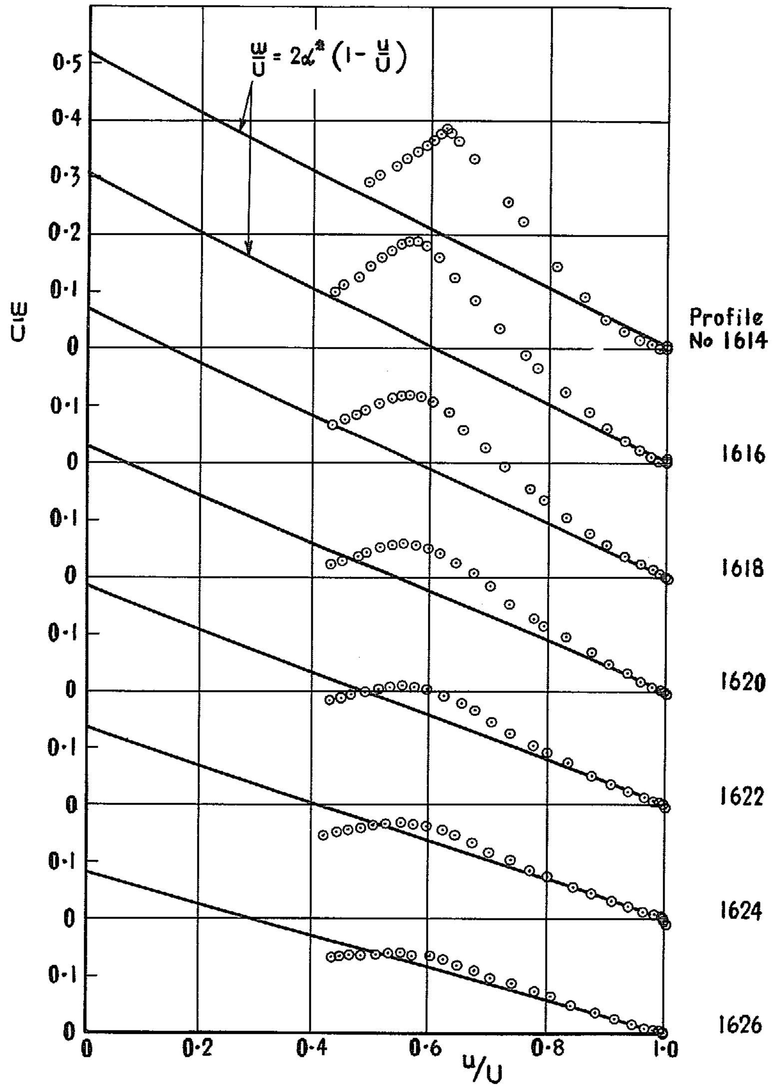

FIG. 5. Johnston plots of a selection of profiles. Z = 16 inches.

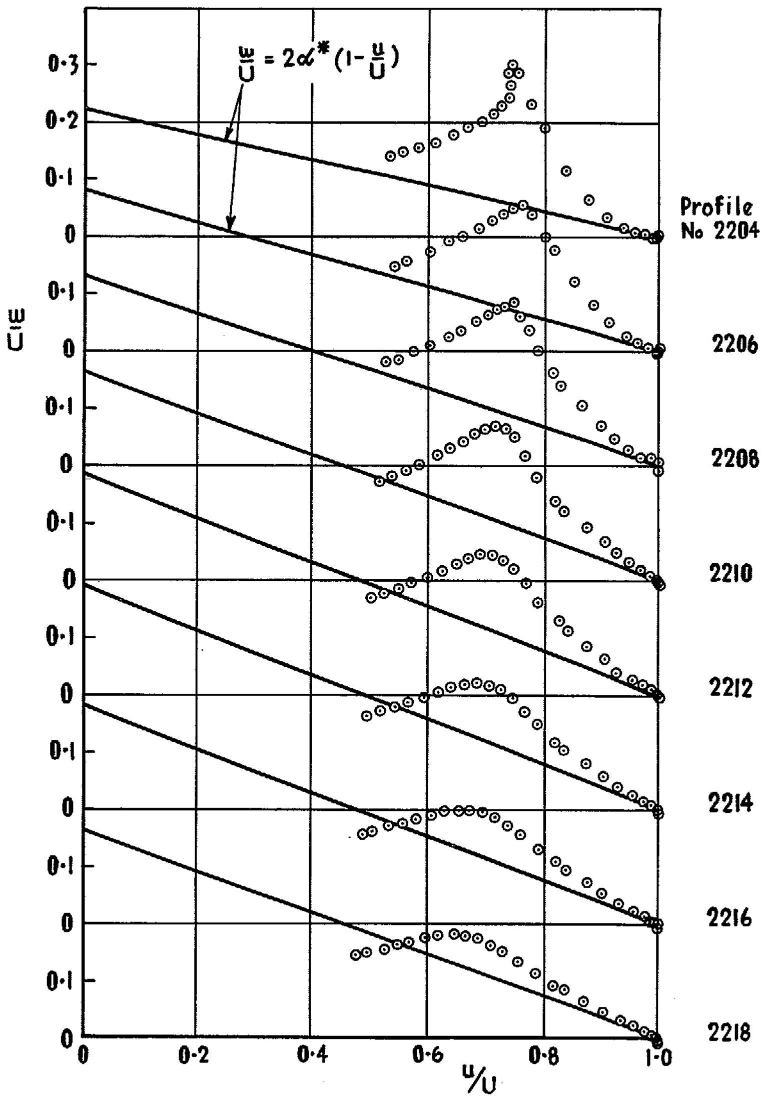

FIG. 5 *contd.* Johnston plots of a selection of profiles. Z = 22 inches.

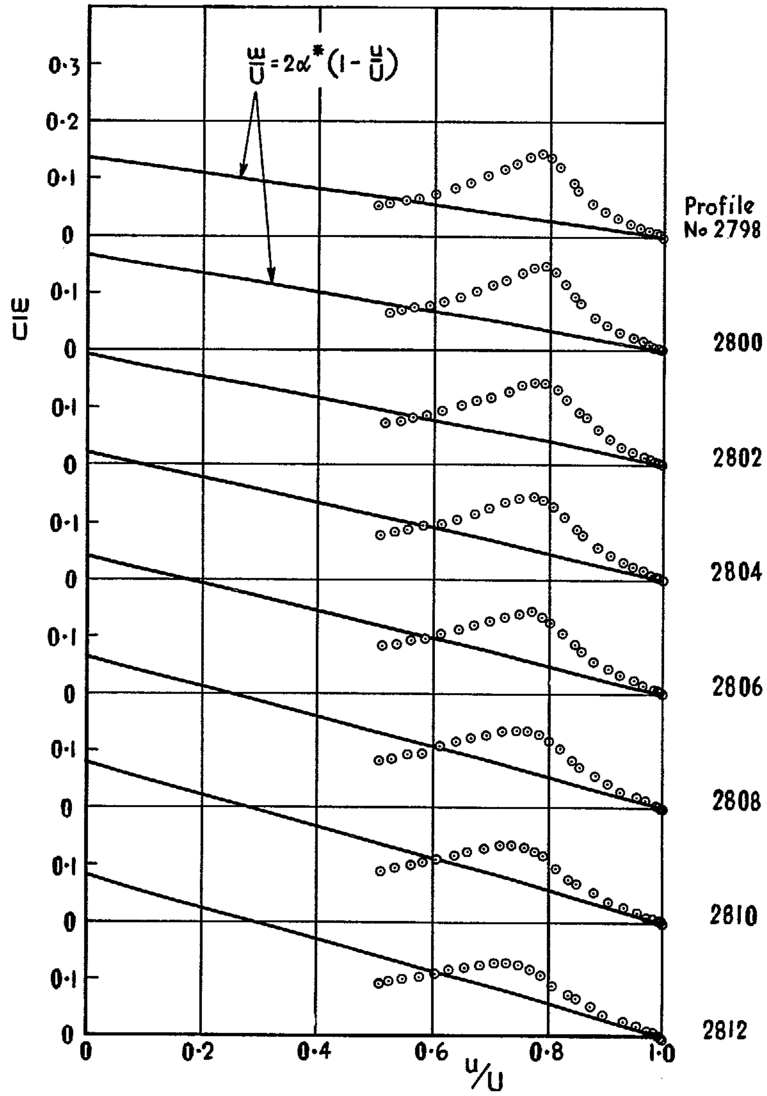

FIG. 5 *concld.* Johnston plots of a selection of profiles. Z = 28 inches.

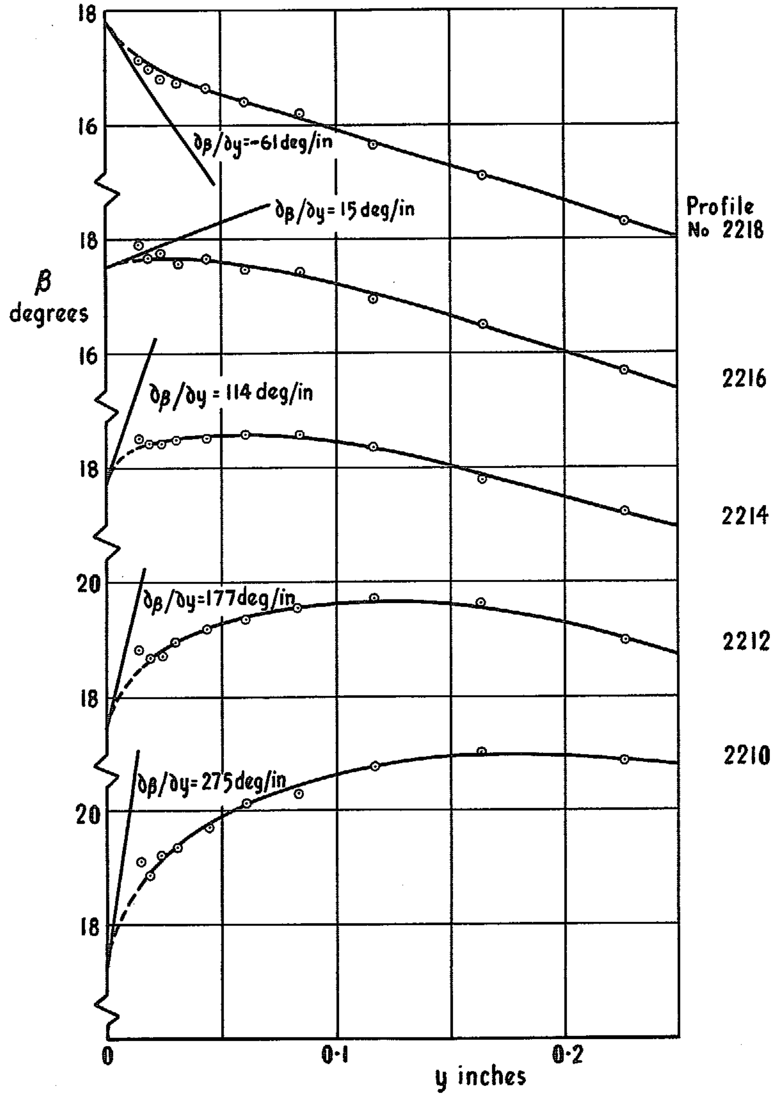

FIG. 6. Variation of cross-flow angle β over the inner region of a selection of profiles.

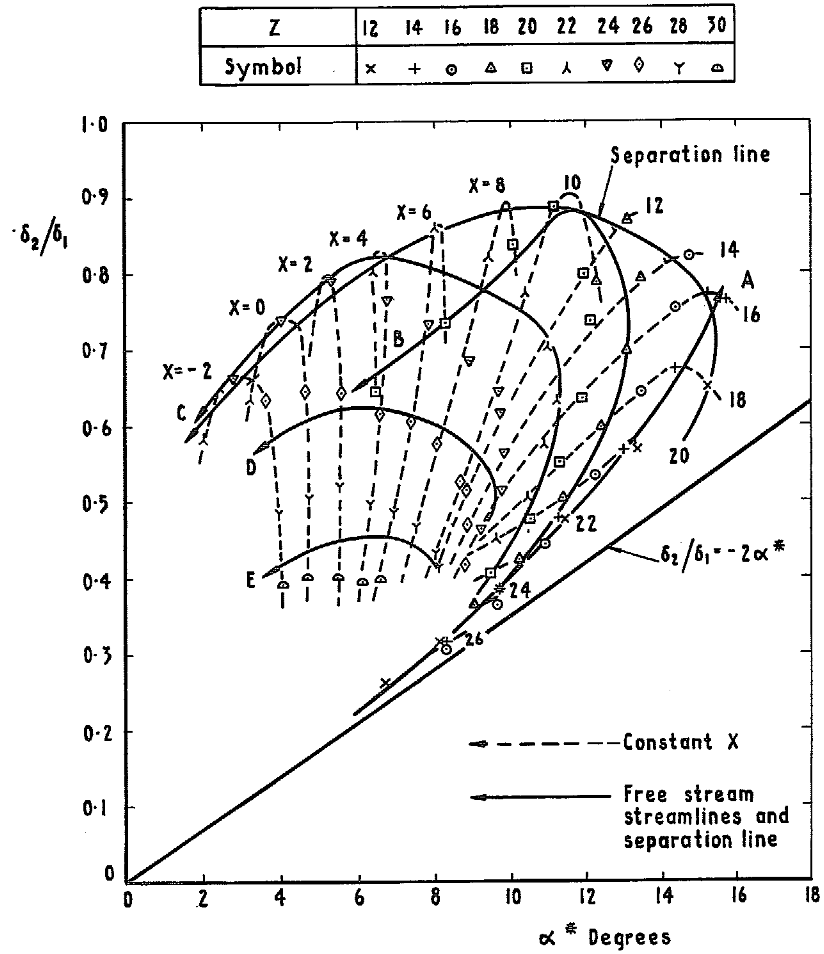

FIG. 7. Plot of ratio of displacement thicknesses against free-stream angle.

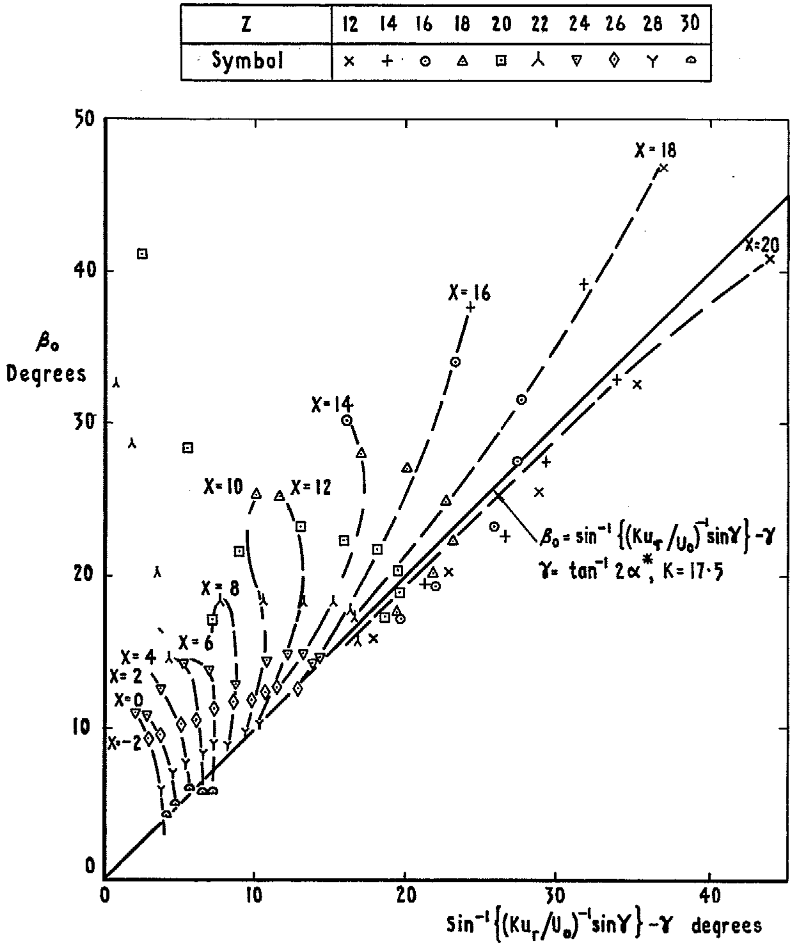

FIG. 8. Surface-flow direction given by equations 5 & 6 compared with data.

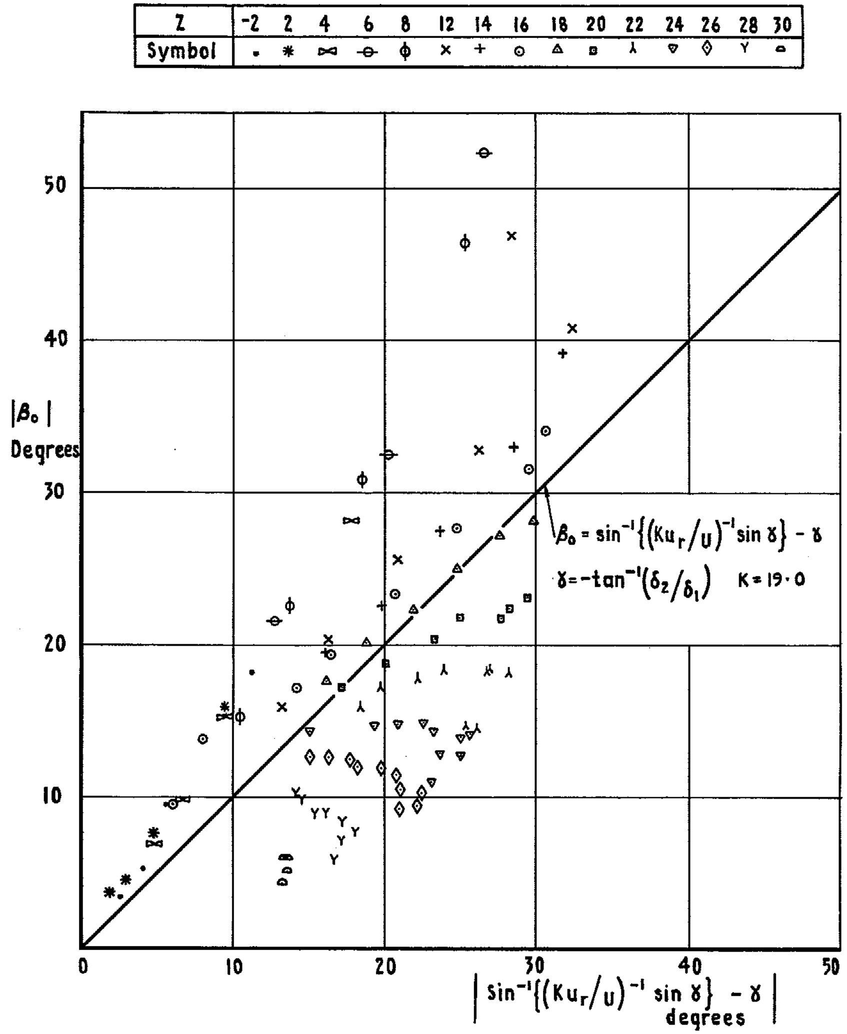

FIG. 9. Surface-flow direction given by equation 8 compared with data from Parts 1 & 2.

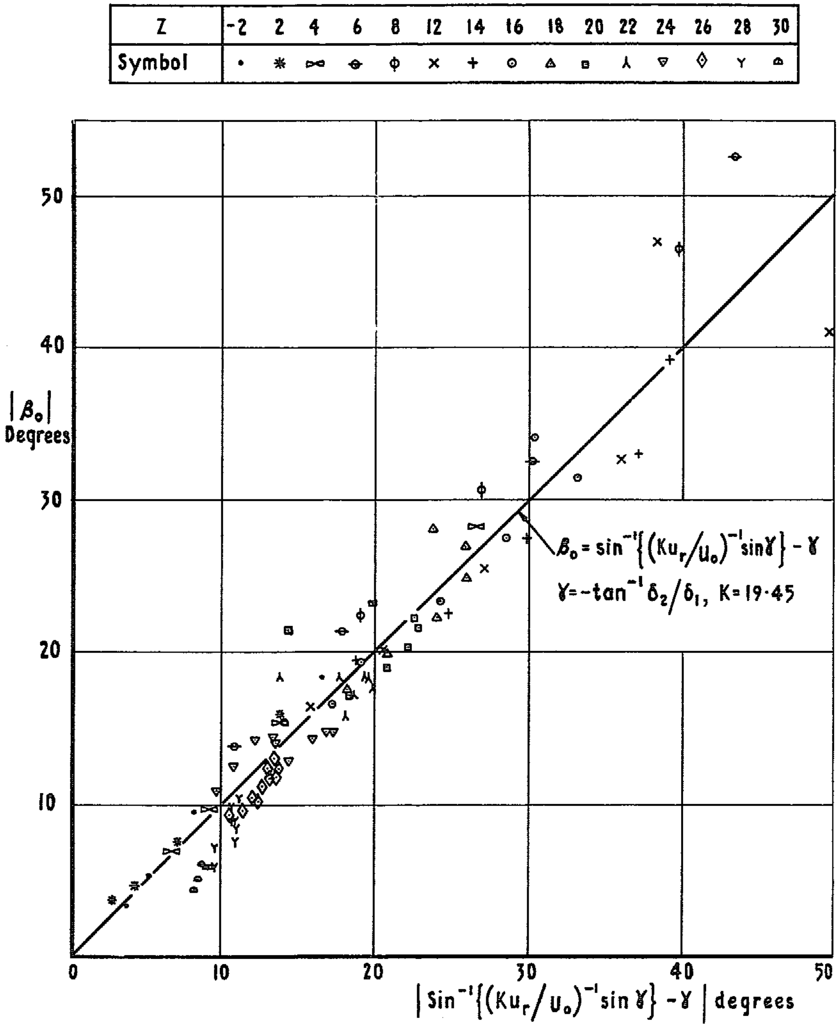

FIG. 10. Surface-flow direction given by equation 9 compared with data from Parts 1 & 2.

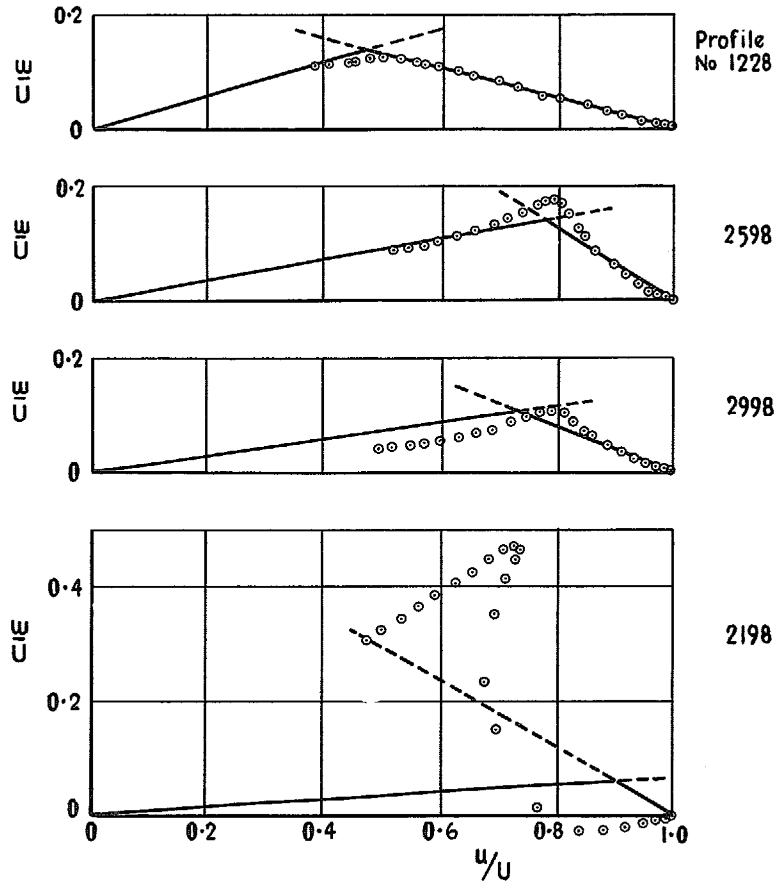

FIG. 11. Various profiles compared with the equivalent triangle used to derive equations 8 & 9.

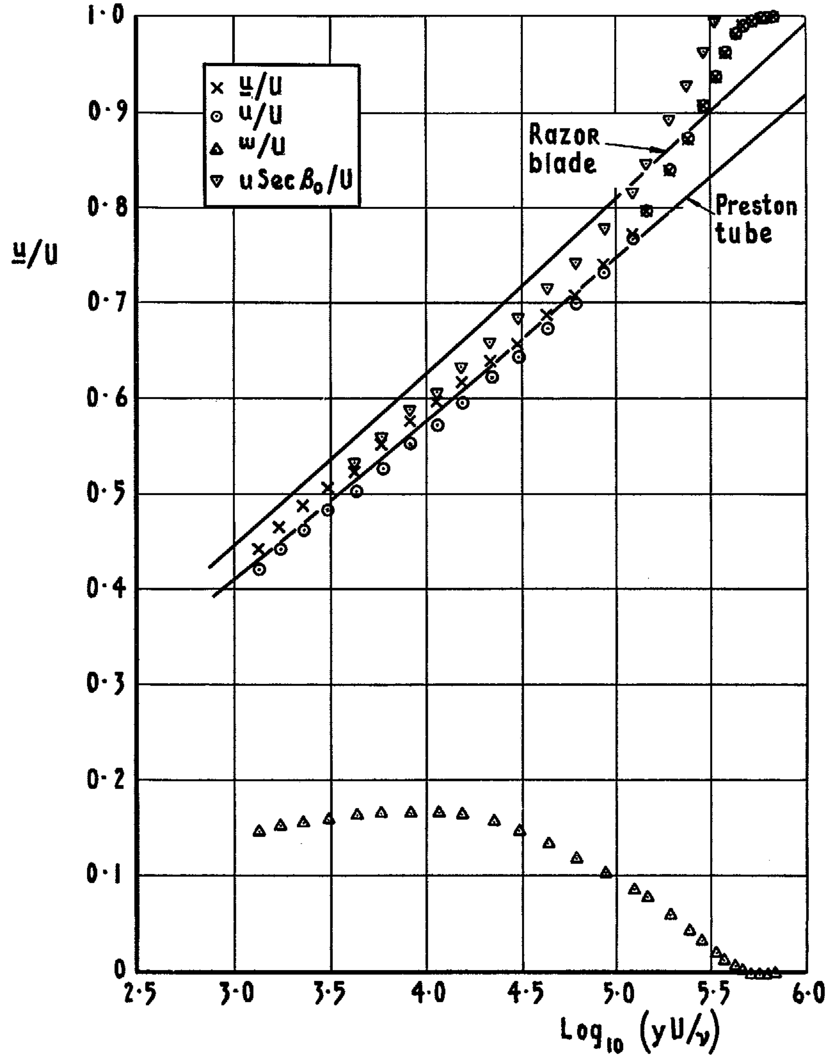

FIG. 12. Logarithmic plots, profile No. 1624.

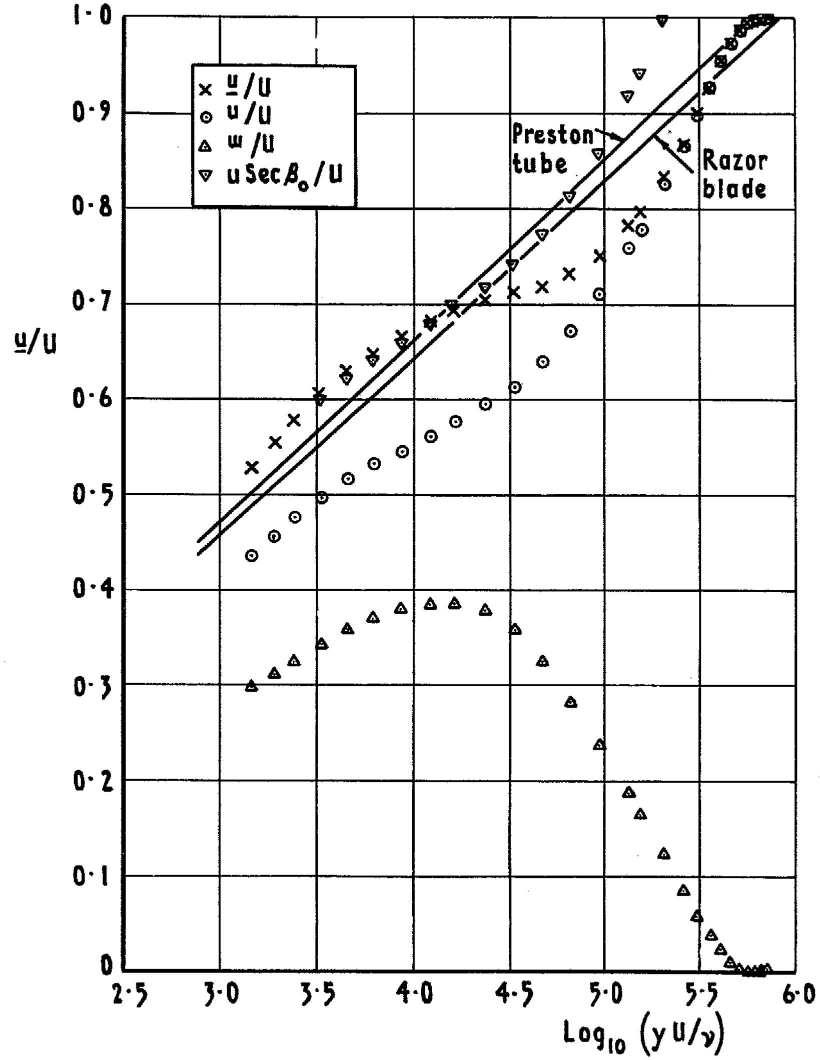

FIG. 12 *contd.* Logarithmic plots, profile No. 1616.

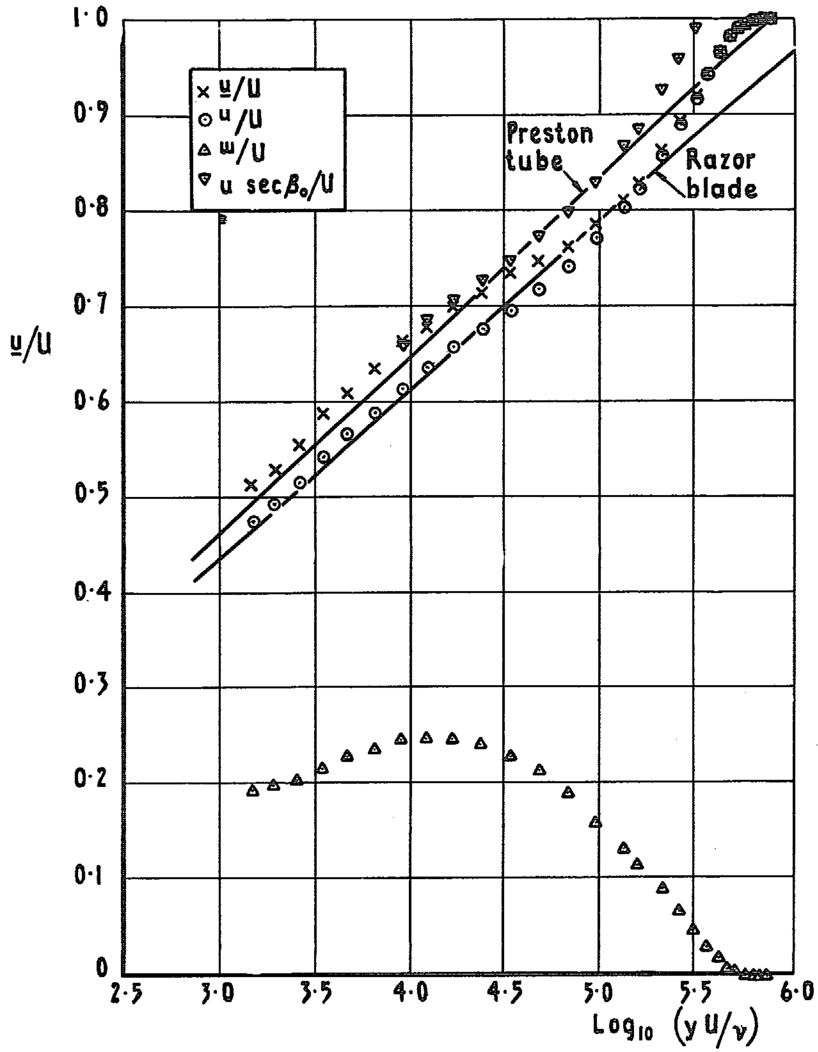

FIG. 12 *contd.* Logarithmic plots, profile No. 2016.

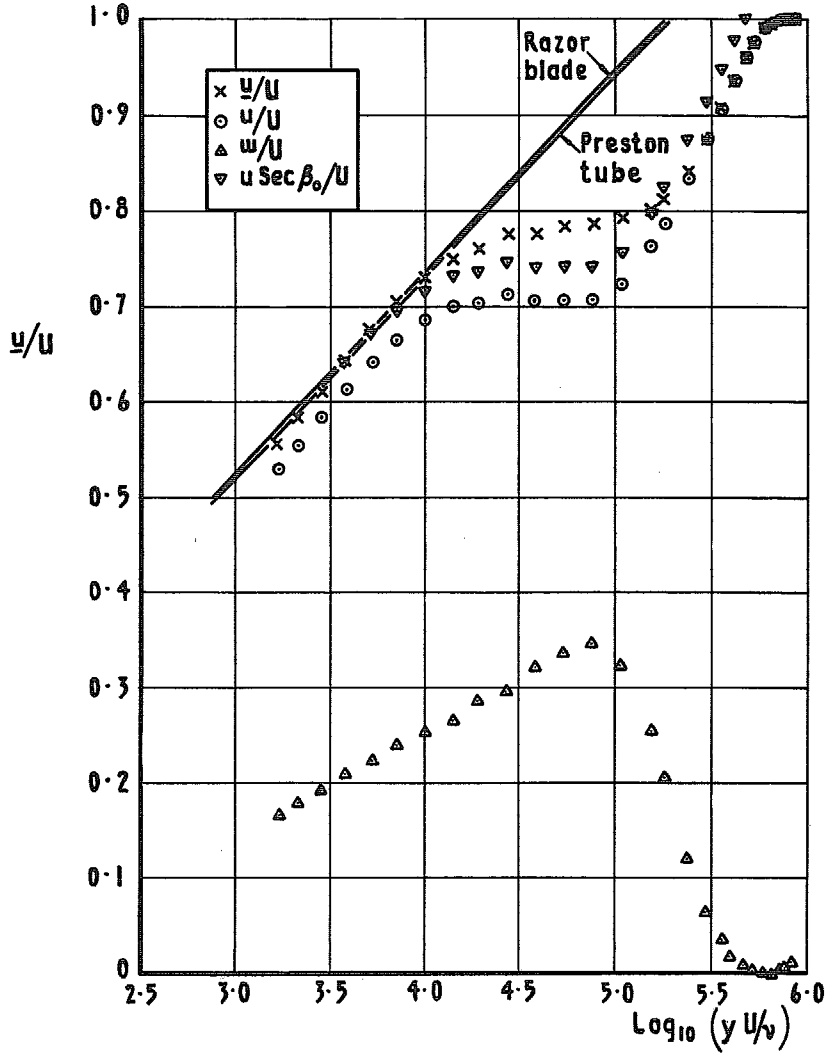

FIG. 12 *contd.* Logarithmic plots, profile No. 2008.

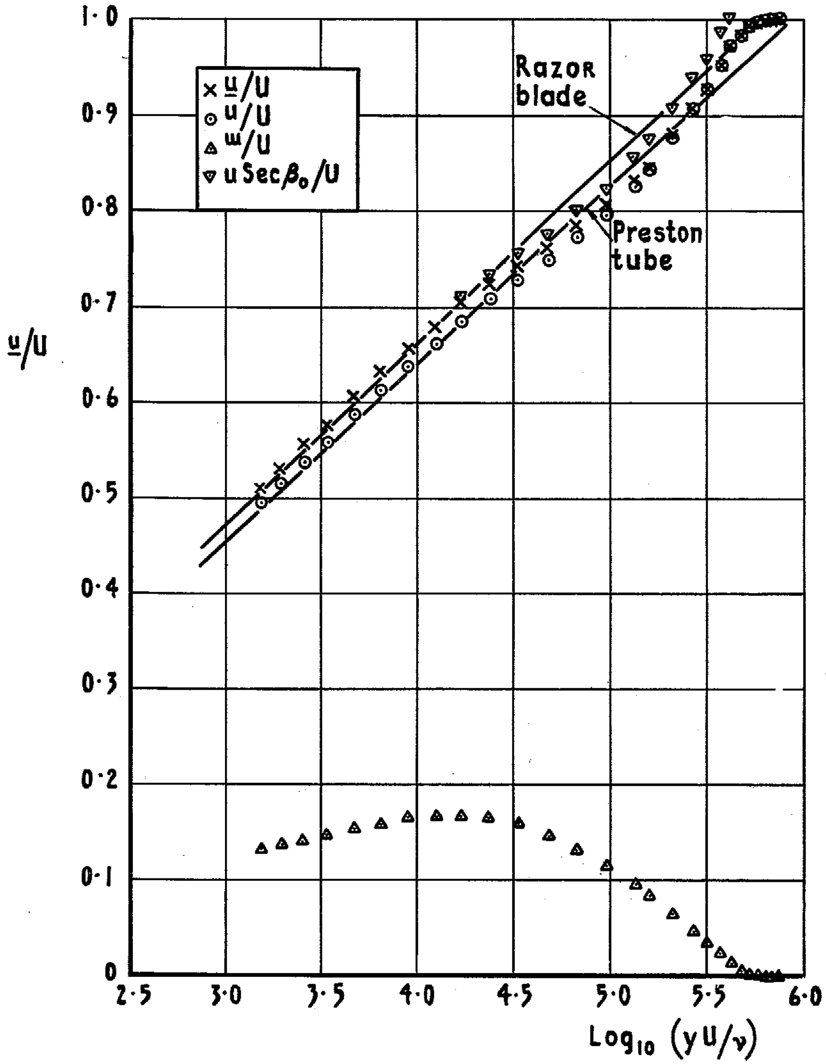

FIG. 12 *contd.* Logarithmic plots, profile No. 2416.

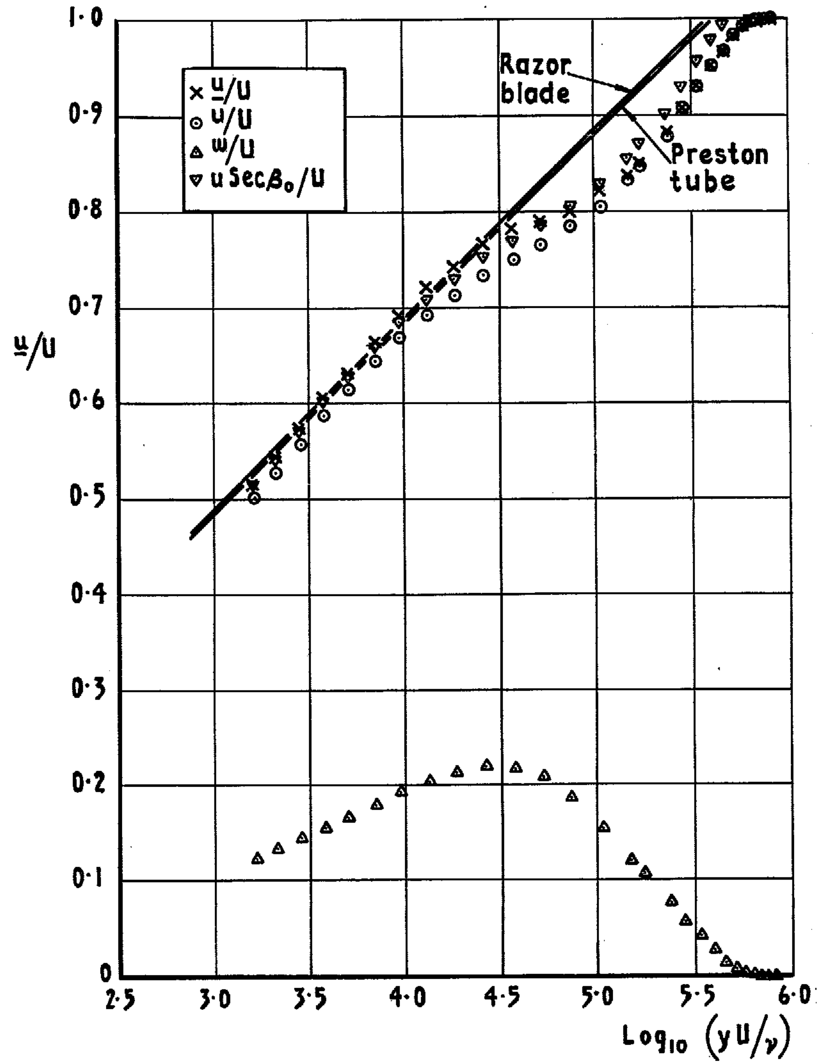

FIG. 12 *contd.* Logarithmic plots, profile No. 2408.

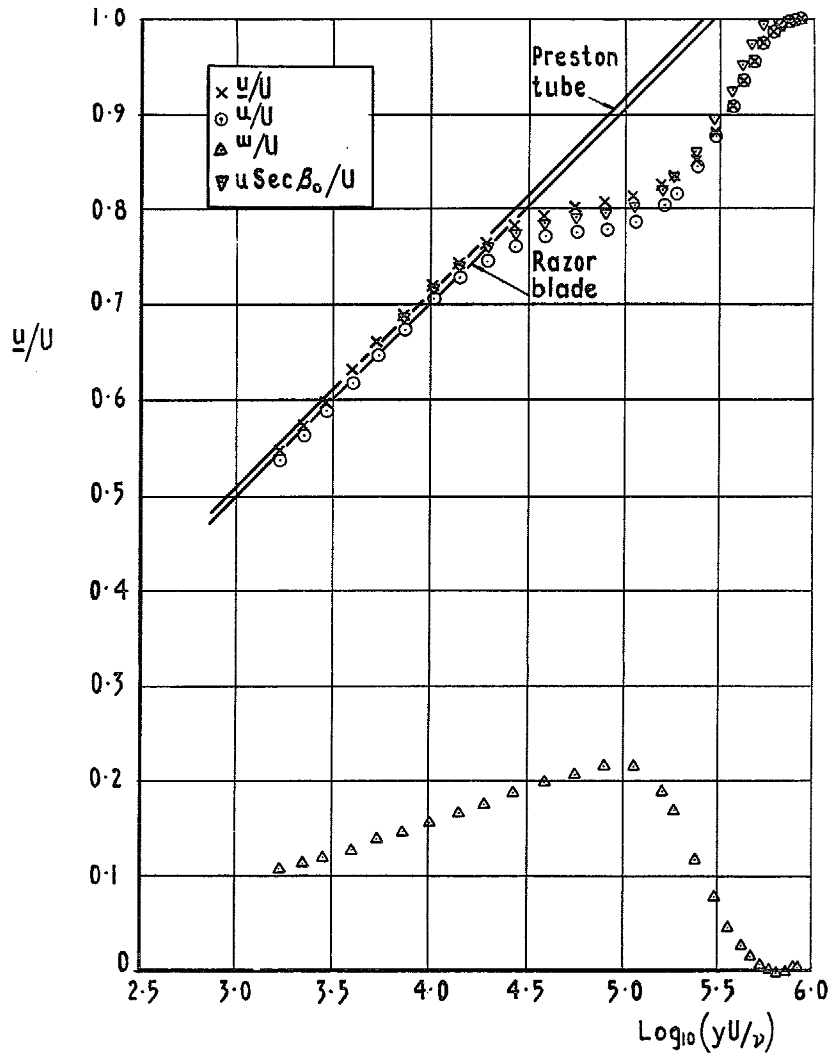

FIG. 12 *contd.* Logarithmic plots, profile No. 2400.

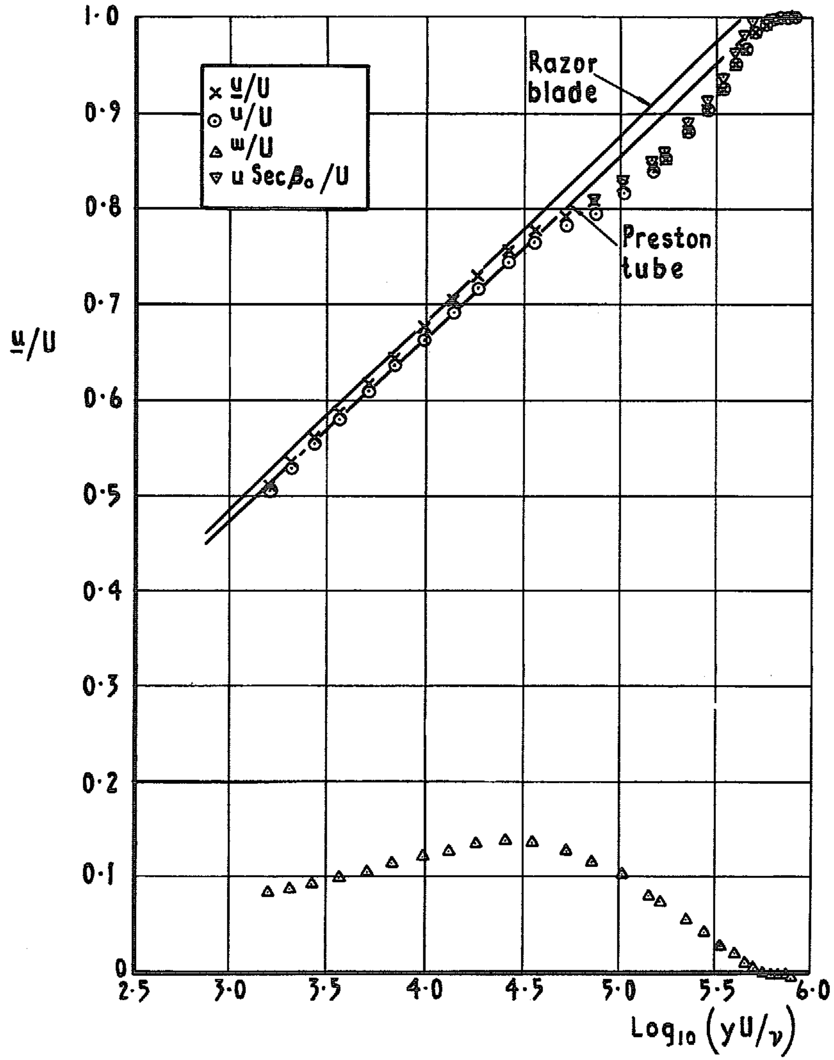

FIG. 12 *contd.* Logarithmic plots, profile No. 2808.

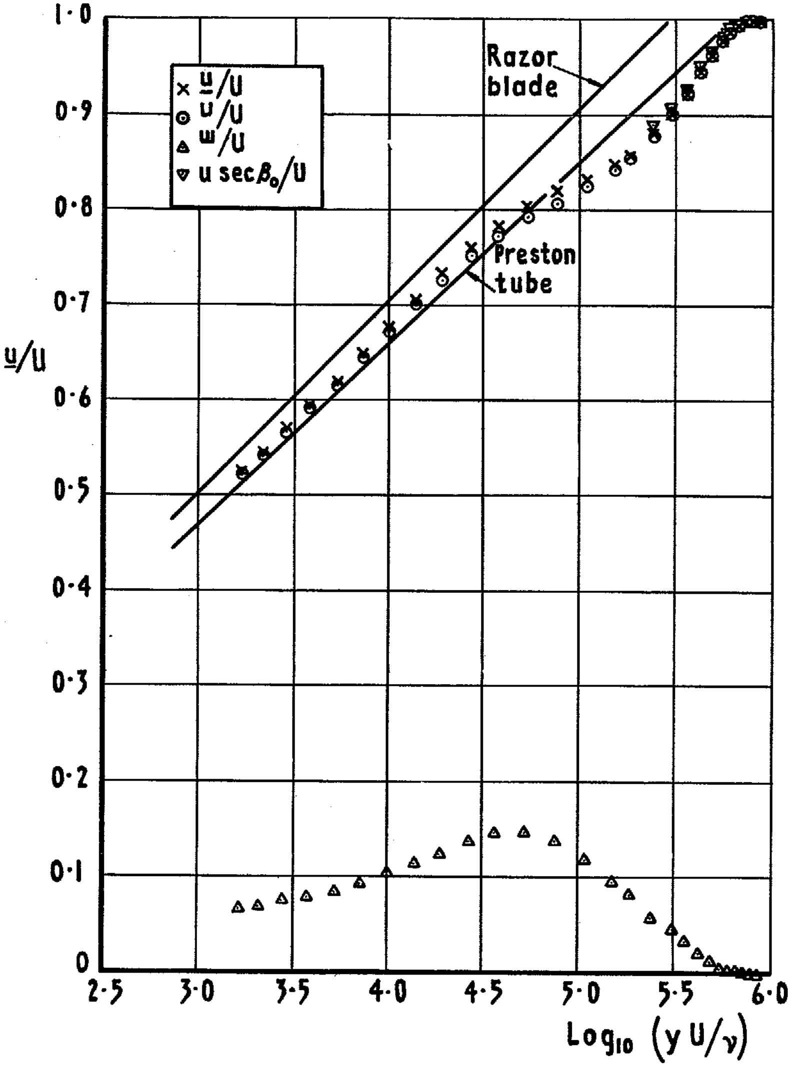

FIG. 12 *concld.* Logarithmic plots, profile No. 2800.

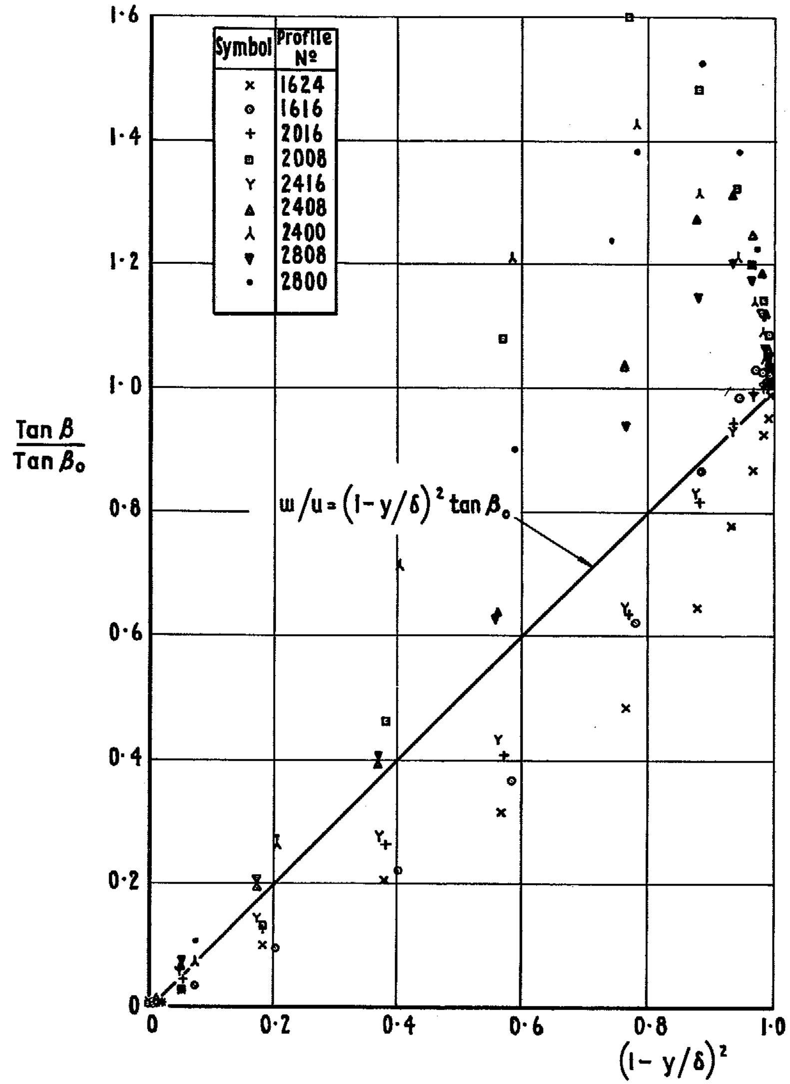

FIG. 13. Test of Mager's cross-flow equation.

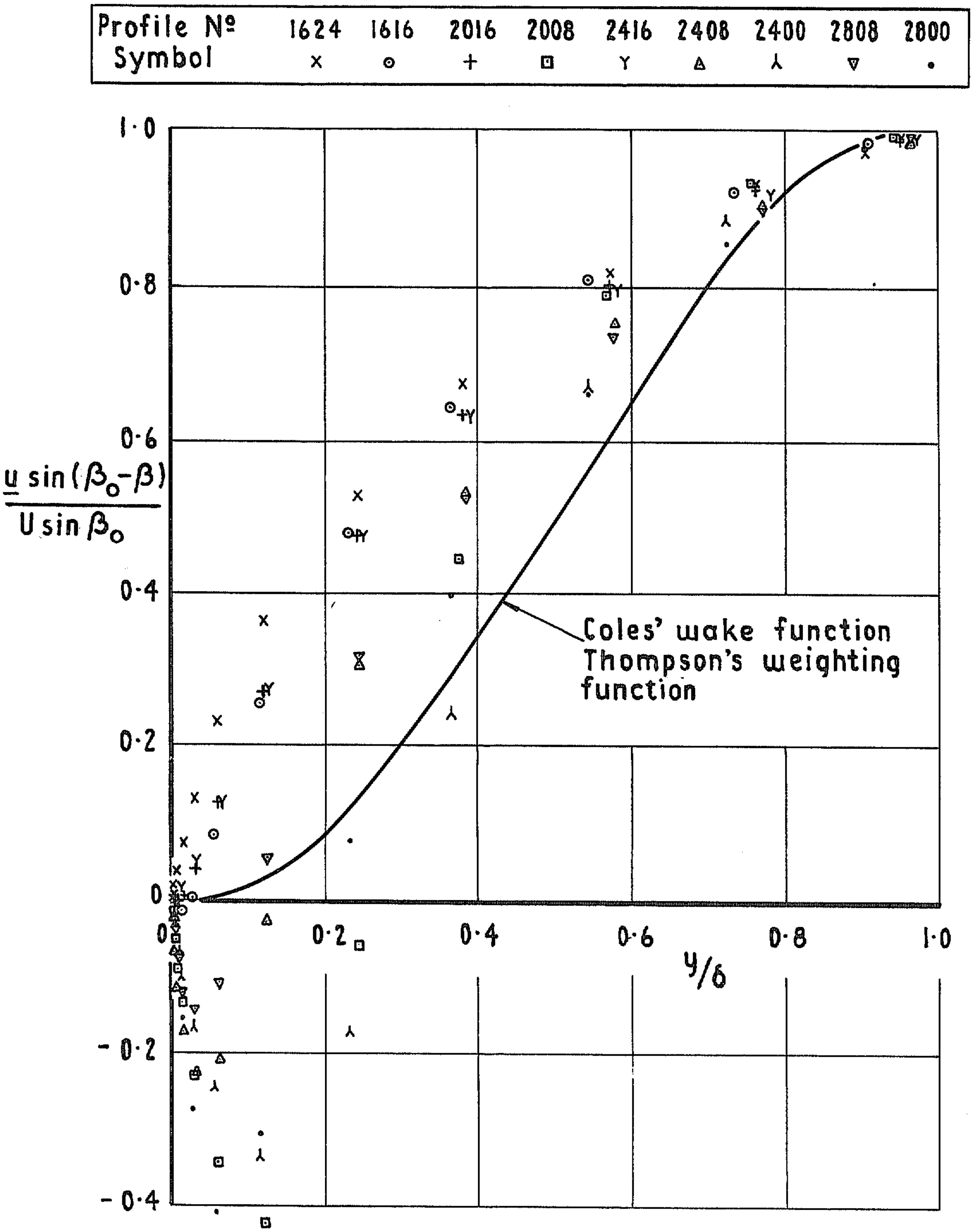

FIG. 14. Velocity profiles normal to surface shear-stress vector compared with Coles' wake function and Thompson's weighting function.

Printed in Wales for Her Majesty's Stationery Office by Allens Printers (Wales) Limited

Dd. 501372 K.5

R. & M. No. 3653

Published by
HER MAJESTY'S STATIONERY OFFICE

To be purchased from
49 High Holborn, London WC1V 6HB
13a Castle Street, Edinburgh EH2 3AR
109 St Mary Street, Cardiff CF1 1JW
Brazennose Street, Manchester M60 8AS
50 Fairfax Street, Bristol BS1 3DE
258 Broad Street, Birmingham B1 2HE
80 Chichester Street, Belfast BT1 4JY
or through booksellers

R. & M. No. 3653
SBN 11 470373 6